Concurrent Design for Optimal Quality and Cycle Time

by

Yu-Feng Wei

M.S., Industrial Engineering
University of Wisconsin-Madison, 1996

B.S., Mechanical Engineering
National Taiwan University, 1993

Submitted to the Department of Mechanical Engineering
in Partial Fulfillment of the Requirement for the Degree of

Doctor of Philosophy in Mechanical Engineering
at the
Massachusetts Institute of Technology

February 2001

Signature of Author _____
Department of Mechanical Engineering
January 19, 2001

Certified by _____
Anna C. Thornton
Assistant Professor of Mechanical Engineering
Thesis Supervisor

Accepted by _____
Ain A. Sonin
Chairman, Department Committee on Graduate Students

Concurrent Design for Optimal Quality and Cycle Time

by

Yu-Feng Wei

Submitted to the Department of Mechanical Engineering on January 19, 2001
in Partial Fulfillment of the Requirement for the Degree of
Doctor of Philosophy in Mechanical Engineering
at the
Massachusetts Institute of Technology

ABSTRACT

Product and manufacturing system design are the core issues in product development and dominate the profitability of a company. In order to assess and optimize the product and manufacturing system design, an objective evaluation framework is needed. Despite the many existing tools for product and manufacturing system design, there is a missing link between the product design and the production performances under system variability.

The goal of the thesis is to explore and understand the interactions among part design and tolerancing, processes and system variability, and system control decision, then provide an integrated model to assess the total cost in a system. This model will be used to aid part design, tolerancing, batching, as well as strategy analysis in process improvement.

A two-stage modeling approach is used to tackle the problem: quality prediction and production prediction. The quality prediction model projects the process variations into the output quality variations at each manufacturing stage, then predict the yield rate from the stochastic behavior of the variations and the tolerance. The production prediction model projects the demand rate and variability, processing times and variability, yield rates and batch-sizes into the manufacturing cycle time and inventories. After the performances are predicted through the previous two models, concurrent optimization of part design, tolerance, and batch-sizes are achieved by varying them to find the minimum cost. A case study at Boeing Tube shop is used to illustrate this approach.

The result shows that the costless decisions in part design, tolerancing, and batch-sizes can significantly improve the system performance. In addition, conducting them separately or without using the system performance as the evaluation criteria may only lead to the local optima.

Thesis Committee:

Prof. Anna Thornton (Chairperson)
Prof. Mary Boyce
Dr. Stanley Gershwin
Prof. David Hardt

DEDICATION

To Florence, for her love and encouragement through my graduate school years.

To my parents, for putting up with me and giving me the total freedom in making my own choice.

ACKNOWLEDGEMENT

First and most, I would like to thank my advisor, Prof. Anna Thornton, for her continuous guidance and support through my doctoral studies. I would also like to thank my thesis committee, Prof. Mary Boyce, Dr. Stanley Gershwin, and Prof. David Hardt, for their advice.

Second, I would like to thank many people at the Boeing Tube Shop who provided much help in my research project. Special thanks are due to Lindsay Anderson for initiating this project and always being supportive, and also to Chris Westenskow, Mike Carnette, Larry Lawrence, Kevin Clark, Mark Weber, Mark Carpenter, Mike Drumheller, Mark Williams, and many others who generously provided many insights, and helped me understand the problem and gather various data.

Third, thanks to all my past and current fellow students in the lab for bringing in laughter and good time.

Finally, I would like to thank the sponsors of the research project: Boeing Commercial Aircraft Group and National Science Foundation Career Award Grant 9702662.

TABLE OF CONTENTS

NOMENCLATURE

α: Angle of bend
β: Angle of rotation
$\delta\bullet$, $d\bullet$: Variation of the random variable
λ_i : Mean batch-arrival rate of part type i
a_j : Availability of workstation j
c_j^* : Adjusted SCV of aggregated processing time at workstation j
c_j : SCV of aggregated processing time at workstation j
c_j^{a*} : SCV of aggregated inter-arrival time at workstation j
c_j^{d*} : SCV of aggregated inter-departure time at workstation j
c_{ij}^s : SCV of batch setup time for part type i at workstation j
c_{ij} : SCV of single-part processing time for part type i at workstation j
c_i^a : SCV of batch inter-arrival time of part type i
c_{ij}^b : SCV of batch processing time for part type i at workstation j
c_{ij}^Q : SCV of batch-size for part type i arriving at workstation j
c_i : Inspection gauge clearance
CI_{ij} : Inventory cost of part type i at workstation j (dollars per unit per unit time)
CO_j : Operation cost of machine and labor at workstation j (dollars per unit time)
CS_{ij} : Scrap cost of part type i at workstation j (dollars per unit)
CT: Mean cycle time through the manufacturing system
CT_j : Mean cycle time at workstation j
d_i : Mean demand rate for part type i
e : Safety coefficient
$f(\bullet)$: Process mapping function
$\mathbf{g}_0$: Nominal position of the inspection point on the tube
$\mathbf{K}$: Stiffness matrix
l : Distance between bends
λ_j^* : Mean aggregated arrival rate at workstation j
m : Number of part types processed in the system
m_j^f : Mean time to failure in a machine at workstation j
m_j^r : Mean time to repair in a machine at workstation j
n : Number of workstations in a manufacturing system
N_j : Number of machines at workstation j
$\mathbf{o}_g$: Nominal orientation of the inspection point on the tube
$\mathbf{o}_t^*$: Actual orientation of one inspection point on the tube before adjustment
$d\mathbf{P}$: Total translation variation vector a point on the tube after the bending operation
$d\mathbf{P}_i$: Translation variation vector a point on the tube contributed by the i^{th} bend cycle
$pdf(\bullet)$: Probability density function

$\tilde{Q}_{ij}$: Random variable of batch-size for part type i arriving at workstation j

Q_{ij} : Mean batch-size for part type i arriving at workstation j

R : Bend radius

r : Reordering point

$\boldsymbol{\sigma}$: Generalized force vector

$\boldsymbol{\delta}_i$: Rotational variation vector of a point on the tube contributed by the i^{th} bend cycle

s : Safety stock

$\boldsymbol{\delta}$: Total rotational variation vector of a point on the tube after the bending operation

$\mathbf{S}$: Variation sensitivity matrix

s_{ij} : Mean batch setup time for part type i at workstation j

$\mathbf{t}_0^*$: Actual position of one inspection point on the tube before adjustment

t_j^* : Adjusted mean aggregated processing time at workstation j

${}^{i}\mathbf{T}_{i-1}$: Homogeneous transform matrix from coordinate system i-1 to i

$\mathbf{T}$: Matrix of tolerance set

t_j : Mean aggregated processing time at workstation j

t_{ij}^b : Mean batch processing time for part type i at workstation j

$\tilde{t}_{ij}^b$: Random variable of batch processing time for part type i at workstation j

$\tilde{t}_j$: Random variable of the aggregated processing time at workstation j

TC : Total cost (dollars per unit time)

TC^I : Total Inventory cost (dollars per unit time)

TC^O : Total operation cost (dollars per unit time)

TC^S : Total quality cost (dollars per unit time)

$\mathbf{T}_*$: Vector of lower specification limits

$\mathbf{T}^*$: Vector of upper specification limits

t_{ij} : Mean single-part processing time for part type i at workstation j

u_j^* : Average utilization rate at workstation j

$\mathbf{u}^{\mathbf{a}}$: Vector of key characteristics on the incoming (arriving) part

$\mathbf{u}^{\mathbf{d}}$: Vector of key characteristics on the output (departing) part

$\mathbf{v}$: Vector of process parameters/key characteristics of the mating part

WIP_i : Mean work-in-process of part-type i in the system

WIP_{ij} : Mean work-in-process of part-type i at workstation j

y : Yield rate at a single operation

Y_i : Mean overall yield rate for part type i through the system ($Y_i = \prod_{j=1}^{n} y_{ij}$)

y_{ij} : Mean yield rate for part type i at workstation j

Y_{ij} : Mean yield rate for part type i up to workstation j ($Y_{ij} = \prod_{k=1}^{j} y_{ik}$)

CHAPTER 1 INTRODUCTION

1.1 BACKGROUND

Product and manufacturing system design are the core issues in product development and dominate the profitability of a company. The objective of product design is to satisfy all the functionality requirements of its customers and to be produced in a cost efficient way. The goal of manufacturing system design is to make the products efficiently and responsively at the minimum cost while maintaining the production flexibility. There are many interactions between these two issues and they cannot be treated separately.

The design of a product will not only determine the value perceived by customer and the production costs, but also inherently constrain and guide the design of the manufacturing system by the selected process, required accuracy, and desired production rate. In case where there is an existing manufacturing system, it constrains the product design by its process flexibility and process capability. Ideally, the product and system should be jointly designed to optimize both.

In order to assess and optimize the product and manufacturing system design, an objective evaluation framework is needed. Many methodologies have been developed during the past decades by the academia and industry, such as *Concurrent Engineering*, *Robust Design*, *Design for Manufacture and Assembly*, *Total Quality Development*, etc. Each of these methods has its advantages and limitations. The frameworks typically comprise a set of design variables, performance measures, constraints, and decision-making procedure. The design variables have two categories: product design variables (*e.g.*, shape or features of the components, weight, thickness, etc.) and system design variables (*e.g.*, number of machines, number of labors, routing, batch-sizes, etc.). The performance measurements may include production rate, manufacturing cycle time[1], inventory, quality, flexibility, and cost. These measures can be converted into overall system cost when the cost structure is applicable. The constraints include the time and resource available for the design tasks.

1.2 MOTIVATION

Despite the many existing tools for product and manufacturing system design, there is a missing link between the product design and the production performances under system variability. For example, how does a part design influence its manufacturing cycle time when the production is subject to random yield loss and variability in demand and processing time? To answer such questions, an analytical framework that bridges the gap between product design and system design are necessitated.

The decision-making procedure is the most crucial part in the evaluation framework. It maps the design variables to the performance measures with the consideration of the constraints, and can be either qualitative or quantitative. The qualitative approach relies on human judgment and group consensus. It is easy to implement and results can be

[1] Manufacturing cycle time is defined as the time span a part spends in a manufacturing system, starting from the time it enters the system until it departs from the system. Manufacturing cycle time is also called *throughput time* or *manufacturing lead time*.

obtained quickly, but the quality of the results depend heavily on the knowledge and experience of the designers and the group dynamics. On the other hand, the quantitative approach requires analytical modeling. It can derive objective and accurate results, and provides more insights. However, such modeling requires longer time and more efforts, and sometime it is infeasible or even impossible to obtain.

Concurrent Engineering (CE) has been recognized as an important manufacturing philosophy over the past decade. It seeks to break down departmentalism and facilitate communication among different groups at early stage of product development. The goal is to identify, avoid, or fix the potential problems that may occur later in the production. CE advocates communication and information flow among different groups of people, especially the design and manufacturing personnel. However, it has two major deficiencies. First, most of the CE techniques only provide qualitative frameworks that require human judgment and assessment. Therefore, the quality of the decisions are very easily biased or distorted due to human errors, insufficient knowledge or inexperience. Secondly, the decision-making process relies heavily on group dynamics. As the result, the decisions reflect more the compromise after negotiation rather than the objective and optimal solutions.

One of the most popular tools linking design and manufacturing, *Design for Manufacture and Assembly* (DFM/A), provides a set of generic design guidelines and a systematic way for assessing the impact of design on manufacturing and assembly. However, its guidelines only emphasizes on the interactions between product design and manufacturing process. In addition, the evaluation method it provides primarily focuses on the material and process costs only. The problem is that its guidelines are more qualitative and may not be applicable for all scenarios, and the system-level costs such as inventory cost, manufacturing cycle-time cost, and quality cost are overlooked. As a consequence, the guidelines are not robust for all cases and the evaluation scheme can be misleading.

Furthermore, the current design and control methodologies for manufacturing system such as lean manufacturing paradigm or operations research techniques have their deficiencies, too. They all treat product design as fixed input and then try to control and optimize the performances of the system. The pitfalls are that the results might still be local optima if the product and system designs are not considered as a whole, and there is no feedback for product design based on the system performances.

1.3 GOAL AND SCOPE OF THE THESIS

The goal of the thesis is to explore and understand the interactions among part design, tolerancing and inspection, manufacturing processes, and manufacturing system, then provide an integrated model to assess the total cost in a system. This model will be used to aid product design, tolerancing and inspection, system control and planning, as well as strategy analysis in process improvement.

The scope of the thesis is two-fold. First, we address three issues in the product development for an existing manufacturing system with variability: part design, tolerancing, and batching[2]. These are decision variables that can be determined

[2] Determining the batch-sizes of the products. Also called lot-sizing or batch-sizing.

simultaneously to optimize the system performance without capital investment. The variability includes process variation, demand variability and processing time variability. Secondly, we seek to find the optimal investment strategy to improve the current system, such as variation reduction or capacity expansion, and the consequences on the three decision variables: part design, tolerancing, and batching.

1.4 HYPOTHESIS

The hypothesis of this thesis is stated as follows: the overall production cost for a product during manufacturing and assembly can be modeled, controlled and minimized only when the interactions among part design, tolerancing, inspection, manufacturing processes, and manufacturing system are modeled and optimized jointly. Any attempt to minimize quality cost through an individual area will only result in local optimum or a possible greater overall loss.

1.5 APPROACH

The overview for the problem structure is illustrated in Figure 1.1. The design variables and the system variability are described in Section 1.3. The problem can be broken into two levels: process and system, as highlighted in the yellow and blue areas in Figure 1.1, respectively. At the process level, the central issue is the quality of the part, which is characterized by the production yield rates at all stage of the manufacturing process. At the system level, the central issue is the system performance, which includes the manufacturing cycle time, inventory level, and cost. It is noteworthy that the yield rates relate the two levels, since they are not only the output of the process but also influence the system performances.

Our approach comprises three steps: quality prediction, production prediction, and concurrent optimization. We seek to model and predict the system performances from the design variables, system settings, and system variability, then use them as the feedback for optimal design and investment strategy. These steps are discussed in the following sections. We first discuss the general modeling strategy, then followed by the three steps.

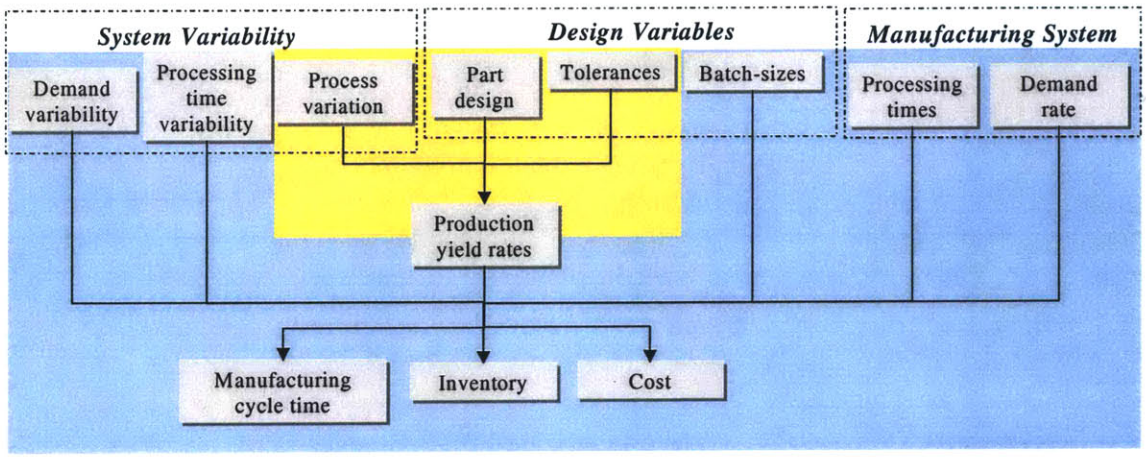

Figure 1.1: Problem structure

Modeling Strategy

There are two modeling approaches: simulation and analytical modeling. Simulation modeling is easy to implement but is also computationally expensive and time consuming. Analytical modeling provides prompt solution and deeper insights, however, it also requires broader knowledge of the object to be modeled and sometimes the model is impossible to derive. Since our problem contains two levels of modeling and an optimization, simulation modeling will be infeasible due to the large number of iterations needed[3]. Therefore, we seek to derive an analytical model and minimize the need for simulation. When the exact analytical expression cannot be found, approximation methods are applied. Each approximation will be followed by the validation and limitation.

Quality Prediction

The quality prediction model projects the process variations into the output quality variations at each manufacturing step, then predict the yield rate from the variations and the tolerances. Changes in the part design will change the variation sensitivities in the manufacturing process, thus the yield rates. The model overview is described in Section 2.2 and a detailed example is elaborated in Chapter 3.

Production Prediction

The production prediction model projects the demand rate and variability, processing times and variability, yield rates and batch-sizes into the manufacturing cycle time and inventories. The model overview is described in Section 2.3 and a detailed example is provided in Chapter 4.

Concurrent Optimization

After the performances are predicted through the previous two models, they can be converted into costs as the commensurate performance measure. Concurrent optimization of part design, tolerance, and batch-sizes are achieved by varying them to find the minimum cost. The formulation is described in Section 2.6 and a detailed example is illustrated in Chapter 5.

In addition, a case study at Boeing Tube shop is used to illustrate the proposed approach. In this case study, the impact of tube design, tolerance and batch-sizes on the manufacturing system is assessed through quantitative modeling of the tube and the system. The expected yield rates during tube production is predicted through variation modeling, then plugged in the production prediction model to evaluate the manufacturing cycle time, inventory level, and overall costs. An example is used to illustrate the optimization of tube design, tolerance and batch-sizes. Finally, the optimal investment strategy for variation reduction is also discussed. We will introduce the tube production

[3] This is because the optimization requires several iterations. Each iteration needs two simulations for both levels, and each simulation requires large run size (usually larger than 500).

systems in the following section, including tube manufacturing and assembly, tube design, and the characteristics of tube production system.

1.6 TUBE PRODUCTION SYSTEMS

Tubes are extensively used in sophisticated vehicles such as aircraft and submarines for hydraulic systems, airflow systems, and waste systems. Because of the functional requirement of transporting substances through a complex structure, tubes are typically bent into complex shapes. Figure 1.2 shows an example of a hydraulic tube system in an aircraft.

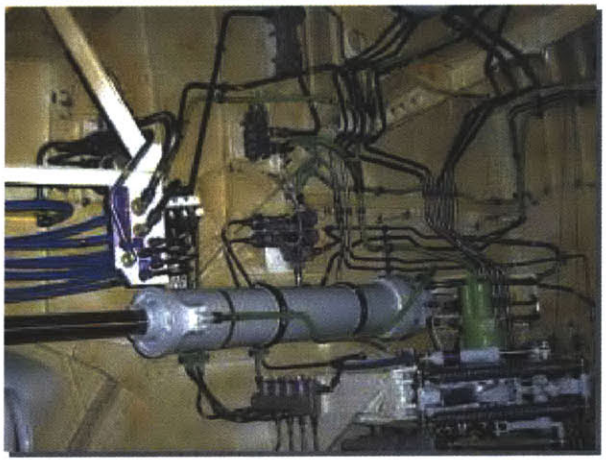

Figure 1.2: Example of a tubing system

A tube production system transforms the raw tubes into desired shapes and installed them onto the mating structure. It comprises two stages: tube manufacturing and tube assembly. We will discuss them in the following sections.

1.6.1 Tube Manufacturing

The tubes need to go through several manufacturing operations prior to the assembly, as shown in Figure 1.3. Among these operations, bending is the most critical one in delivering the shape and determining the variations on the tubes. The raw tubes are sent to the bending workstation to transform into the desired shape. The output *key characteristics*[4] (KCs) of a bent tube are usually the positions and orientations of the install points on the tube, and they are due to the incoming part variations (springback) and the process variations (distance of stroke, angel of bend, and angle of rotation). The bending operation is followed by the inspection to ensure the output KC variations are within some acceptable range. There are several methods can be used for inspection, such as gauge fitting, CMM measuring, and optical method. The tubes failing the inspection are scrapped, and those passing the inspection are sent to the finishing workstations. The

[4] A set of predefined and important measures, such as dimensions, weight, surface finish, etc, used to determined the acceptability of a part during manufacturing and assembly process (Lee and Thornton 1996).

finishing operations may include trimming and deburring, swaging or welding of the connectors, painting, and pressure test. Tubes will also be scrapped during these operations. However, most of the scrap is due to material problems such as particle inclusions, cracks, scratches, etc.

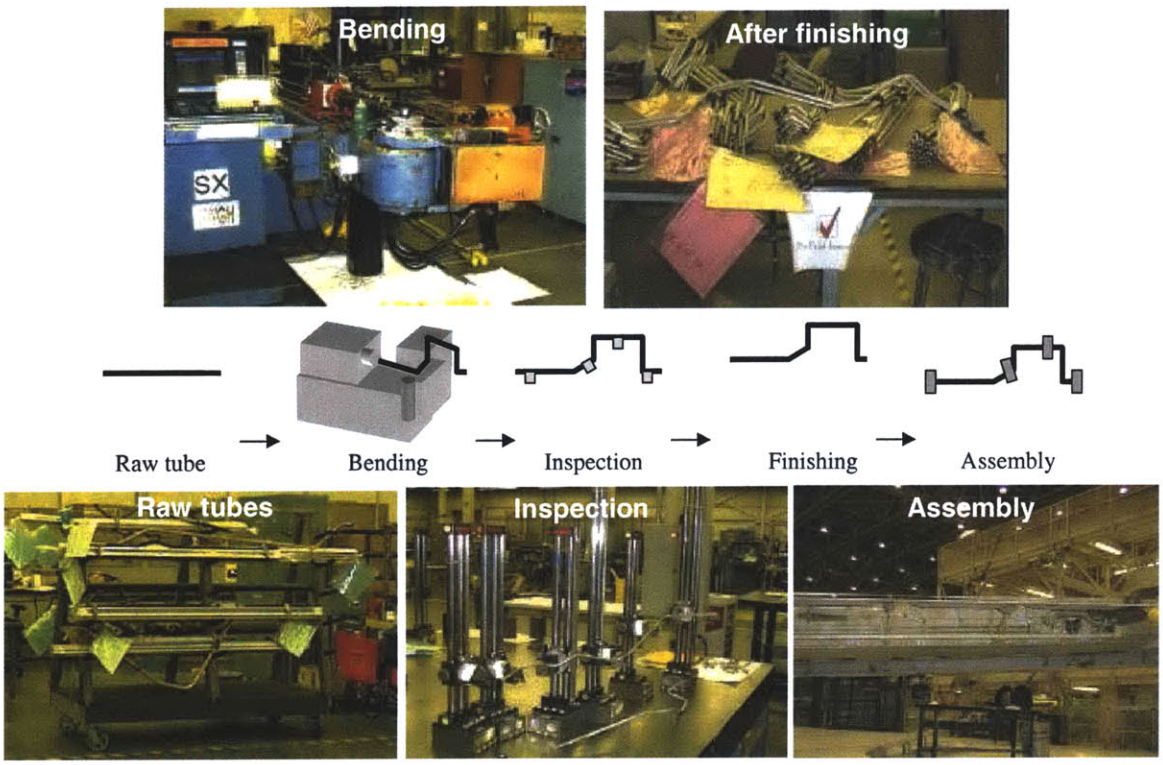

Figure 1.3: Typical tube manufacturing and assembly process

1.6.2 Tube Assembly

Figure 1.4 illustrates the assembled tube. In the tube assembly operation, the tube ends are connected to either a structural part on the aircraft or another tube. It must pass through holes in the structure and bend around obstructions. In addition, the tube is typically *tied-down* at a series of points. These tie-downs prevent vibration, ensure the proper location of the tubes, and provide structural support.

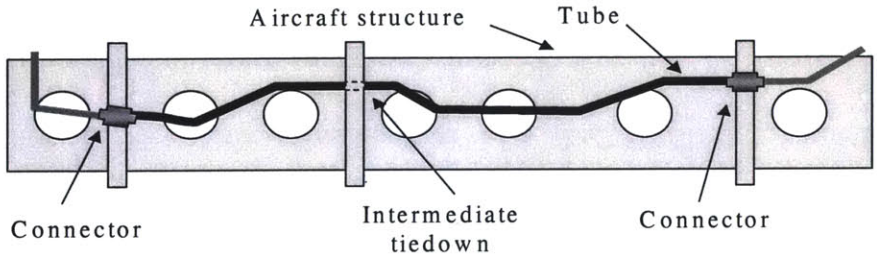

Figure 1.4: Example of assembled tube

In general, there is variation in connection points, tie-down points and the tube. The assembler must apply compensating load (force and moment) to fit the tube into the install points. Because the tube has bends, a large aspect ratio, and is thin-walled, the tube compliance is used to enable assembly. However, applying load on the tube can impact the life-cycle performance of the tubes. As a result, a maximum load is specified at each connection point. Therefore, the assembly loads are the output KC used to qualify the acceptance of the tube assembly. If a tube cannot be installed without exceeding that load, the tube is rejected. Figure 1.5 shows that the assembly with geometrical variations in both tube and structure requires compensating loads.

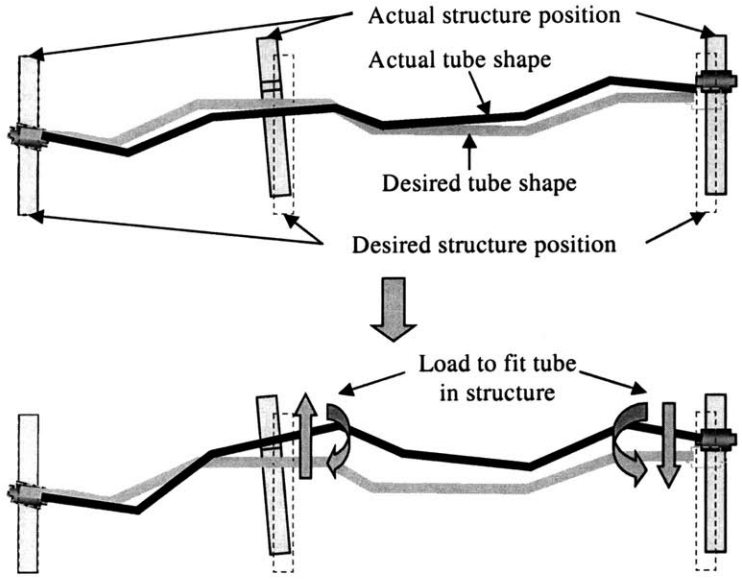

Figure 1.5: Variations in tube assembly and the compensating load

The deformation on the mating parts during assembly is governed by the stiffness and the variations of the mating parts. Variations on the mating parts are absorbed by their deformation and determine the variation on the assembled part. As a general rule, the stiffer part has less deformation and its variations are more dominant in the variations of assembled part.

1.6.3 Tube Design and Robustness

The task of tube design is to find a routing path to connect two preset points under the geometric constraints (objects to avoid, supports to pass through), manufacturing constraints (minimum and maximum bend angles, machine interference), and functionality constraints (maximum weight, maximum number of bends to maintain internal fluid pressure). Figure 1.6 shows an example of two tube design alternatives that connect point 1 and 3 via an intermediate support.

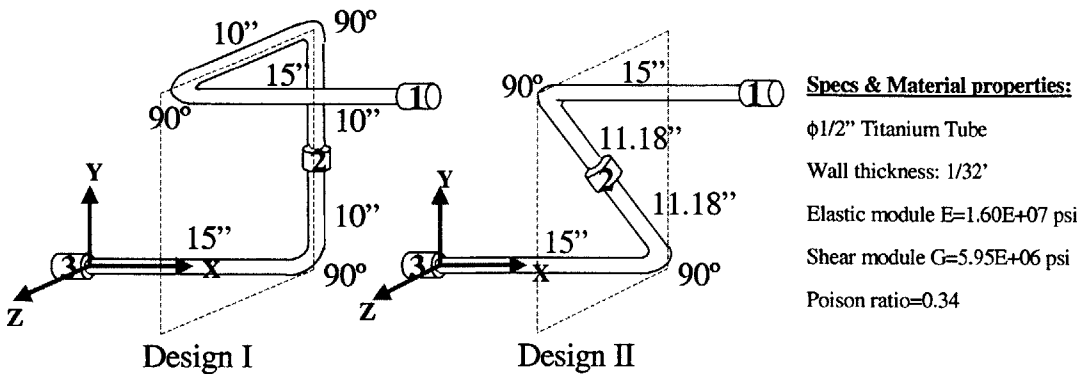

Figure 1.6: Example of tube design

Tube design also determines the robustness in manufacturing and assembly, in which robustness is defined by the sensitivity to variations. In many cases they cannot be concurrently minimized thus tradeoff between them needs to be made. As a general rule, increasing the number of bends on a tube can increase the compliance (higher assembly robustness), but it also introduces more variations onto the tube (lower manufacturing robustness). In the example above, Design I has higher assembly robustness but lower manufacturing robustness than Design II.

1.6.4 Characteristics of Tube Production System

The aircraft tubes have very high part variety. It is estimated that there are on average more than ten thousand unique tubes in a commercial aircraft. Due to the high part-variety, each type of tube is usually manufactured in batches to reduce the setups. The demand for tubes depends on the demand for the aircraft. Usually the tubes are treated as commodity in the aircraft assembly site, and are stored in the finished tube inventories. The inventory for each tube has a reordering point, reordering quantity, and safety stock. When the number of tubes on stock reaches the reordering point, an order with a predetermined quantity will be sent to the tube manufacturing plant, which in turn will be the batch-size for the tube manufacturing plant. The safety stock provides the buffer for the uncertainties in demand and delivery. In short, the tube production system can be characterized as a make-to-order batch-production system with inventories controlled by reordering-points.

1.7 RELATED WORK

Related research falls into three categories: concurrent engineering, design under quality-related variability, and production control under uncertainties.

1.7.1 Concurrent Engineering

Concurrent Engineering (CE) rooted from the early automobile industry (Evans 1988), and gained its popularity around 1980. The relevant literature is broad. The history and different applications of CE are reviewed in Parsaei and Sullivan (1993). There are

two categories of CE: team-based approaches and computer-aided tools. For the former the most commonly used are House of Quality (Hauser and Clausing 1988, Clausing and Pugh 1991, Clausing 1993), which selects the design concept based on a set of criteria and relative rating, and Failure Mode and Effects Analysis, which seeks to diagnose the potential problem at the design stage.

For the computer-aided tools, Design for Manufacture and Assembly (DFM/A) is the most recognized. Boothroyd and his colleagues developed a series of guidelines and cost estimation methods for manufacturing and assembly process at the design stage. Software package is also available based on their methodology.

Some researchers studied the effect of product design on the production performance. Govil and Magrab (1999) estimated the manufacturing cycle time of product design based on the assembly tree and used the information to predict the production rate. Herrmann and Chincholkar (2000) presented a set of queueing models to predict the manufacturing cycle time for a new product design. Veeramani *et al.* (1997, 1999) proposed a quoting system that allows users to modify the standard products online then generates the CAD model, bill-of-materials, process plan and shop-floor schedule to calculate the price and delivery date. All these methods do not take the process variability into account, *i.e.*, the robust design issue is not considered.

1.7.2 Design under Quality-related Variability

There are three subcategories: robust design, variation modeling, and optimal tolerancing.

Robust Design

Robust design seeks to minimize the quality variations of the output parts under the uncertainties in the manufacturing process. The robust design community studies two types of robustness: robust process design and robust part design. For the former researchers seek to find the process parameter set that minimizes output quality variations. For the latter, researchers seek to minimize the sensitivity to quality variation through part design. Kazmer *et al.* (1996) use predictive model to analyze part variation and robustness in the injection molding process. Frey (1997) proposes the Process Capability Matrix method to propagate variations of multiple key characteristics and predict the yield in multiple operations manufacturing. Suri and Otto (1999) present the *Integrated System Model* method that predicts variations in manufacturing system, and provides a feed-forward control scheme for the stretch forming process. Most of the robust design work focus on modeling the quality performance of the production, *i.e.*, the effects of operational settings and process variations on the variations of part features. Other system performances are not considered.

Variation Modeling

Research in variation modeling seeks to predict the quality variations of the output parts under uncertainties in the assembly process. There are two types of variation modeling in assembly: rigid assembly modeling, and compliant assembly modeling.

Previous works in rigid-part assembly include tolerance representation and analysis. In their terminology tolerance analysis and variation modeling are interchangeable. One class of researchers (*e.g.*, Daniel *et al.* 1986, Turner 1990, Takahashi 1991) uses MCS or numerical methods to propagate variation in assembly. Simulation-based commercial software is also available (*e.g.* VSA-3D). Turner and Gangoiti (1991) present a comprehensive survey on these commercial packages. Another class of researcher adopts statistical approach to predict the variation and assemblability in the final assembly. Bjorke (1978) studies the one-dimensional variation stack-up for tolerance analysis. Whitney and his colleagues (1994) introduce homogeneous transform matrix (HTM) for 3-D geometric representation and tolerance analysis. Their method predicts the spatial distribution of position and orientation of parts in assembly, and calculates the assemblability by Gaussian approximation. Gao and his colleagues (Gao *et al.* 1998) generalize the method for assembly with kinematic adjustment. The linearized matrix transform method significantly reduces the computational requirement and shows high accuracy compared to MCS (Gao *et al.* 1995). In this thesis we modify this method and apply it to the variation modeling for tube bending. Since the preceding research has the assumption of rigid parts, they do not consider part deformation during process and assembly.

The variation modeling for compliant part assembly is a growing research area. Liu *et al.* (1996) and Hu (1997) first derive the variation propagation equations for simple 2-D sheet metal assembly from beam theory and use MCS to attain the variation distribution. They further extend the work to more complex cases by using a simplified FEM approach with MCS (Liu and Hu 1997). Their approach obtains the stiffness matrix for the nominal part shape through FEM first, then uses MCS to get the variation distribution. Chang (1996) uses similar approach to investigate the deformation and variation of sheet metal assembly with fixture. These methods still rely on intensive simulation, thus are infeasible for robust design that needs to quickly evaluate a large amount of designs. Lee *et al.* (2000) derive the sensitivity matrix for compliant assembly and use its largest Eigenvalue as an index for the robustness. This method can provide instant feedback for robust design. However, its result may not truly reflect the assemblability because it does not use variations and tolerances as input. In addition, all the abovementioned works only consider the geometric variations. Assemblability issue subject to load constraints is not considered in the previous research.

Optimal Tolerancing

Research in optimal tolerancing seeks to make tradeoffs in manufacturing cost caused by tight tolerance and quality cost caused by loose tolerance. Ostwald and Huang (1977) used linear programming method to minimize cost in tolerance allocation. They assumed linear cost model and treated tolerance as linear inequality constraints. Diplaris and Sfantsikopoulos (2000) determined the optimal tolerance by minimizing the costs in manufacturing and dimensional accuracy. Zhang *et al.* (1992) simultaneously determined the optimal machining process and tolerances for multiple parts to be assembled. Their formulation is to minimize the total manufacturing cost associated with the tolerances through all machining process for all parts, under the machining constraints and overall

tolerance allowance after assembly. Dong (1997) used similar formulation except that the cost of performance of the assembled part is taken into account.

All these approach only consider costs in manufacturing process and product quality or performance. However, there are other costs in the manufacturing system such as manufacturing cycle time and inventory cost will also be influenced by the tolerance. This is because tolerance will determined the yield rate at each manufacturing stage, and yield rate will in turn affect the manufacturing cycle time and inventory. In addition, these approaches assume that the tolerance-related manufacturing cost model can be obtained from statistical data. However, such data might be biased, inaccurate, or even unavailable.

1.7.3 Production Control under Uncertainties

Manufacturing Cycle Time Calculation

The major portion of the manufacturing cycle time is due to queueing caused by the uncertainties in demand arrival and processing. The calculation is studied extensively by the queueing theory community. Kleinrock (1975, 1976) provided a general review on the theoretical background for different types of queueing systems. The exact solution for queueing time relies on the Markovian assumption in either the arrival or the service. For some simple cases, such as single-item-individual-arrival or single-item-batch-arrival systems, standard models such as *M/M/1* and *M/G/1* can be applied and the queueing time can be obtained by the Pollaczek-Khintchine formula. For other generic cases, such as multi-item system or the Markovian assumption is invalid, *G/G/1* or more complex models need to be used. In such cases only approximation and bounds on the queueing time can be obtained. Yao (1984) provided the approximation for batch-arrival-individual-service and Whitt (1983) provided the approximation for batch-arrival-batch-service. Papadopoulos *et al.* (1993) summarized the different applications and approaches of queueing theory in the manufacturing systems.

Optimal Batching

There are two classes of optimal batching literature: infinite capacity and finite capacity. The former focuses on the issue of quantity. It started with the classic study of *Economic Ordering Quantity* (EOQ), where the ordering lead-time (manufacturing cycle time of the supplier) and yield loss are negligible and the demand is constant. The optimal batch-sizes seek to balance the inventory cost and the setup cost. For system with yield and demand uncertainties, more sophisticated models are used to balance the inventory cost, setup cost, and backlog cost. Yano and Lee (1995) provided a comprehensive review.

The optimal batching with regard to finite capacity focuses on the issue of time. The effect of batch-sizes on the manufacturing cycle time was first studied by Karmarkar and his colleagues (1985, 1987, 1992). They introduced the concept of *Q-lots*, where the average queueing time has a convex relation with the batch-sizes. In general, large batch-size increases the batch waiting time and small batch-size causes congestion, which leads to long queueing time. Other researchers (Jönsson 1985, Bertrand 1985, Zipkin 1986)

used different approaches to investigate the same issue. Kuik and Tielemans (1999) studied the relation between batch-sizes and the lead-time variability by using the *M/G/1* model. Lambrecht and Vandaele (1995) used Whitt's approximations to get the mean and variance of the queueing time, then fit them into lognormal distribution so that approximated lead-time can be quoted under a specific service level.

1.8 STRUCTURE OF THE THESIS

The rest of the thesis is arranged in the following structure: Chapter 2 introduces the theoretical foundations and the research methodologies: *Joint System Performance Model* (JSPM) and *Concurrent Optimal Design* (COD). The former synthesizes the variation model and queuing model to predict the system performances at the product design stage, while the latter provides an integrated approach for system optimization by combining robust design, tolerancing, and batching based on JSMP. Chapter 3 elaborates the quality prediction in JSPM for aircraft tube design. Chapter 4 develops the cycle time prediction in JSPM for aircraft tube production system with inventories controlled by reordering-points. Chapter 5 applies the method of COD for aircraft tube design and production, and discuss the optimal investment strategy for variation reduction. Chapter 6 concludes the thesis with the key findings, major contributions, method generalization, and opportunities for future research.

CHAPTER 2 JOINT SYSTEM PERFORMANCE MODEL

2.1 INTRODUCTION

In Chapter 1 we briefly introduce the research approach. In this chapter, we will elaborate it by introducing the theoretical foundations and the research methodologies. We first describe the quality model for yield rate and end-of-line variation prediction. Secondly, the production model for manufacturing cycle time and work-in-process prediction is depicted. Thirdly, the cost model that converts the predicted performances is explained. Finally, we introduce the novel concept of *Joint System Performance Model* (JSPM) and *Concurrent Optimal Design* (COD). The former synthesizes the quality model and production model to predict the system performances at the product design stage, while the latter provides an integrated approach for system optimization by combining robust design, tolerancing, and batch-sizing based on JSMP.

2.2 QUALITY MODEL

A process to produce a product usually comprises several operations. In each operation the incoming parts are transformed into desired shape, geometry, material property or subassemblies. The output parts are qualified by a set of KCs. Due to the variability in incoming part, machine and worker, the KCs will deviate from their target values. As the result, tolerances are imposed on the KCs to define their acceptable ranges. If any of the KCs falls outside its tolerance, the part is either scrapped or needs rework.

There are two performance measures for the production quality in a manufacturing system. The first performance measure is the yield rates at all stages of the process. Yield rate is defined as the probability that a raw material becomes a finished part without being rejected during the process. Yield rate is directly associated with the internal quality cost, which includes scrap cost, rework cost, and other indirect costs by deteriorating the system performance.

The other quality performance is the end-of-line variation on the KCs. It is the result of variation propagated through the process and filtered by the tolerance. End-of-line variation is associated with the external quality cost because it might affect the functionality of the product or become a source of variation for the downstream customers.

2.2.1 Representation

The manufacturing process can be represented mathematically. Each manufacturing operation can be represented as a mapping process from the incoming part KCs and the process parameters to the output part KCs, bounded by the tolerance. Figure 2.1 illustrates the scheme.

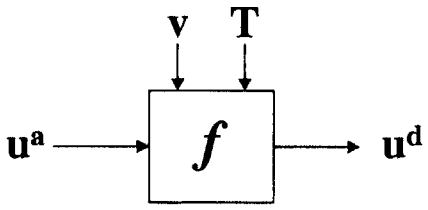

$\mathbf{u}^a$: Vector of key characteristics on the incoming part

$\mathbf{v}$: Vector of process parameters/ key characteristics of mating part

$\mathbf{T}$: Tolerance set

$\mathbf{u}^d$: Vector of key characteristics on the output part

Figure 2.1: Schematic representation of KC in a single operation

In this scheme, the incoming part has a key characteristic vector (KCV), $\mathbf{u}^a$. As mentioned previously, the KCV is a complete set of measures used to quantify the quality of the part. The KCV of output part is denoted as $\mathbf{u}^d$. Note that $\mathbf{u}^a$ and $\mathbf{u}^d$ need not have the same dimensions and components. For example, in a tube bending process, $\mathbf{u}^a$ may contain the length and wall thickness of a raw tube, while $\mathbf{u}^d$ may contains the positions and orientations of some points of interest of the finished tube. Vector $\mathbf{v}$ has two definitions. It is either the complete set of process parameters that the workstation performs to make the part, or the KCV of the mating part in an assembly operation. For example, in the tube bending operation, $\mathbf{x}$ includes the bending angle, rotation angle and translational distance in a bend cycle. In the tube assembly operation, $\mathbf{v}$ is the KVC that contains the positions and orientations of the install points.

Due the stochastic nature of the manufacturing operation, the values of $\mathbf{u}^a$, $\mathbf{v}$ and $\mathbf{u}^d$ are randomly distributed in the manufacturing operation. To control the variations within acceptable ranges, tolerances are imposed on $\mathbf{u}^d$. Matrix $\mathbf{T}$ is the tolerance set that defines the admissible ranges for the variations in $\mathbf{u}^d$. In simple cases where one tolerance corresponds to one output KC, it has two columns and is defined as $\mathbf{T} = \left(\mathbf{T}_* \;\; \mathbf{T}^*\right)$. The first column is the lower specification limit vector, and the second is the upper specification limit vector, both on the output KCV, $\mathbf{u}^d$.

For example, the tolerance vector for a tube may contain the maximum and minimum angular and translational variations for each point of interest on the tube. In more complex cases, $\mathbf{T}$ is defined as a set of linear or nonlinear combinations of the output KCs to form the admissible zone. For example, some inspection methods use gauges to check if the part can fit in. In such cases, $\mathbf{T}$ can be represented as some spatial "zones" that the part must falls inside. In either case, the probability that $\mathbf{u}^d$ falls outside $\mathbf{T}$ is denoted as y, which is also the long-term yield rate if a large quantity of parts are produced. The yield rate is determined by the variability in incoming KCs and process parameters, as well as the tolerance. It will be discussed in the next section. The mapping process among $\mathbf{u}^a$, $\mathbf{v}$, $\mathbf{u}^d$ and $\mathbf{T}$ are expressed as follows.

$$\mathbf{u}^d = f(\mathbf{u}^d, \mathbf{v}, \mathbf{T}) \tag{2.1}$$

Where $f(\bullet)$ is the process mapping function. This equation predicts the output KCs given that the incoming part KCs and process parameters are known. However, in practice the global process mapping function is difficult or impossible to derive due to the inherent complexity of the manufacturing operations. Since in reality a manufacturing operation is usually operated under a finite set of $\mathbf{u}^a$ and $\mathbf{v}$, we can obtain the linearized

process mapping functions at these points instead of the whole space of $\mathbf{u}^a$ and $\mathbf{v}$. The advantage of this approach is that the process mapping function is easier to derive thus the prediction of the output KCs and yield rate is enabled. Many researchers have used similar approaches for different types of manufacturing operations (*e.g.* Frey and Otto 1996, Kazmer and Barkan *et al.* 1996, Suri and Otto 1998). This method is described in the following section.

2.2.2 Variation Model for A Single Operation

Letting $\mathbf{u}_0^a$ be the nominal incoming KCV, $\mathbf{v}_0$ be the nominal process parameter vector, and $\mathbf{u}_0^d$ be the target output KCV, then through Taylor series expansion, Equation (2.1) can be expressed as:

$$\delta\mathbf{u}^d = \left(\frac{\partial f}{\partial \mathbf{u}^a}\right)_{\mathbf{u}^a=\mathbf{u}_0^a} \delta u^a + \left(\frac{\partial f}{\partial \mathbf{v}}\right)_{\mathbf{v}=\mathbf{v}_0} \delta\mathbf{v} + H.O.T. \tag{2.2}$$

In the equation above, $\delta\mathbf{u}^a$, $\delta\mathbf{v}$ and $\delta\mathbf{u}^d$ are the variation vectors of incoming KCs, process parameters, and output KCs, respectively. Specifically, $\delta\mathbf{u}^a = \mathbf{u}^a - \mathbf{u}_0^a$, $\delta\mathbf{v} = \mathbf{v} - \mathbf{v}_0$, $\delta\mathbf{u}^d = \mathbf{u}^d - \mathbf{u}_0^d$ and $\mathbf{u}_0^d = f(\mathbf{u}_0^a, \mathbf{v}_0)$. The two matrices, $\left(\frac{\partial f}{\partial \mathbf{u}^a}\right)_{\mathbf{u}^a=\mathbf{u}_0^a}$ and $\left(\frac{\partial f}{\partial \mathbf{v}}\right)_{\mathbf{v}=\mathbf{v}_0}$, are the sensitivity matrices of output KCs to the incoming KCs and the process parameters evaluated at $\mathbf{v}_0$ and $\mathbf{u}_0^a$, respectively. Based on Equation (2.2), the stochastic behavior of output KC variations and the yield rate can be predicted, as shown in Figure 2.2. We will discuss the calculation in two steps: before inspection and after inspection.

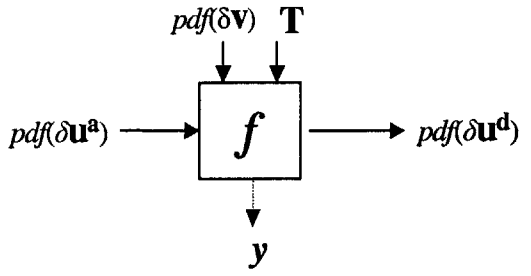

Figure 2.2: Stochastic behavior of the variation propagation in a single operation

Variation Propagation before Inspection

Letting the sensitivity matrices, $\mathbf{S}_{\mathbf{u}_0^a} = \left(\frac{\partial f}{\partial \mathbf{u}^a}\right)_{\mathbf{u}^a=\mathbf{u}_0^a}$, $\mathbf{S}_{\mathbf{v}_0} = \left(\frac{\partial f}{\partial \mathbf{v}}\right)_{\mathbf{v}=\mathbf{v}_0}$, and ignoring the high order terms in Equation (2.2), we get:

$$pdf_{\mathbf{u}_0^d}(\delta\mathbf{u}^d) = \int\int pdf_{\mathbf{v}_0}(\mathbf{S}_{\mathbf{v}_0}^{-1}\delta\mathbf{u}^d - \mathbf{S}_{\mathbf{v}_0}^{-1}\mathbf{S}_{\mathbf{u}_0^a}\delta\mathbf{u}^a)\cdot pdf_{\mathbf{u}_0^a}(\delta\mathbf{u}^a)\cdot d\mathbf{u}^a \cdot d\mathbf{v} \tag{2.3}$$

$$E(\delta\mathbf{u}^d) = \mathbf{S}_{\mathbf{u}_0^a}E(\delta\mathbf{u}^a) + \mathbf{S}_{\mathbf{v}_0}E(\delta\mathbf{v}) \tag{2.4}$$

$$Var(\delta\mathbf{u}^d) = \mathbf{S}_{\mathbf{u}_0^a}Var(\delta\mathbf{u}^a)\mathbf{S}_{\mathbf{u}_0^a}^T + \mathbf{S}_{\mathbf{v}_0}Var(\delta\mathbf{v})\mathbf{S}_{\mathbf{v}_0}^T \tag{2.5}$$

where $Var(\bullet)$ is the covariance matrix and $pdf_{\mathbf{u}_0^d}(\bullet)$ is the multivariate joint probability density function (pdf) of $\delta\mathbf{u}^d$ around $\mathbf{u}_0^d$. Similarly, $pdf_{\mathbf{v}_0}(\bullet)$ is the joint pdf of $\delta\mathbf{v}$ around $\mathbf{v}_0$, and $pdf_{\mathbf{u}_0^a}(\bullet)$ is the joint pdf of $\delta\mathbf{u}^a$ around $\mathbf{u}_0^a$.

Yield Rate Prediction

During inspection, the part will be rejected if output KC variations exceed the tolerances. Therefore, the new distribution of output KC variations after inspection is truncated and pushed up. Figure 2.3 illustrates the distribution change.

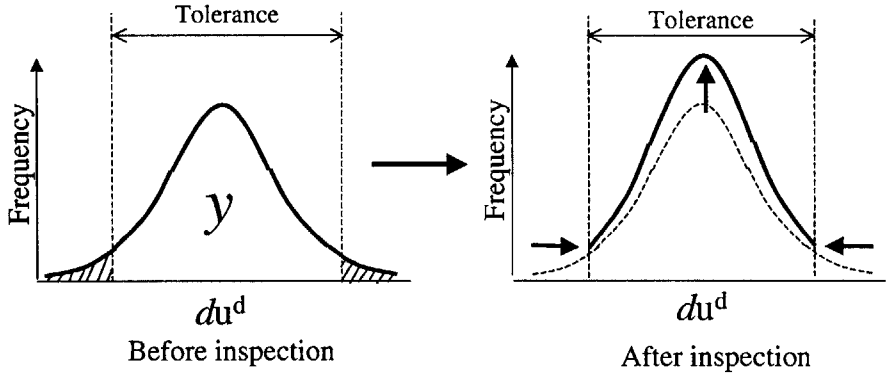

Figure 2.3: Distribution of output KCs before and after inspection

The non-shaded area under the distribution curve of $\delta\mathbf{u}^d$ before inspection is the probability of passing the inspection, *i.e.*, the production yield rate, y. In the cases where tolerance set simply contains the upper and lower bound for each of the output KC variations, it can be calculated through the following equation:

$$y = \int_{\mathbf{T}_* \le \delta\mathbf{u}^d \le \mathbf{T}^*} pdf_{\mathbf{u}_0^d}(\delta\mathbf{u}^d)\cdot d\mathbf{u}^d \tag{2.6}$$

where $pdf_{\mathbf{u}_0^d}(\delta\mathbf{u}^d)$ is obtained from Equation (2.3). In more complex cases, Monte Carlo simulation can be used to estimate the yield rate. We will illustrate the method in Chapter 3.

Variation Propagation after Inspection

If the yield rate can be calculated through Equation (2.6), the new pdf of $\mathbf{u}^d$ after inspection becomes (Chen and Thornton 1999):

$$pdf^*_{\mathbf{u}_0^d}(\delta\mathbf{u}^d)=\begin{cases}\frac{1}{y}pdf_{\mathbf{u}_0^d}(\delta\mathbf{u}^d) & , \mathbf{T}_* \le \delta\mathbf{u}^d \le \mathbf{T}^* \\ 0 & , \text{else}\end{cases} \tag{2.7}$$

With the modified joint pdf, the expected value and variance of $\delta\mathbf{u}^d$ after inspection can be calculated as follows:

$$E(\delta\mathbf{u}^d) = \int_{\mathbf{T}_* \le \delta\mathbf{u}^d \le \mathbf{T}^*} pdf^*_{\mathbf{u}_0^d}(\delta\mathbf{u}^d)\cdot d\mathbf{u}^d \tag{2.8}$$

$$Var(\delta\mathbf{u}^d) = \int_{\mathbf{T}_* \le \delta\mathbf{u}^d \le \mathbf{T}^*} \left(\delta\mathbf{u}^d - E(\delta\mathbf{u}^d)\right)^2 \cdot pdf^*_{\mathbf{u}_0^d}(\delta\mathbf{u}^d)\cdot d\mathbf{u}^d \tag{2.9}$$

Otherwise they can be obtained from the simulation result.

2.2.3 Variation Model for A System

Having deriving the variation propagation equations in a single operation, we can use that to calculate the quality performance through a manufacturing system. A typical manufacturing system contains several operations, as shown in Figure 2.4. Raw materials are processed through a series of operations, and are assembled with other parts into finished products. For example, an aircraft tube need to go through bending, trimming, painting, and swaging, then is installed onto the aircraft structure.

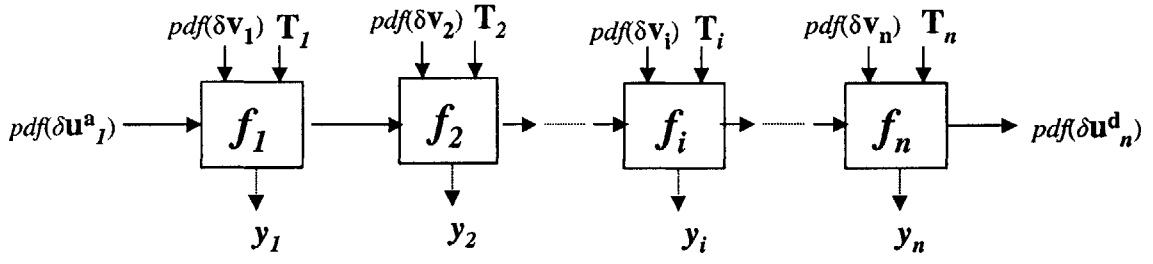

Figure 2.4: Quality performances in a manufacturing system

From Figure 2.4 it can be seen that the output KC variations at an operation become the input KC variations for the next. At each stage there is a yield rate, y_i. The ultimate output KC variations at the end of the line are $\delta \mathbf{u}_n^{\mathbf{d}}$. The variation propagation mechanism is illustrated in Figure 2.5. The output KC variations from operation i becomes the input KC variations of operation i+1, *i.e.*, $pdf^{*}_{\mathbf{u}^{\mathbf{d}}_{0i}}(\delta \mathbf{u}_i^{\mathbf{d}}) = pdf_{\mathbf{u}^{\mathbf{a}}_{0i+1}}(\delta \mathbf{u}_{i+1}^{\mathbf{a}})$. Using Equation (2.3) through (2.9) or simulation, the yield rates and pdf for the variation on output KC variations, $pdf^{*}_{\mathbf{u}^{\mathbf{d}}_{0i+1}}(\delta \mathbf{u}_{i+1}^{\mathbf{d}})$, can be calculated.

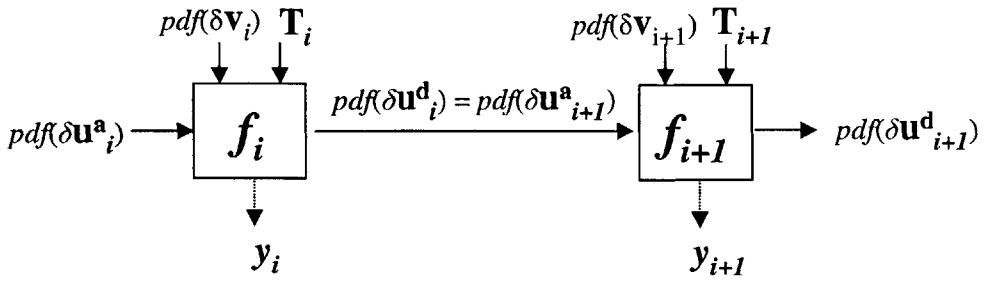

Figure 2.5: Key characteristics transfer in serial operations

By repeating the foregoing procedures, the statistical behavior of the variations on the end-of-line KC variations and the yield rate at each operation can be calculated throughout the manufacturing system.

2.2.4 Modeling Methods for Sensitivity Matrices

The procedures to model the sensitivity matrices are shown in Figure 2.6. The first step is identifying the key input (incoming KCs and process parameters) and output (output KCs) variables that are relevant in the manufacturing operation. After that, there are two ways to construct the relationship among these variables: mechanistic modeling and empirical modeling. We will discuss them in the next section.

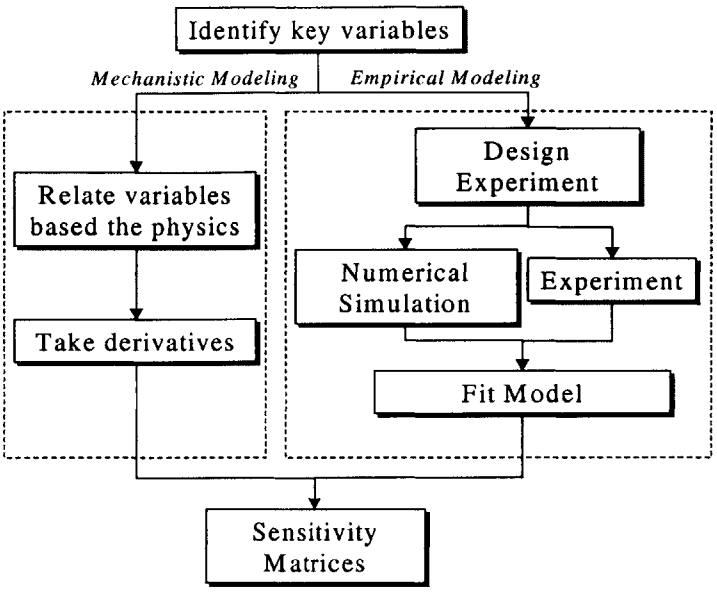

Figure 2.6: Modeling procedure of sensitivity matrices

Mechanistic Modeling

Mechanistic modeling relates the input and output variables based on the physics of the operation. Analytical closed-form expressions for the sensitivity matrices can be obtained by taking derivatives of the output variables with respect to the input variables. Mechanistic modeling usually requires deep understanding of the physics in the operation, and oftentimes needs several iterations to validate the model. The difficulty of such modeling increases significantly when the operation is complex. However, once the mechanistic model is established and validated, it is usually valid over the whole variable space rather than localized regions at the operating points. Therefore, it reduces repetitive modeling tasks that are needed by empirical models and facilitates process analysis and optimization.

Empirical Modeling

The notion of empirical modeling is to conjecture the mapping function by observing the changes in output variables corresponding to the changes in input variables. Several techniques can apply to empirical modeling, we will discuss the three most popular techniques: Design of Experiments (DoE), numerical simulation, and Response Surface Methods (RSM)

DoE is a methodology for planning and allocating the resource for experiments in empirical modeling, such as the number of experiment runs or time required. It provides a framework to reduce the total number of experiment runs and determine the combination of the predefined levels of the input variables (*factors*) for each run. For example, consider an experiment with three factors each with two levels, instead of doing 2^3 experiments for all possible combination of the factors, a 2^2 *partial-factorial* experiments

can be run to obtained the desired results. Details about DoE can be found in (DeVor *et. al.* 1992) and (Box *et. al.* 1978).

Numerical simulation methods such as Monte Carlo Simulation are often used as the surrogate when real experiments are infeasible or too expensive to conduct. In such simulation, random numbers are generated as the input variables and the statistics on the output variables are collected. These data are used to fit the conjectured model.

RSM is a multivariate regression method for model fitting. A response surface for the output variables around the region of interests are obtained by conducting experiments or simulation at some points around the region and fit the results with low-order polynomial regression. Details about RSM can be found in (Montgomery 1984).

2.3 PRODUCTION MODEL

Now that we have discussed the quality model, we will proceed to the production model for system performance prediction. The production model applies queueing theory with some approximation methods to estimate the average manufacturing cycle time (MCT) and work-in-process (WIP). Manufacturing cycle time is defined as the duration of time that a part spends in a manufacturing system. It is an important performance measure because it determines the responsiveness to customers and the inventory cost in a plant. MCT comprises several components: transport time, queueing time, and processing time. Queueing time is caused by the variability of the system, such as the randomness of the order arrivals, variability in process time and setup time, machine breakdowns, reworks, etc. We will show how these factors affect the MCT in a system in the following sections.

2.3.1 Representation

The cycle time in a workstation with N machines, or *servers*, is determined by five factors: mean arrival rate, inter-arrival variability, mean processing time, processing time variability, and number of machines. In addition, the variability of inter-arrival time and processing time propagate into the variability of inter-departure time, which is determined by these five factors. Figure 2.7 illustrates the scheme. Note that the mean departure rate is the minimum of the mean arrival rate and the mean service rate (N/t^*). In order to maintain a stable system, the total mean service rate must be larger than the mean arrival rate, *i.e.*, $\frac{N}{t^*} > \lambda^*$, otherwise the arrivals will keep queueing up. We use the squared coefficient of variation (SCV) to characterize the variability. SCV is defined as the ratio of variance to the squared mean of the time between to events. For example, let A be the inter-arrival time of a customer, then the SCV of A is calculated by $SCV(A) = \frac{Var(A)}{E^2(A)}$.

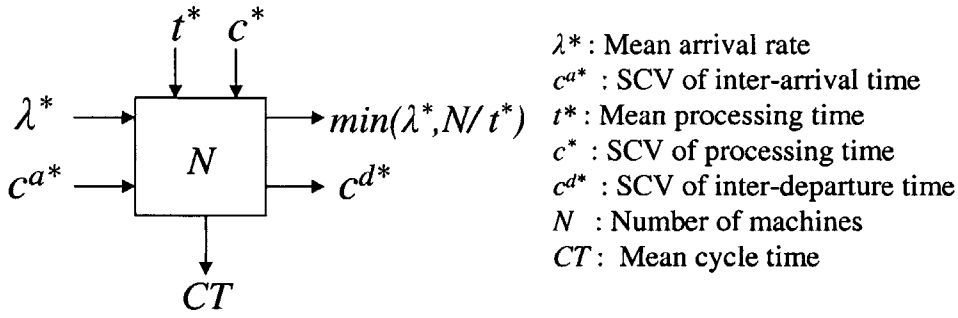

Figure 2.7: Schematic representation of queueing behavior in a single operation

The means and SCV of inter-arrival and processing time are determined by many other factors, such as part mix, batch-sizes, yield rates, machine failures, etc. We will illustrate the calculation below.

2.3.2 Queueing Model for A Flow Line System

Consider a flow line manufacturing system consisting of n workstations, each with N_j machines ($1 \leq j \leq n$), and there is an infinite buffer between any two consecutive workstations. The machines in workstation j have the same mean time to failure, m_j^f, and mean time to repair, m_j^r. The system makes m types of parts and all parts go through every workstation in the system without skipping. Part type i ($1 \leq i \leq m$) has a mean demand rate of d_i, and arrives in batches randomly with predetermined batch-size Q_i, and a SCV for its batch arrival, c_i^a. Each batch of part i is processed on one machine in the workstation j with mean setup time, s_{ij}, mean single-part process time, t_{ij}, and mean yield rate y_{ij}. The average cycle time for a batch of any part type spending in workstation j is CT_j. Assume that the product-mix and the system resource do not change over time, and the system has been producing the products for a long time thus is in steady-state. In order to calculate the means and SCV of the inter-arrival and processing time at each workstation, we need to aggregate the arrivals and processing of all part types. The model is described below, where the notations are summarized in the nomenclature section.

Arrival Aggregation

The batch arrival rate of a part type is its demand divided by the average batch-size arriving at the first workstation, and adjusted by the overall yield rate to fulfill the demand. Namely,

$$\lambda_i = \frac{d_i}{Y_i Q_{i1}} \tag{2.10}$$

The aggregated batch arrival rate at the first workstation is the sum of the batch arrival rates of all part types, *i.e.*,

$$\lambda_1^* = \sum_{i=1}^{m} \lambda_i \tag{2.11}$$

Assuming the mean batch arrival rates for all part types are of the same order of magnitude, the SCV of aggregated inter-arrival time at the first workstation can be approximated by the weighted average of the SCV of batch inter-arrival time of all part types (Herrmann and Chincholkar 2000):

$$c_1^{a*} = \frac{\sum_{i=1}^{m} \lambda_i c_i^a}{\sum_{i=1}^{m} \lambda_i} \tag{2.12}$$

The SCV of inter-arrival time for individual part, c_i^a, is either estimated directly from the demand data for the plant, or derived form the demand data in the downstream supply chain if the ordering mechanism is known. For example, if a manufacturing plant produces parts to replenish the inventory of its customer with known ordering policy (*e.g.*, reordering point), the SCV of inter-arrival time for the parts can be derived from the customer's demand information. We will discuss it with an example in Section 3.3.2.

Validation

The approximation for the mean and SCV of the aggregated inter-arrival time is validated by the simulation method, as shown in Figure 2.8. The scenario for (a) is that three types of parts arrive with the same mean inter-arrival times of 1 and SCVs ranging from 0.2 to 2. The scenario for (b) is that three types of parts arrive with the same mean inter-arrival times of 1 but different SCVs. One of the part type has a SCV of 1 and the other two have higher and lower SCVs with the same discrepancy. This discrepancy rages from 0 to 0.9. For example, the SCVs for the three part types can be (0.5, 1, 1.5), (0.7, 1, 1.3), etc. The scenario for (c) is that three types of parts arrive with the same SCVs of inter-arrival times of 1 and means ranging from 0.2 to 2. The scenario for (d) is that three types of parts arrive with the same SCVs of inter-arrival times of 1 but different means. One of the part type has a mean of 1 and the other two have higher and lower means with the same discrepancy. This discrepancy rages from 0 to 0.9. In the simulation, the inter-arrival times are generated from Gamma distribution.

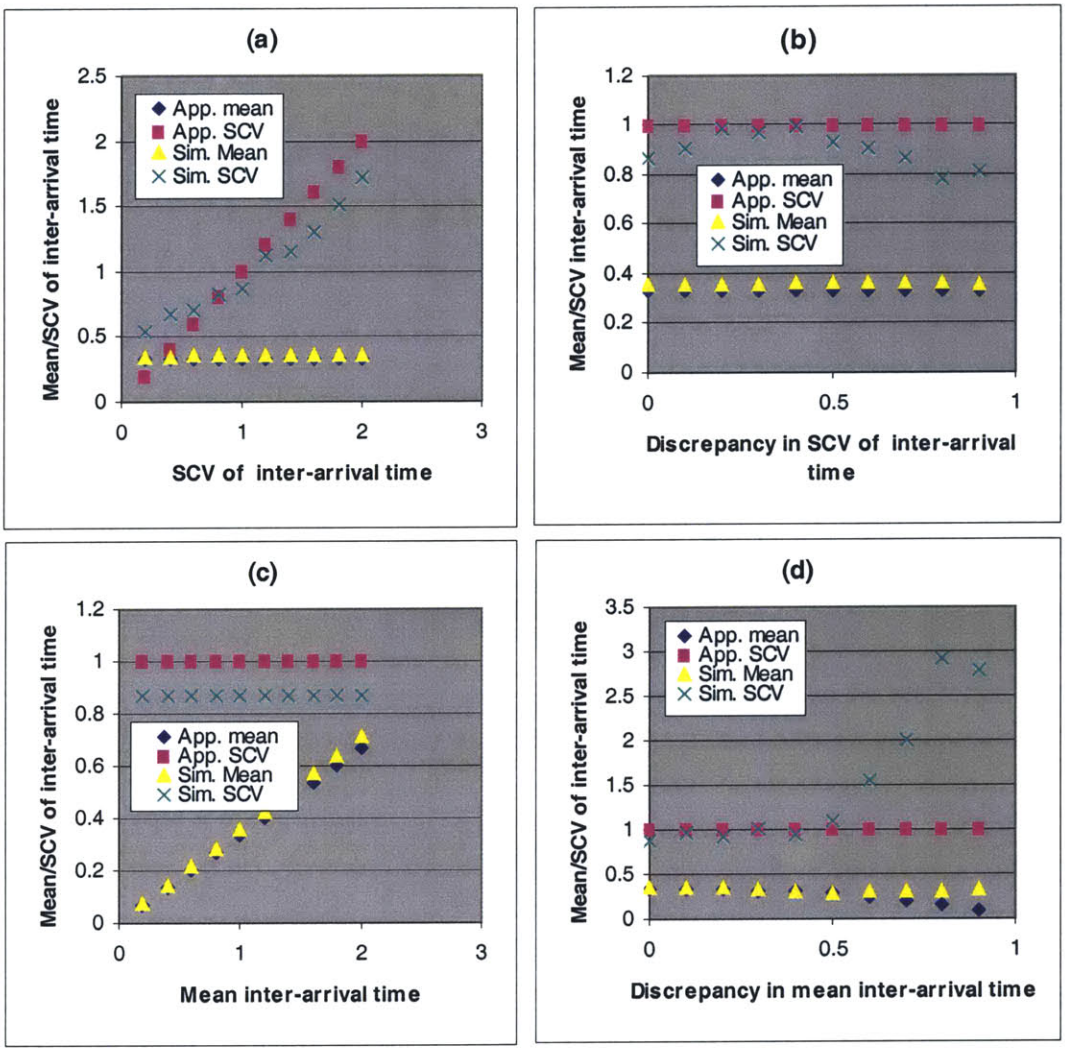

Figure 2.8: Simulation and approximation results for the mean and SCV of the aggregated inter-arrival time

It can be seen that the approximation for the aggregated mean inter-arrival times are good in all scenarios. The approximation for the aggregated SCV is good as the individual SCVs approach 1 (become closer to exponential) and the individual mean inter-arrival times have less discrepancies. It is also noteworthy that the SCV approximation becomes unreliable as the individual arrival rates become highly heterogeneous (large discrepancies in the mean inter-arrival times), as shown in Figure 2.8(d).

Processing Time Aggregation

There are four steps in the processing time aggregation: First, deriving the mean and the variability of the arriving quantity for individual parts. Second, calculating the mean and variability of the batch processing time for individual parts. Third, aggregating the

mean and variability of the processing time in the workstation. Fourth, adjusting for machine failure or downtime.

Arriving Quantity

Due to the yield loss through the previous workstations, the actual number of parts in the arrived batch is smaller than the original batch-size, Q_{i1}. Assuming at each workstation, each part in a batch has the same probability of y_{ij} to be rejected, then the number of parts proceeding to the next workstation without being rejected can be assumed to have a binomial distribution.

For $j > 1$, the average arriving quantity at workstation j equals

$$Q_{ij} = E(\tilde{Q}_{ij}) = Q_{i1}Y_{ij-1} \tag{2.13}$$

The variance can be calculated by conditional expectation:

$$\begin{aligned} Var(\tilde{Q}_{ij}) &= EE(\tilde{Q}_{ij}^2 \mid \tilde{Q}_{ij-1}) - E^2E(\tilde{Q}_{ij} \mid \tilde{Q}_{ij-1}) \\ &= E\left(\tilde{Q}_{ij-1}y_{ij-1}\left(1-y_{ij-1}\right) + \left(\tilde{Q}_{ij-1}y_{ij-1}\right)^2\right) - E^2(\tilde{Q}_{ij-1}y_{ij-1}) \\ &= y_{ij-1}\left(1-y_{ij-1}\right)E(\tilde{Q}_{ij-1}) + y_{ij-1}^2 Var(\tilde{Q}_{ij-1}) \end{aligned} \tag{2.14}$$

Plug Equation (2.13) into Equation (2.14) and expand the last term on the right hand side, we have

$$\begin{aligned} Var(\tilde{Q}_{ij}) &= Q_{i1}Y_{ij-1}\left(1-y_{ij-1}\right) + y_{ij-1}^2 Var(\tilde{Q}_{ij-1}) \\ &= Q_{i1}Y_{ij-1}\left(1-y_{ij-1}\right) + y_{ij-1}^2 Q_{i1}Y_{ij-2}\left(1-y_{ij-2}\right) + y_{ij-2}^2 Var(\tilde{Q}_{ij-2}) \\ &= Q_{i1}Y_{ij-1}\left(1-y_{ij-1}+y_{ij-1}-y_{ij-1}y_{ij-2}\right) + y_{ij-2}^2 Var(\tilde{Q}_{ij-2}) \\ &= Q_{i1}Y_{ij-1}\left(1-y_{ij-1}y_{ij-2}\right) + y_{ij-2}^2 Var(\tilde{Q}_{ij-2}) \end{aligned} \tag{2.15}$$

By further expansion and manipulation, equation (2.14) can be expressed as

$$Var(\tilde{Q}_{ij}) = Q_{i1}Y_{ij-1}\left(1-Y_{ij-1}\right) + Y_{ij-1}^2 Q_{i1}^2 c_{i1}^Q \tag{2.16}$$

From Equation (2.13) and (2.16), it can be seen that the multi-stage binomial process is equivalent to a single-stage binomial process with the probability that is the product of the probabilities in all stages. Divide both sides of Equation (2.16) by Q_{ij}^2, we get

$$c_{ij}^Q = \frac{1-Y_{ij-1}}{Q_{i1}Y_{ij-1}} + c_{i1}^Q \tag{2.17}$$

From the Equation (2.13) and (2.17), it can be seen that the average quantity decreases and quantity variability increases through the line due to the yield loss at each

stage. In addition, any decreases in the upstream yield rates will not only decrease the quantity, but also increase the quantity variability in the downstream stages.

Batch Processing Time

The mean batch process time is the sum of the mean batch setup time and the mean total processing time. The mean total processing time is the mean single-part processing time multiplied by the mean number of parts in the arrived batch, *i.e.*,

$$t_{ij}^{b} = s_{ij} + Q_{ij} t_{ij} \tag{2.18}$$

Assuming the batch setup time and single-part process time are independent, the variance of batch processing time is the sum of the variance of setup time and total processing time. The variance of total processing time is contributed by the variance in single-part processing time and the variance in the arrived batch-size[5]. Hence,

$$\left(t_{ij}^{b}\right)^2 c_{ij}^{b} = \left(s_{ij}\right)^2 c_{ij}^{s} + Q_{ij}\left(t_{ij}\right)^2 c_{ij} + \left(t_{ij}\right)^2 Q_{ij}^2 c_{ij}^{Q} \tag{2.19}$$

Manipulating the equation above, we can get

$$c_{ij}^{b} = \left(\frac{s_{ij}}{t_{ij}^{b}}\right)^2 c_{ij}^{s} + \left(\frac{t_{ij}}{t_{ij}^{b}}\right)^2 \left(Q_{ij} c_{ij} + Q_{ij}^2 c_{ij}^{Q}\right) \tag{2.20}$$

Aggregation

The aggregated mean processing time at the workstation is the weighted average of the mean batch processing time of all part types. The weighted average of each part type is assessed by its arrival rate over the aggregated arrival rate, which is the probability that the part type is found at the workstation. Therefore, the first and second moments of $\tilde{t}_j$ are

$$t_j = E\left(\tilde{t}_j\right) = \frac{\sum_{i=1}^{m} \lambda_i E\left(\tilde{t}_{ij}^{b}\right)}{\sum_{i=1}^{m} \lambda_i} \tag{2.21}$$

$$E\left(\left(\tilde{t}_j\right)^2\right) = \frac{\sum_{i=1}^{m} \lambda_i E\left(\left(\tilde{t}_{ij}^{b}\right)^2\right)}{\sum_{i=1}^{m} \lambda_i} \tag{2.22}$$

[5] Let X_i (i=1, 2, ...) be independent-and-identically distributed random variables, then the variance of the sum of a random number of X_i, $Y=(X_1+ X_2+\ldots,+X_n)$, is calculated by $Var(Y)=EE(Y^2|n)-E^2E(Y|n)= E(n)Var(X_i)+E(n^2)E^2(X_i))-E^2(n)E^2(X_i) =E(n)Var(X_i)+E^2(X_i)Var(n)$.

Equation (2.22) can be rewritten as

$$Var\left(\tilde{t}_j\right)+\left(t_j\right)^2=\frac{\sum_{i=1}^{m}\lambda_i\left(Var\left(\tilde{t}_{ij}^b\right)+\left(t_{ij}^b\right)^2\right)}{\sum_{i=1}^{m}\lambda_i} \tag{2.23}$$

Dividing both sides in by $\left(t_j\right)^2$ and manipulating the terms in Equation (2.23), we can get

$$c_j=\frac{\sum_{i=1}^{m}\lambda_i\left(t_{ij}^b\right)^2\left(c_{ij}^b+1\right)}{\left(t_j\right)^2\sum_{i=1}^{m}\lambda_i}-1 \tag{2.24}$$

Downtime Adjustment

Equation (2.24) gives the SCV of aggregated processing time at the workstation without considering machine unavailability. However, due to the machine failures or downtime (*e.g.*, scheduled maintenance), the actual processing time will take longer thus needs to be adjusted. The percentage of time that a workstation is available is

$$a_j=\frac{m_j^f}{m_j^f+m_j^r} \tag{2.25}$$

The adjusted mean aggregated time and SCV of aggregated time become

$$t_j^*=\frac{t_j}{a_j} \tag{2.26}$$

$$c_j^*=c_j+2a_j(1-a_j)\frac{m_j^r}{t_j} \tag{2.27}$$

Flow Variability Propagation and Cycle Time Calculation

There are four factors determining the variability of the inter-departure time and the cycle time: workstation utilization, number of machines, variability of the aggregated inter-arrival time, and variability of the aggregated processing time.

Workstation Utilization

The average utilization rate at a workstation is the percentage of time that it is busy. It is calculated by the following equation:

$$u_j^* = \frac{\lambda_j^* t_j^*}{N_j} \tag{2.28}$$

Approximation for Flow Variability Propagation

Assuming that the system is stable (*i.e.*, $u_j^* < 1$ for all j), then the departure rate at each workstation equals the arrival rate because of the flow conservation. Namely,

$$\lambda_j^* = \lambda_1^*, \; 2 \le j \le n \tag{2.29}$$

The variability of inter-departure time at each workstation is propagated from the variability of inter-arrival and processing time. It can be approximated by the following equation (Herrmann and Chincholkar 2000):

$$c_j^{d*} = 1 + \left(1 - \left(u_j^*\right)^2\right)\left(c_j^{a*} - 1\right) + \frac{\left(u_j^*\right)^2}{\sqrt{N_j}}\left(c_j^* - 1\right) \tag{2.30}$$

The equation above indicates that when the workstation utilization is high, the inter-departure time variability is dominated by the processing time variability. Since there is no workstation blocking because of the infinite buffers, the inter-departure time variability from upstream workstation transfers to the inter-arrival time variability of downstream workstation, *i.e.*,

$$c_{j-1}^{d*} = c_j^{a*}, \; 2 \le j \le n \tag{2.31}$$

Approximation for Cycle Time Calculation

With all the information about λ_j^*, c_j^{a*}, t_j^*, and c_j^* through the manufacturing system, we can use them to calculate the cycle time at each workstation. Assuming the workstation utilization is high, the mean cycle time can be approximated by the GI/G/*N* queueing model through the following equation (Hopp and Spearman 1996):

$$CT_j = \left(\frac{c_j^{a*} + c_j^*}{2}\right)\frac{\left(u_j^*\right)^{\left(\sqrt{2(N_j+1)}-1\right)}}{N_j\left(1-u_j^*\right)} t_j^* + t_j^* \tag{2.32}$$

The first term on the right hand side of Equation (2.32) is the approximated queueing time. It can be seen that the queueing time is composed of three factors: variability, utilization, and processing time. The queueing time increases linearly with the sum of arrival and processing SCV, as well as the processing time. In addition, the queueing time increases non-linearly and approaches infinity as the workstation utilization approaches

one, which indicates the system instability. The mean system cycle time is the sum of the workstation cycle time:

$$CT = \sum_{j=1}^{n} CT_j \tag{2.33}$$

It can be seen from Equation (2.30) that the variability of inter-arrival time and processing time from the upstream workstations propagates to the downstream workstations and determined the cycle time at each stage. Figure 2.9 illustrates this propagation process.

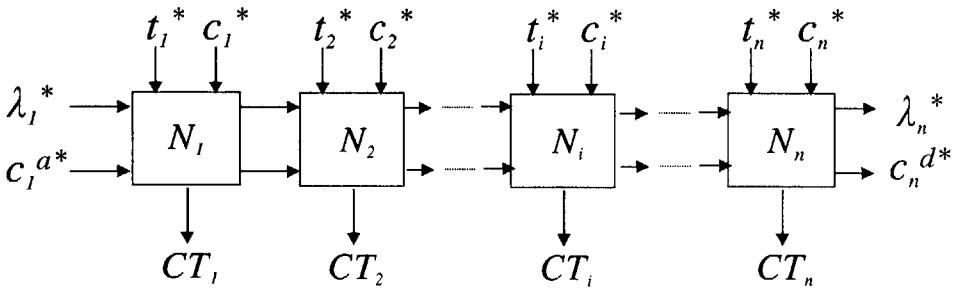

Figure 2.9: Flow variability propagation and cycle time in a manufacturing system

Validation

The results from the approximation method are compared against the simulation results, as shown in Figure 2.10. In the simulation setting, the inter-arrival times are generated from Gamma distribution, and the mean and SCV of the aggregated processing time are 25 and 0.36, respectively. It can be seen from Figure 2.10 (a) that the average cycle time increases sharply as the workstation utilization approaches one. The approximation for the average cycle time is close to the simulation results, with the error margins less than 10%. The error increases as the utilization rate and the SCV of the aggregated inter-arrival time increase. From Figure 2.10 (b) it can be seen that the SCV of the inter-departure time approaches the SCV of the aggregated batch processing time as the workstation utilization approaches one, and the error margins between the approximation and simulation methods range from 10% to 30%. This implies that it will cause 5% to 15% of error for the average cycle time approximation in the downstream workstation.

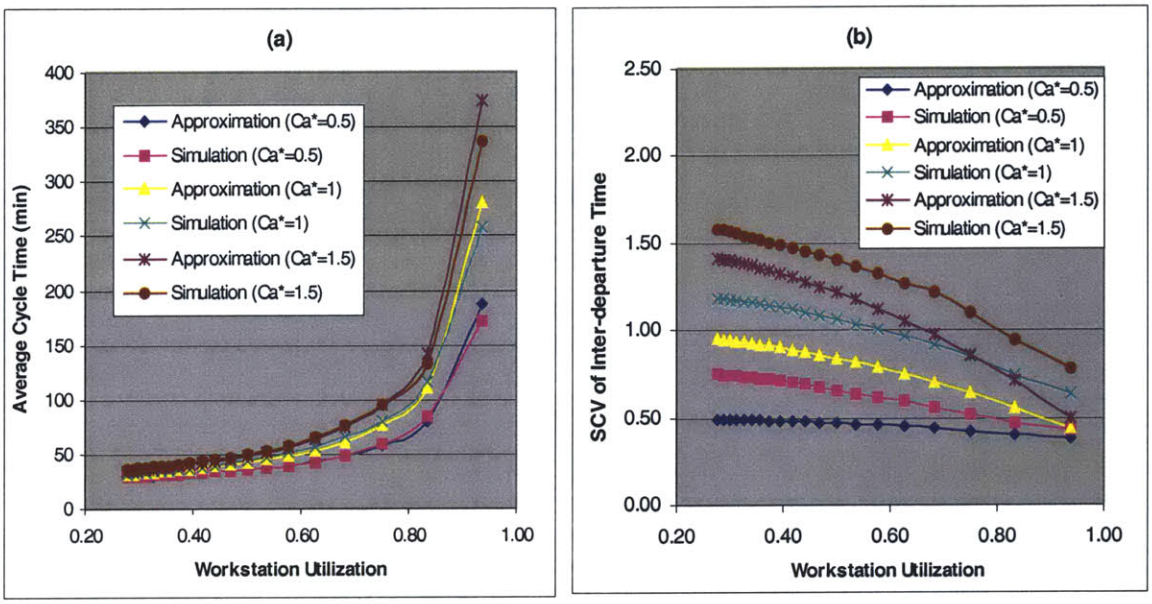

Figure 2.10: Simulation and approximation results for (a) the average cycle time and (b) SCV of the inter-departure time

Work-in-Process

According to Little's Law, the average work-in-process (WIP) is the product of mean arrival rate and the mean cycle time in the system. The mean arrival rate of a part-type at a workstation is the mean batch arrival rate multiplied by the mean batch-size at the workstation. Therefore, from Equation (2.10) and (2.13), the average WIP for a part type at a workstation can be expressed as:

$$WIP_{ij} = \lambda_i \cdot Q_{ij} \cdot CT_j = \frac{d_i}{Y_i Q_{i1}} Q_{i1} \left(\prod_{k=1}^{j-1} y_{ik} \right) CT_j = \frac{d_i}{\prod_{k=j}^{n} y_{ik}} CT_j \tag{2.34}$$

The total WIP of a part-type in the system is the sum of WIP at all workstations:

$$WIP_i = \sum_{j=1}^{n} WIP_{ij} \tag{2.35}$$

2.4 COST PREDICTION

There are three categories of costs incurred during the production. The first is the quality cost due to yield loss, the second is the inventory cost of work-in-process, and the third is the operation cost for machine and labor hours. The calculation for these costs is discuss as follows.

2.4.1 Total Cost

The quality cost of a batch of part type i at workstation j is the product of unit scrap cost multiplied by the expected quantity loss. The quality cost per unit time of part type i is the scrap cost per batch multiplied by the batch arrival rate, *i.e.*,

$$TC^S = \sum_{i=1}^{m}\sum_{j=1}^{n} CS_{ij}\lambda_i Q_{i1}\left(\prod_{k=1}^{j-1} y_{ik}\right)\left(1-y_{ij}\right) \tag{2.36}$$

The total inventory cost is the sum of all WIP costs, *i.e.*,

$$TC^I = \sum_{i=1}^{m}\sum_{j=1}^{n} CI_{ij}WIP_{ij} \tag{2.37}$$

The operation cost of a machine at a workstation is the machine and labor cost per unit time multiplied by the portion of time that the machine is busy, *i.e.*, the utilization rate. Therefore, the total operation cost is calculated by

$$TC^O = \sum_{j=1}^{n} CO_j N_j u_j^* = \sum_{j=1}^{n} CO_j \lambda_j^* t_j^* \tag{2.38}$$

Finally, the total cost in a system is the sum of the three costs, namely,

$$TC = TC^S + TC^I + TC^O \tag{2.39}$$

2.5 JOINT SYSTEM PERFORMANCE MODEL

Having derived the quality and queueing models for a manufacturing system in the previous sections, we can combine them to investigate the interaction between quality performance and the queueing behavior of the system. Figure 2.11 shows the schematic representation of the Joint System Performance Model (JSPM), in which the quality model and queueing model are linked by the yield rates. In this model, the process and part variations in the production of a part type propagate through the system and lead to the yield rates at all stages as described in Equation (2.3) to (2.9). These yield rates in turn influence the arrival and service processes of the workstation, and thus the manufacturing cycle time and WIP of all other part types in the system. It can be seen from Equation (2.10) to (2.12) that a low overall yield rate of a part type will either increase the aggregated arrival rate and arrival variability or require a larger batch size. In either case, the aggregated processing time and service variability will also increase due to the higher relative arrival rate or the larger batch size of the part type, as described from Equation (2.13) to (2.24). As a result, the manufacturing cycle time and WIP of all part type will increase, as it can be seen in Equation (2.30) and (2.34).

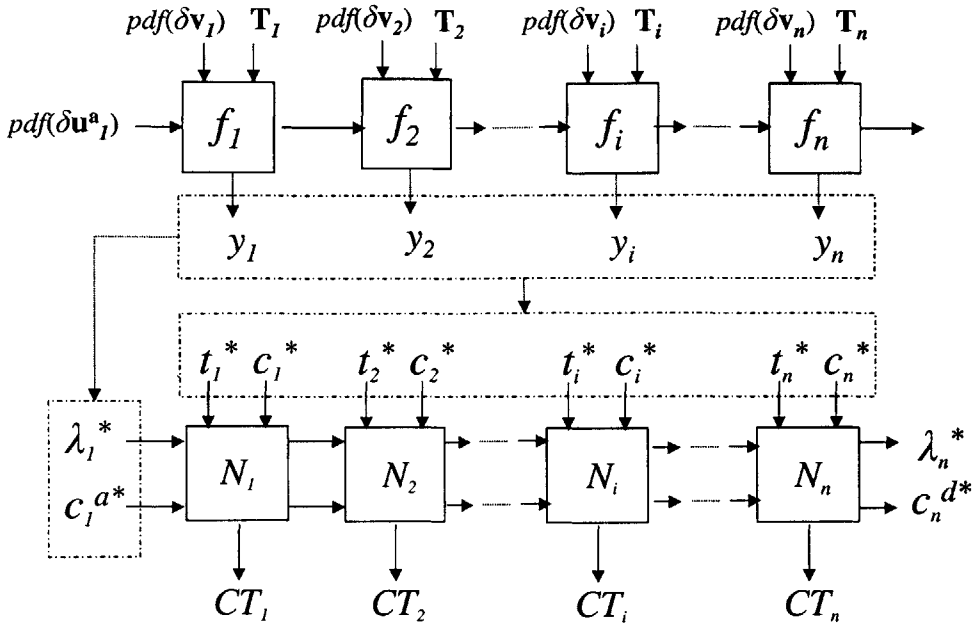

Figure 2.11: Schematic representation of Joint System Performance Model

The JSPM provides an integrated framework to optimize the system performances through the following three ways: robust design, tolerancing, and batch-sizing. We call this optimization methodology for system performances Concurrent Optimal Design (COD) and discuss it in the following section.

2.6 CONCURRENT OPTIMAL DESIGN

The notion of COD is to minimize the total system cost during the production of a part type through concurrent design of part, tolerance, and batch-sizes, so that the system is robust to the process and flow variability. Traditionally, the three aforementioned tasks are treated independently. However, it can be seen from JSPM that they are interrelated. Treating them separately to optimizing the system performances will only result in a local optimal solution. In light of this, COD seeks to achieve the global optimal solution by treating them concurrently through the JSPM.

2.6.1 Design Variables

There are three design variables in COD: part design, tolerances, and batch-sizes, which are discussed in details below.

Part Design

Part design determines the variation sensitivity at each stage of the production, therefore it influences the output KC variations and yield rate. In many cases, the variation sensitivities cannot always be minimized simultaneously and tradeoffs need to be made. Traditional robust design methodologies seek to minimize the end-of-line variations or quality cost due to yield loss. However, as mentioned previously, the

process and part variations in the production of a part type will propagate into the production flow variability thus deteriorate the cycle time and WIP performances of all parts produced in the system. As the objective of traditional robust design methodologies, minimizing the end-of-line variations or quality cost does not always guarantee the minimum cost in the system when the system performances are converted into costs as described in Equation (2.36) to (2.38). In COD, a part design is mapped into the variation sensitivities at all stages of production and evaluated based on JSPM.

Tolerances

The part design determines the variation sensitivities thus the KC variations before inspection at each operation, and the decision on inspection and tolerancing determine the yield rates at the immediate and downstream stages. In general, loose tolerancing makes a high yield rate at the stage but also worsens the downstream yield rates because larger KC variations are passed down. Therefore, there are tradeoffs between upstream and downstream yield rates in tolerancing. The decision of whether to perform inspection or not at a stage is similar to tolerancing, since no inspection is equivalent to infinitely wide tolerance.

Batch-sizes

The decision on the batch sizes for all part types will influence the cycle time and consequently the WIP performances. In general, a large batch size increases the waiting time of the parts in a batch, while a small batch size increases the setups, which in turn increase the flow congestion that leads to longer cycle time. Batch sizes can be chosen to optimize the system performances for a system setting, including arrival rates, yield rates, setup time, processing time, etc. Therefore, there is a corresponding set of optimal batch sizes for any combination of part design and tolerancing decision that determines the yield rates.

2.6.2 Procedure and Formulation

The procedures of COD is described as follows:

- Determine the design parameters for a part type
- Explore all possible designs under the design constraints and functionality requirements
- For each design, derive the sensitivity functions to input KC variation and process variation at each stage
- Determine key characteristics to inspect
- Allocate tentative tolerances on the key characteristics
- Assign a tentative batch-size for the part type
- Start the optimization iterations and use the JSPM to evaluate the total cost for each iteration
- Select the part design, tolerances, and batch-sizes that minimize the total cost

The optimization formulation for COD is as follows:

$$
\begin{aligned}
&\underset{\mathbf{D}_i,\mathbf{T}_i,\mathbf{Q}}{Minimize} \quad TC \\
&S.T. \quad 0 < y_{ij} \le 1 \\
&\qquad 0 < u_j < 1 \\
&\qquad Q_i \in \{1,2,\cdots\} \\
&\qquad for \quad 1 \le i \le m, 1 \le j \le n
\end{aligned}
$$

where $\mathbf{D}_i = (D_{i1}, D_{i2}, \cdots, D_{ik})$ is the design parameter vector for part type i, $\mathbf{T}_i$ is the tolerance set as described in Section 2.2.1, and $\mathbf{Q} = (Q_1, Q_2, \cdots, Q_m)$ is the batch-size vector that contains the batch-sizes for all part types produced in the system. The relationship among TC, $\mathbf{D}_i$, $\mathbf{T}_i$, and $\mathbf{Q}$ can be constructed through JSPM.

2.7 CHAPTER SUMMARY

This chapter depicts the theoretical foundations for modeling system performances in quality, manufacturing cycle time, work-in-process, and costs. The Joint System Performance Model is introduced for the simultaneous evaluation and optimization of the system performances. Based on the model, the Concurrent Optimal Design methodology is formulated for optimal part design, tolerancing, and batch-sizing that minimize the system cost under the process and flow variability.

CHAPTER 3 QUALITY PREDICTION FOR AIRCRAFT TUBE DESIGN

3.1 INTRODUCTION

In this chapter we derive the quality performance model for tube production system. We focus on the quality issues related to the tube bending and assembly operations, rather than the material problems occurring in the finishing operations. Mechanistic modeling techniques are used to model the process mapping functions in tube bending and assembly operations. We first summarize the approach adopted and the advantages. Secondly, we describe the model representation. Thirdly, we derive the variation propagation equations for tube bending and assembly. Lastly, we demonstrate two approaches for yield rates prediction: simulation method and Gaussian approximation.

3.2 SUMMARY OF APPROACH

Monte Carlo Simulation (MCS) plus FEM are often the *de facto* variation modeling approach for compliant parts. However, such approach is very computational intensive (Liu and Hu 1997), thus is infeasible for high-variety part design. For instance, in a typical aircraft there are thousands of unique tubes. In order to obtain meaningful statistical data, it would be necessary to model and simulate each design numerous times. Given the large number of parts, using simulation and FEM packages will be too time-consuming and expensive. The proposed approach uses mechanistic models when feasible thus minimizes the dependency on simulation and FEM. The only need for simulation is the modeling for gauge inspection after the bending operation.

The proposed method is summarized as follows:

1. Represent the geometry of a tube design by its process plan instead of the CAD model.
2. Use linearized homogeneous matrix transforms to model the sensitivity matrices in tube bending operation.
3. Derive the sensitivity matrices for compliant-part assembly from the stiffness matrices of tube and mating structure.
4. Calculate the characteristic stiffness matrix through matrix operations. Because the tube geometry is a series of straight and circular sections, its stiffness matrix can be calculated through composing the section stiffness matrices on a tube. Such matrices can be obtained from an engineering handbook.
5. Calculate yield rates in the tube bending and assembly operations through simulation with numerical method, or Gaussian approximation.

The advantage of this method is that it only needs the digital definition of the tube (*i.e.*, the process plan) as the input instead of CAD/FEM models. As a result, only one of simulation is required for the yield rates prediction thus the modeling and computational efforts are minimized. These models are programmed in MS Excel. The CPU time for geometry and compliance computation is 5 seconds and 20 minutes for the yield rates simulation with a Pentium II 300 MHZ processor with 128M RAM.

3.3 MODEL REPRESENTATION

Figure 3.1 illustrates the model for quality performances. This model assumes small variations and uses linear approximation. It contains three stages: tube bending, inspection, and assembly. In the tube bending stage, **U** and **V** are the variation vectors on the incoming tube and process, respectively. **X** is the geometric variation vector of output tube. $\mathbf{S_1}$ and $\mathbf{S_2}$ are the sensitivity matrices that map **U** and **V** to **X**. $\mathbf{S_1}$ and $\mathbf{S_2}$ are determined by the geometry of the tube, and is derived in Section 3.4.3. If there are n features (install points) on the output tube for assembly, then [6] $\mathbf{X}=(\mathbf{X}_1,\mathbf{X}_2,\cdots,\mathbf{X}_n)^T$. Similarly, $\mathbf{U}=(\mathbf{U}_1,\mathbf{U}_2,\cdots,\mathbf{U}_l)^T$ contains variation vectors at the l features (bends) on the part that will be processed, and $\mathbf{V}=(\mathbf{V}_1,\mathbf{V}_2,\cdots,\mathbf{V}_m)^T$ includes variation vectors in the m operations (bend cycles) that need to be performed in the tube bending stage. Since the tube and process variation vectors are geometric, each component of the variation vectors has six degrees-of-freedom.

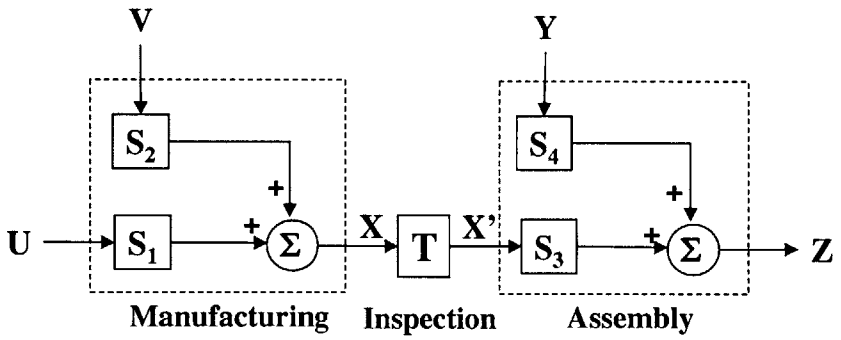

Figure 3.1: Variation model for compliant part manufacturing and assembly

In the inspection stage, **T** is the tolerance set that defines the admissible range of **X**. **X'** is the output variation vector after inspection, such that

$$\mathbf{X}' = \{\mathbf{X} \mid \mathbf{T}_* < \mathbf{X} < \mathbf{T}^*\}$$

where $\mathbf{T}_*$ and $\mathbf{T}^*$ are the lower and upper specification limits. Note that **X'** has the same dimension as **X**. In the assembly stage, **Y** is the geometric variation vector on the mating part. **Z** is the output KCV and can be the geometric variation or assembly load. $\mathbf{S_3}$ and $\mathbf{S_4}$ are the sensitivity matrices that map **X'** and **Y** to **Z**, and can be calculated from the

[6] $\mathbf{X}_i=(dx_i,dy_i,dz_i,\delta x_i,\delta y_i,\delta z_i)^T$, including the three translational and three rotational variations on the i^{th} feature.

stiffness matrices[7] of the incoming part from manufacturing and the mating part, $\mathbf{K_1}$ and $\mathbf{K_2}$, respectively. Since the numbers of features (install points) on the mating parts are equal, the dimensions of **X'**, **Y** and **Z** are the same. Specifically, $\mathbf{Y}=(\mathbf{Y}_1,\mathbf{Y}_2,\cdots,\mathbf{Y}_n)^T$ and $\mathbf{Z}=(\mathbf{Z}_1,\mathbf{Z}_2,\cdots,\mathbf{Z}_n)^T$. The values of **X'**, **Y** and **Z** are measured from the same nominal positions and orientations of all features on the final assembled part.

The dimensions of $\mathbf{K_1}$ and $\mathbf{K_2}$ are $(6n*6n)$ for n mating features. Three methods can be applied to model the stiffness matrix (Chang 1996): For parts with simple geometry such as beams, blocks, and rings, it can be obtained by solving the set of differential equations of equilibrium. For parts that can be dissected and approximated by elements with simple geometry, it can be calculated directly through matrix operations on the stiffness matrices of its components. For parts with complex geometry, it can be modeled by FEM. In Section 3.4.5, we will introduce a direct calculation method through matrix operations.

3.3.1 Variation Propagation

Two equations can be derived from the model that describe the full variation propagation process from manufacturing to assembly:

$$\mathbf{X} = \mathbf{S_1}\mathbf{U} + \mathbf{S_2}\mathbf{V} \tag{3.1}$$

$$\mathbf{Z} = \mathbf{S_3}\mathbf{X}' + \mathbf{S_4}\mathbf{Y} \tag{3.2}$$

The adjacency of matrices indicates matrix multiplication. Equation (3.1) and (3.2) indicate the variation of output part as the sum of the effects by the manufacturing and assembly process and incoming part variations. The derivation of $\mathbf{S_1}$, $\mathbf{S_2}$, $\mathbf{S_3}$ and $\mathbf{S_4}$ is demonstrated in the next section.

3.4 VARIATION SENSITIVITY FUNCTIONS

In this section we derive the detailed model for tube bending and assembly operations. We first describe the methods used by industry, in which tubes are described in terms of bend plans sent to the tube bender. Secondly, we describe how this plan can be used to describe the 3-D geometry of the tube. Then based on the 3-D geometry model, we present the mathematical models for geometric variation and the characteristic compliance of tubes for the variation sensitivity matrices. Lastly, we introduce methods that incorporate these models to predict the yield rates.

---

[7] The stiffness matrix is symmetric and independent of the assembly process according to Betti's reciprocal theorem. It has the following format: $\mathbf{K} = \begin{pmatrix} \mathbf{K}_{1,1} & \mathbf{K}_{1,2} & & \leftarrow & \mathbf{0} \\ \mathbf{K}_{2,1} & \mathbf{K}_{2,2} & \mathbf{K}_{2,3} & & \downarrow \\ & \mathbf{K}_{3,2} & \mathbf{K}_{3,3} & & \\ \uparrow & & & \ddots & \mathbf{K}_{n-1,n} \\ \mathbf{0} & \rightarrow & & \mathbf{K}_{n,n-1} & \mathbf{K}_{n,n} \end{pmatrix}$, where $\mathbf{K_{i,j}}$ linearly maps the generalized displacement $\mathbf{X}_j = (dx_j, dy_j, dz_j, \delta x_j, \delta y_j, \delta z_j)$ at feature j to the generalized force $\mathbf{F}_i = (F_{i,x}, F_{i,y}, F_{i,z}, M_{i,x}, M_{i,y}, M_{i,z})$ at feature i, so that $\mathbf{F}_i = \mathbf{K}_{i,j} * \mathbf{X'}_j$.

3.4.1 Model for Tube Bending Operation

Tubes are built through a cold forming operation. This operation is a single-machine-multi-cycle tube bending that transforms straight raw tubes into desired three-dimensional shapes. A tube is uniquely described by the specifications of raw tube and the bend plan. The specifications include material, diameter, wall thickness and length. The bend plan is composed of a series of triplets. Each triplet describes the distance between bends (shoot), the angle of rotation (rotate) and the angle of bend (bend). In addition, the bend radius is set by the forming die and is the same for all bends. Table 3.1 shows the bend plans for the two designs in Figure 3.2.

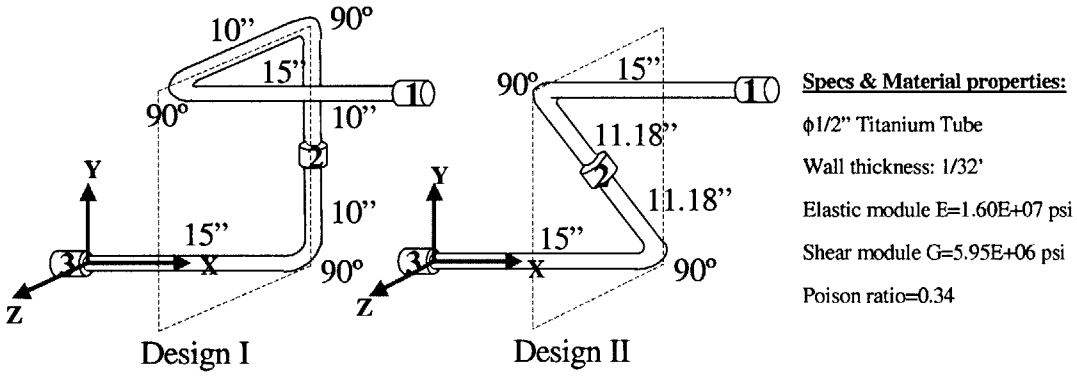

Figure 3.2: Example of tube design

Table 3.2: Bend plan for Design I and II

Bend cycle	Design I			Design II		
	l	β	α	l	β	α
1	15"	0°	90°	15"	0°	90°
2	10"	-90°	90°	22.36"	180°	90°
3	20"	-90°	90°			

The bend plan for design I comprises three cycles, and the bend plan for design II has two cycles. The parameters in the table are l (shoot), α (bend), and β (rotate). Figure 3.3 shows these values and the global coordinate system[8] that will be used throughout the chapter.

[8] The global coordinate system is attached to the bender.

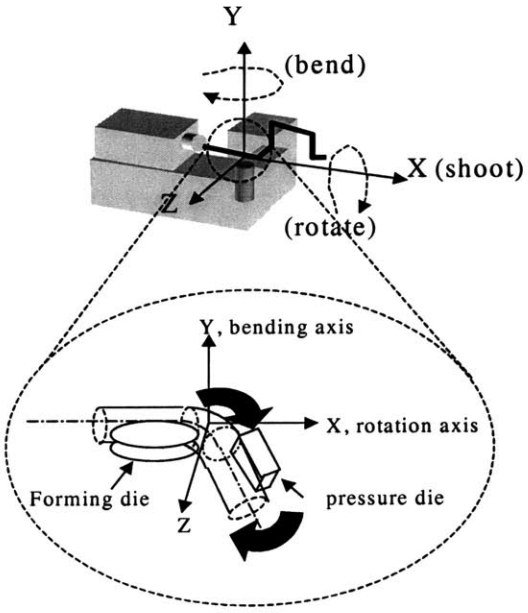

Figure 3.3: Global coordinate system XYZ and the three motions in a bend cycle

Shooting is a translation along the **X**-axis by an amount l, rotation is a negative rotation around the **X**-axis by an amount β, and bending is a negative rotation around the **Y**-axis by an amount α. Each bend cycle is a three-step coordinate transformation comprising one translation and two rotations of the bent part of the tube. A tube with n bends needs to go through n bend cycles to achieve the desired shape. Figure 3.4 shows the bend cycle with the three parameters and the complete bending operation.

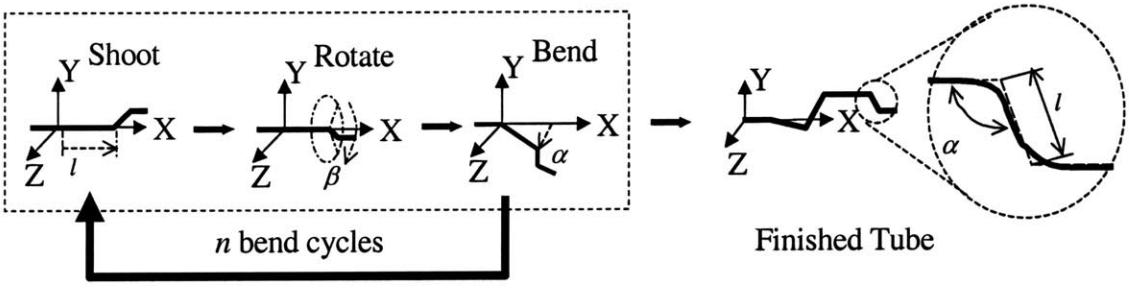

Figure 3.4: Tube bending operation and the process parameters

3.4.2 Geometry Representation of A Tube

From the bend plan it is possible to generate the geometry of the tube in 3-D space. This is done using the Homogeneous Transformation Matrix (HTM) to transform the location and orientation of the bends as the bend plan is executed.

To simplify the modeling, we break the model into two parts. In the first model, the linear centerline model, we represent the tube as if the bending radius was zero (*i.e.*, all sections are straight). We predict for each bend the theoretical breakpoint: the location of the bend if the bending radius is zero. The linear centerline model enables us to simplify

the variation propagation model. The second model, the curvilinear centerline model, includes the bending radius. The curvilinear model is used to more accurately predict variation and the compliance. The conversion is described at the end of this section. Figure 3.5 shows both representations.

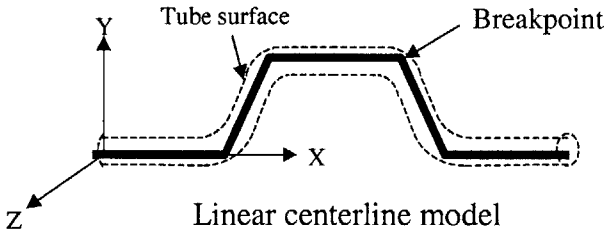

Linear centerline model

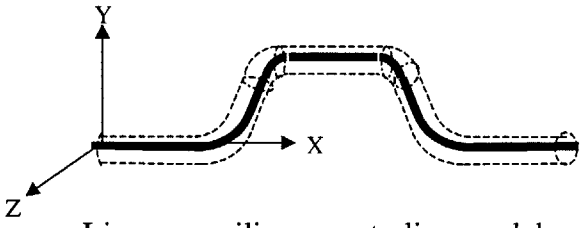

Linear-curvilinear centerline model

Figure 3.5: Representation of tube geometry

The overall shape of a tube can be described by the 3-D positions of all breakpoints plus the two end points in the global coordinate system, as shown in Figure 3.6. There are n bends and point $\boldsymbol{u}$ is an arbitrary point on the tube centerline. We will use this representation throughout our model derivation.

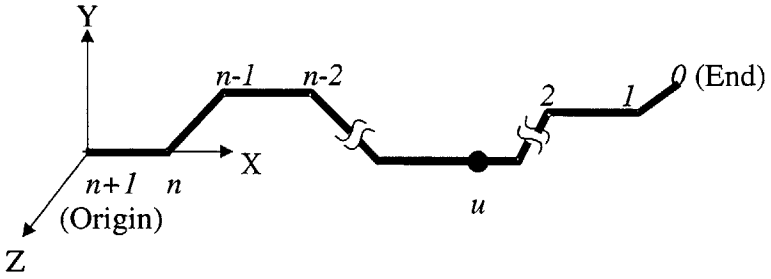

Figure 3.6: Representation of tube geometry in global coordinate system

We locate these points by setting point $n+1$ as the origin (the left end of the tube) and calculating the HTM for each bend cycle. When the i^{th} bend is created, point $\boldsymbol{u}$ undergoes the following coordinate transformation.

$$ {}^{i}\mathbf{T}_{i-1} = \mathbf{B}_i\mathbf{R}_i\mathbf{S}_i = \begin{pmatrix} \cos\alpha_i & \sin\alpha_i\sin\beta_i & -\sin\alpha_i\cos\beta_i & l_i\cos\alpha_i \\ 0 & \cos\beta_i & \sin\beta_i & 0 \\ \sin\alpha_i & -\cos\alpha_i\sin\beta_i & \cos\alpha_i\cos\beta_i & l_i\sin\alpha_i \\ 0 & 0 & 0 & 1 \end{pmatrix} \tag{3.3} $$

where $\mathbf{S}_i$, $\mathbf{R}_i$, and $\mathbf{B}_i$ are the HTMs for shooting, rotating, and bending in each bend cycle. Their definitions and the detailed matrix transforms in a bend cycle are illustrated in Figure 3.7.

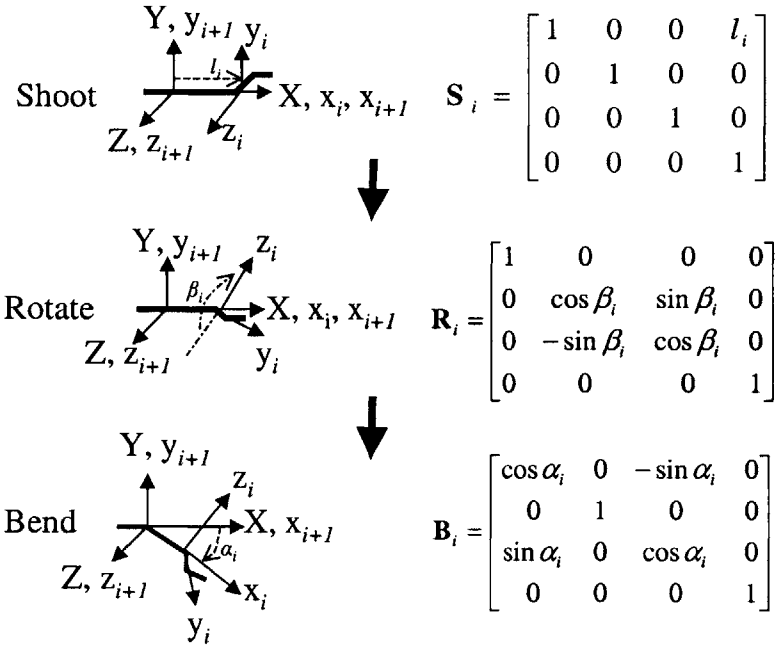

Figure 3.7: Detailed matrix transforms of a bend cycle

The effect of multiple bends can be combined into one HTM through a series of matrix multiplications. The following HTM is the total transformation matrix from the i^{th} to the $(n+1)^{th}$ bend cycle:

$$ \mathbf{T}_i = {}^{n+1}\mathbf{T}_n\,{}^{n}\mathbf{T}_{n-1}\cdots{}^{i+1}\mathbf{T}_i = \begin{pmatrix} \mathbf{R}_i & \mathbf{P}_i \\ \mathbf{0} & 1 \end{pmatrix} \tag{3.4} $$

Later in the paper we will use parts of the total transformation matrix to calculate variation propagation. These parts are the 3x3 rotational matrix $\mathbf{R}_i$ and the 3x1 translational vector, $\mathbf{P}_i$. [9]

[9] Note that ${}^{n+1}\mathbf{T}_n$ is the HTM from the last breakpoint to the origin of XYZ with translation of l_{n+1} only ($\alpha_{n+1} = \beta_{n+1} = 0$).

The linear-curvilinear centerline model can be derived from the linear centerline model by plugging in the curvilinear sections and calculating the tangent points. Figure 3.8 illustrates the procedure.

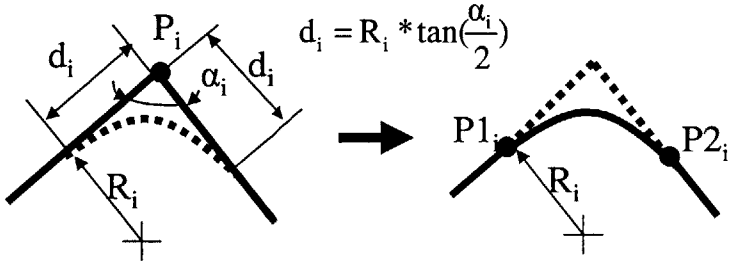

Figure 3.8: Conversion of linear-curvilinear centerline model

3.4.3 Variation Propagation in Tube Bending Operation

Now that we have described the 3-D shape in global coordinate system, the HTM $\mathbf{T}_i$ can be used to calculate the impact of process variation on the resultant geometry. Each shoot, bend, and rotation introduces variation into the geometry. For example, the effect of gravity makes the tubes sag making the rotation less accurate; springback and material variation introduces variation into the bends; variations in indexing, slip and other machine problem introduce variations in the three bending parameters. To simplify the problem, we will first derive the variation propagation model for the linear centerline model, then extend it for curvilinear centerline model.

Linear Centerline Model

From Equation (3.1), the variation propagation in bending process can be written as $\mathbf{X} = \mathbf{S}_1\mathbf{U} + \mathbf{S}_2\mathbf{V}$. The following section derives $\mathbf{S}_1$ and $\mathbf{S}_2$ from the HTM matrices. For simplification, we will demonstrate the derivation at one point on the tube, $\boldsymbol{u}$, as shown in Figure 3.6.

The geometrical variation at an arbitrary point $\boldsymbol{u}$ contains two parts, translational variation $d\mathbf{P} = (dx, dy, dz)^T$ and rotational variation $\delta = (\delta x, \delta y, \delta z)^T$. The bending machine introduces a set of variations affecting point $\boldsymbol{u}$ during the m bend cycles[10] that make the bends between point $\boldsymbol{u}$ and the end of tube that we choose as the origin. These variations are denoted as $d\mathbf{l} = (dl_1, dl_2, \ldots, dl_m)^T$, $d\alpha = (d\alpha_1, d\alpha_2, \ldots, d\alpha_m)^T$ and $d\beta = (d\beta_1, d\beta_2, \ldots, d\beta_m)^T$. The geometrical and process variations can be linked through the following linear equations (Veitschegger 1986; Whitney 1994):

[10] If u locates between the $(j-1)^{th}$ and j^{th} breakpoints, m equals $(n-j+1)$, i.e., $(n-j)$ bends plus the last straight section.

$$\begin{pmatrix} d\mathbf{P} \\ \boldsymbol{\delta} \end{pmatrix} = \begin{pmatrix} \mathbf{W}_1 & \mathbf{W}_2 & \mathbf{W}_3 \\ \mathbf{0} & \mathbf{W}_4 & \mathbf{W}_5 \end{pmatrix} \begin{pmatrix} d\mathbf{l} \\ d\boldsymbol{\alpha} \\ d\boldsymbol{\beta} \end{pmatrix} \tag{3.5}$$

where $\mathbf{W}_1$ through $\mathbf{W}_5$ are 3xm sensitivity matrices.[11] The derivation of $\mathbf{W}_1$ through $\mathbf{W}_5$ is explained below.

Consider a point $\boldsymbol{u}$ located between point j-1 and j (j<i), as shown in Figure 3.9. The process variations dl_i, $d\alpha_i$ and $d\beta_i$ contribute to the translational and rotational variations at the point of interest $\boldsymbol{u}$ through the following relationship.

$$\boldsymbol{\delta}_i = \mathbf{R}_i \begin{pmatrix} -d\beta_i \\ -d\alpha_i \\ 0 \end{pmatrix} \tag{3.6}$$

$$d\mathbf{P}_i = \mathbf{R}_i \begin{pmatrix} dl_i \\ 0 \\ 0 \end{pmatrix} + \boldsymbol{\delta}_i \times (\mathbf{R}_i {}^i\mathbf{P}_u) \tag{3.7}$$

In the equation above, ${}^i\mathbf{P}_u$ is the 3x1 translational vector from i^{th} breakpoint to point $\boldsymbol{u}$ in the global coordinate system when i^{th} bend cycle is to be executed. It can be obtained through the following equation:

$${}^i\mathbf{T}_u = {}^i\mathbf{T}_{i-1}\,{}^{i-1}\mathbf{T}_{i-2} \cdots {}^j\mathbf{T}_u = \begin{pmatrix} {}^i\mathbf{R}_u & {}^i\mathbf{P}_u \\ \mathbf{0} & 1 \end{pmatrix} \tag{3.8}$$

In Equation (3.8), ${}^j\mathbf{T}_u$ equals ${}^j\mathbf{T}_{j-1}$ with l_u replacing l_j. The product vector of $\mathbf{R}_i {}^i\mathbf{P}_u$ is the translational vector from the i^{th} breakpoint to $\boldsymbol{u}$ in the global coordinate system when the last bend cycle is finished. The last term of Equation (3.7) is the Abbe variation caused by the rotational variations at the i^{th} breakpoint.

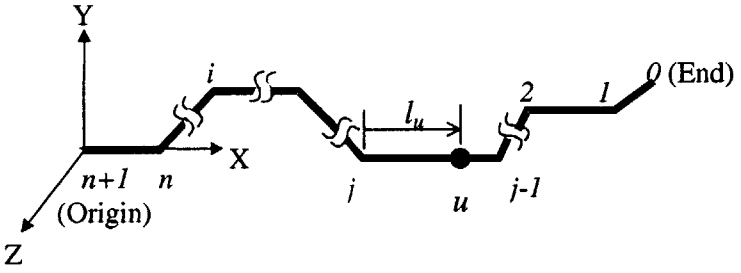

Figure 3.9: Arbitrary point $\boldsymbol{u}$ on the tube

[11] The rotational variation vector is determined only by rotational variations in bending process, while the positional variation vector is determined by both translational and rotational variations.

Since we assume the variations to be small, the total geometrical variations can be obtained by summing up the variations introduced by individual bend cycles. Therefore,

$$\boldsymbol{\delta} = \sum_{i=j}^{n+1} \boldsymbol{\delta}_i^u \tag{3.9}$$

$$d\mathbf{P} = \sum_{i=j}^{n+1} d\mathbf{P}_i^u \tag{3.10}$$

By summarizing Equation (3.6)-(3.10), we can express Equation (3.5) through the following equations:

$$\mathbf{W}_1 = \begin{pmatrix} \mathbf{R}_j^1 & \mathbf{R}_{j+1}^1 & \cdots & \mathbf{R}_{n+1}^1 \end{pmatrix} \tag{3.11}$$

$$\mathbf{W}_2 = -\begin{pmatrix} \mathbf{R}_j^2 \times \left(\mathbf{R}_j{}^j \mathbf{P}_u\right) & \mathbf{R}_{j+1}^2 \times \left(\mathbf{R}_{j+1}{}^{j+1} \mathbf{P}_u\right) & \cdots & \mathbf{R}_{n+1}^2 \times \left(\mathbf{R}_{n+1}{}^{n+1} \mathbf{P}_u\right) \end{pmatrix} \tag{3.12}$$

$$\mathbf{W}_3 = -\begin{pmatrix} \mathbf{R}_j^1 \left(\mathbf{R}_j{}^j \mathbf{P}_u\right) & \mathbf{R}_{j+1}^1 \left(\mathbf{R}_{j+1}{}^{j+1} \mathbf{P}_u\right) & \cdots & \mathbf{R}_{n+1}^1 \left(\mathbf{R}_{n+1}{}^{n+1} \mathbf{P}_u\right) \end{pmatrix} \tag{3.13}$$

$$\mathbf{W}_4 = -\begin{pmatrix} \mathbf{R}_j^2 & \mathbf{R}_{j+1}^2 & \cdots & \mathbf{R}_{n+1}^2 \end{pmatrix} \tag{3.14}$$

$$\mathbf{W}_5 = -\mathbf{W}_1 \tag{3.15}$$

where $\mathbf{R}_j^1$ represents the first column (3x1 vector) and $\mathbf{R}_j^2$ is the second column of $\mathbf{R}_j$. In the tube bending process, the bender contributes variations in the shoot lengths, the bend angles and the rotation angles. The incoming tube only has significant effects on the bend angle because of the variations on springback. Therefore, the elements in Equation (3.1) can be written as: $\mathbf{X}=(d\mathbf{P}, \boldsymbol{\delta})^T$, $\mathbf{U}=(d\mathbf{l}, d\alpha, d\beta)^T$, $\mathbf{V}=(\mathbf{0}, d\alpha, \mathbf{0})^T$, and

$$\mathbf{S}_1 = \mathbf{S}_2 = \begin{pmatrix} \mathbf{W}_1 & \mathbf{W}_2 & \mathbf{W}_3 \\ \mathbf{0} & \mathbf{W}_4 & \mathbf{W}_5 \end{pmatrix} \tag{3.16}$$

The above expression is for the variation propagation at one point on the tube. To obtain the variation propagation equation for multiple points, the forgoing procedures are repeated for each point of interest and organize them into matrix form.

Curvilinear Centerline Model

When the bend radius is not ignorable or for higher accuracy in variation propagation, the curvilinear centerline model needs to be considered. In the model there are dependencies between $d\alpha$ and $d\mathbf{l}$ because of the non-zero bend radius. Figure 3.10

shows their relationships in the two cases: machine over-/under-bend and variation on springback.

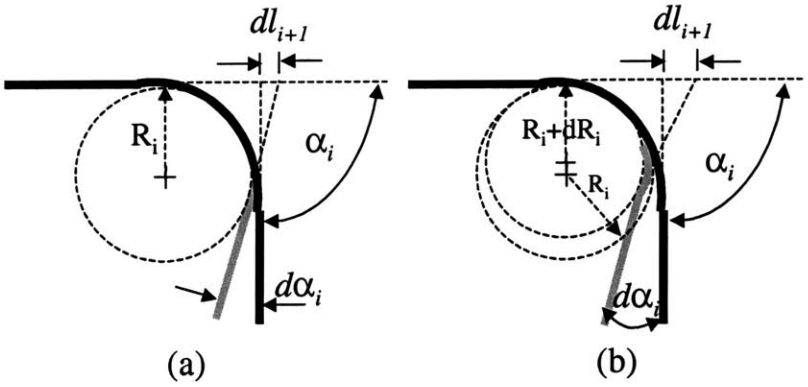

Figure 3.10: Dependency of $d\alpha$ and dl with nonzero bend radius caused by (a) machine over/under bend and (b) variation on springback after compensation

The machine over-/under-bend is caused by the excess/insufficient stroke of the pressure die. The bend radius remains unchanged but the arc length is changed. The variation in bend angle affects the variations in the neighboring shoot lengths through the following equation:

$$dl_i = dl_{i+1} = R_i \tan(\frac{\alpha_i + d\alpha_i}{2}) - R_i \tan(\frac{\alpha_i}{2}) = R_i \frac{d}{d\alpha_i / 2} \tan(\frac{\alpha_i}{2})$$
$$= \frac{R_i}{2}(1 + \tan^2 \frac{\alpha_i}{2}) d\alpha_i \qquad (3.17)$$

In a bending process the springback is compensated by some preset values. However, due to the variation in material properties, the actual springback may be larger or smaller than the compensating values, *i.e.*, there are variations. The springback variation changes the bend radius but the arc length remains the same, *i.e.*, $(R_i + dR_i)(\alpha_i + d\alpha_i) = R_i \alpha_i$. Ignoring the high-order terms, we get $dR_i = -\frac{R_i}{\alpha_i} d\alpha_i$. The relationship between $d\alpha$ and dl can be obtained from the following equation:

$$
\begin{aligned}
dl_{i+1} = dl_i &= (R_i + dR_i)\tan(\frac{\alpha_i + d\alpha_i}{2}) - R_i \tan(\frac{\alpha_i}{2}) \\
&= \frac{R_i}{2}(1+\tan^2(\frac{\alpha_i}{2}))d\alpha_i + dR_i \tan(\frac{\alpha_i + d\alpha_i}{2}) \\
&= \frac{R_i}{2}(1+\tan^2(\frac{\alpha_i}{2}))d\alpha_i - \frac{R_i}{\alpha_i}\tan(\frac{\alpha_i + d\alpha_i}{2})d\alpha \\
&= \frac{R_i}{2}(1-\frac{2}{\alpha_i}\tan(\frac{\alpha_i}{2}) + \tan^2(\frac{\alpha_i}{2}))d\alpha_i
\end{aligned}
\tag{3.18}
$$

Let $C_i = \frac{R_i}{2}(1+\tan^2\frac{\alpha_i}{2})$, $D_i = \frac{R_i}{2}(1-\frac{2}{\alpha_i}\tan(\frac{\alpha_i}{2}) + \tan^2(\frac{\alpha_i}{2}))$ and define

$$
\mathbf{W}_6 = \begin{pmatrix} C_i & 0 & \cdots & 0 \\ C_i & C_{i+1} & \cdots & 0 \\ 0 & C_{i+1} & \ddots & \vdots \\ \vdots & \vdots & \ddots & C_n \\ 0 & 0 & \cdots & C_n \end{pmatrix} \quad \mathbf{W}_7 = \begin{pmatrix} D_i & 0 & \cdots & 0 \\ D_i & D_{i+1} & \cdots & 0 \\ 0 & D_{i+1} & \ddots & \vdots \\ \vdots & \vdots & \ddots & D_n \\ 0 & 0 & \cdots & D_n \end{pmatrix} \tag{3.19}
$$

The new sensitivity matrices for single point on the tube become

$$
\mathbf{S}_1 = \begin{pmatrix} \mathbf{W}_1 & \mathbf{W}_1\mathbf{W}_6 + \mathbf{W}_2 & \mathbf{W}_3 \\ \mathbf{0} & \mathbf{W}_4 & \mathbf{W}_5 \end{pmatrix} \tag{3.20}
$$

$$
\mathbf{S}_2 = \begin{pmatrix} \mathbf{W}_1 & \mathbf{W}_1\mathbf{W}_7 + \mathbf{W}_2 & \mathbf{W}_3 \\ \mathbf{0} & \mathbf{W}_4 & \mathbf{W}_5 \end{pmatrix} \tag{3.21}
$$

Example

In the following section we derive the sensitivity matrices in the tube bending operation for the two design examples in Figure 3.2. Linear centerline model is used for the two designs since the bend radius is small.

Design I: Let the process variations in the three bend cycles be $d\mathbf{l}=(dl_1\ dl_2\ dl_3)^T$, $d\boldsymbol{\alpha}=(d\alpha_1\ d\alpha_2\ d\alpha_3)^T$ and $d\boldsymbol{\beta}=(d\beta_1,\ d\beta_2,\ d\beta_3)^T$. Assuming install point 3 is fixed, let the geometrical variations at install point 1 be $d\mathbf{P}_2=(dx_1,\ dy_1,\ dz_1)^T$ and $\boldsymbol{\delta}_1=(\delta x_1,\ \delta y_1,\ \delta z_1)^T$. Similarly, let the geometrical variations at install point 2 be $d\mathbf{P}_2=(dx_2,\ dy_2,\ dz_2)^T$ and $\boldsymbol{\delta}_2=(\delta x_2,\ \delta y_2,\ \delta z_2)^T$. Note that all angles are in radians. Through the procedures in Section 3.4.3 we derive the individual variation propagation equations as follows:

$$\begin{pmatrix} dx_1 \\ dy_1 \\ dz_1 \\ \delta x_1 \\ \delta y_1 \\ \delta z_1 \end{pmatrix} = \begin{pmatrix} 1 & 0 & 0 & 0 & 0 & -20 & 0 & 0 & -10 \\ 0 & 0 & 1 & 0 & -10 & 15 & 0 & -15 & 0 \\ 0 & 1 & 0 & -15 & 0 & 0 & 0 & 0 & 15 \\ 0 & 0 & 0 & 0 & 1 & 0 & -1 & 0 & 0 \\ 0 & 0 & 0 & 1 & 0 & 0 & 0 & 0 & -1 \\ 0 & 0 & 0 & 0 & 0 & 1 & 0 & -1 & 0 \end{pmatrix} \begin{pmatrix} dl_1 \\ dl_2 \\ dl_3 \\ d\alpha_1 \\ d\alpha_2 \\ d\alpha_3 \\ d\beta_1 \\ d\beta_2 \\ d\beta_3 \end{pmatrix}$$

$$\begin{pmatrix} dx_2 \\ dy_2 \\ dz_2 \\ \delta x_2 \\ \delta y_2 \\ \delta z_2 \end{pmatrix} = \begin{pmatrix} 0 & -10 & 0 \\ 1 & 0 & 0 \\ 0 & 0 & 0 \\ 0 & 0 & 0 \\ 0 & 0 & -1 \\ 0 & 1 & 0 \end{pmatrix} \begin{pmatrix} dl_3 \\ d\alpha_3 \\ d\beta_3 \end{pmatrix}$$

Since point 3 is assumed fixed, it has null sensitivity to the process variations. Combining the two matrices above and adding zeros for the null sensitivity, we can obtain the overall variation propagation equation:

$$\begin{pmatrix} dx_1 \\ dy_1 \\ dz_1 \\ \delta x_1 \\ \delta y_1 \\ \delta z_1 \\ dx_2 \\ dy_2 \\ dz_2 \\ \delta x_2 \\ \delta y_2 \\ \delta z_2 \\ dx_3 \\ dy_3 \\ dz_3 \\ \delta x_3 \\ \delta y_3 \\ \delta z_3 \end{pmatrix} = \begin{pmatrix} 1 & 0 & 0 & 0 & 0 & -20 & 0 & 0 & -10 \\ 0 & 0 & 1 & 0 & -10 & 15 & 0 & -15 & 0 \\ 0 & 1 & 0 & -15 & 0 & 0 & 0 & 0 & 15 \\ 0 & 0 & 0 & 0 & 1 & 0 & -1 & 0 & 0 \\ 0 & 0 & 0 & 1 & 0 & 0 & 0 & 0 & -1 \\ 0 & 0 & 0 & 0 & 0 & 1 & 0 & -1 & 0 \\ 0 & 0 & 0 & 0 & 0 & -10 & 0 & 0 & 0 \\ 0 & 0 & 1 & 0 & 0 & 0 & 0 & 0 & 0 \\ 0 & 0 & 0 & 0 & 0 & 0 & 0 & 0 & 0 \\ 0 & 0 & 0 & 0 & 0 & 0 & 0 & 0 & 0 \\ 0 & 0 & 0 & 0 & 0 & 0 & 0 & 0 & -1 \\ 0 & 0 & 0 & 0 & 0 & 1 & 0 & 0 & 0 \\ 0 & 0 & 0 & 0 & 0 & 0 & 0 & 0 & 0 \\ 0 & 0 & 0 & 0 & 0 & 0 & 0 & 0 & 0 \\ 0 & 0 & 0 & 0 & 0 & 0 & 0 & 0 & 0 \\ 0 & 0 & 0 & 0 & 0 & 0 & 0 & 0 & 0 \\ 0 & 0 & 0 & 0 & 0 & 0 & 0 & 0 & 0 \end{pmatrix} \begin{pmatrix} dl_1 \\ dl_2 \\ dl_3 \\ d\alpha_1 \\ d\alpha_2 \\ d\alpha_3 \\ d\beta_1 \\ d\beta_2 \\ d\beta_3 \end{pmatrix}$$

Design II: Design II has only two bends. Through a similar process, we have

$$
\begin{pmatrix} dx_1 \\ dy_1 \\ dz_1 \\ \delta x_1 \\ \delta y_1 \\ \delta z_1 \\ dx_2 \\ dy_2 \\ dz_2 \\ \delta x_2 \\ \delta y_2 \\ \delta z_2 \\ dx_3 \\ dy_3 \\ dz_3 \\ \delta x_3 \\ \delta y_3 \\ \delta z_3 \end{pmatrix} = \begin{pmatrix} 1 & 0 & 0 & -22.36 & 0 & 0 \\ 0 & 0.89 & -13.42 & 0 & 0 & -6.71 \\ 0 & 0.45 & -6.71 & 0 & 0 & 13.42 \\ 0 & 0 & 0 & 0 & -1 & 0 \\ 0 & 0 & 0.45 & -0.45 & 0 & -0.89 \\ 0 & 0 & -0.89 & 0.89 & 0 & -0.45 \\ 0 & 0 & 0 & -11.18 & 0 & 0 \\ 0 & 0.89 & 0 & 0 & 0 & 0 \\ 0 & 0.45 & 0 & 0 & 0 & 0 \\ 0 & 0 & 0 & 0 & 0 & 0 \\ 0 & 0 & 0 & -0.45 & 0 & -0.89 \\ 0 & 0 & 0 & 0.89 & 0 & -0.45 \\ 0 & 0 & 0 & 0 & 0 & 0 \\ 0 & 0 & 0 & 0 & 0 & 0 \\ 0 & 0 & 0 & 0 & 0 & 0 \\ 0 & 0 & 0 & 0 & 0 & 0 \\ 0 & 0 & 0 & 0 & 0 & 0 \\ 0 & 0 & 0 & 0 & 0 & 0 \end{pmatrix} \begin{pmatrix} dl_1 \\ dl_2 \\ d\alpha_1 \\ d\alpha_2 \\ d\beta_1 \\ d\beta_2 \end{pmatrix}
$$

Validation

The foregoing linearized HTM method is validated against the simulation method. A tube is to be designed to connect point 1 and 3 as shown in Figure 3.2, with varying number of bends from two to ten. The range for the number of bends is the most representative for the majority of the aircraft tubes. The statistics on the process variations are listed in Table 2. Note that the process is centered without biases.

Table 3.3: Statistics on process variations

Process Variations	l	β	α
Mean	0	0	0
Standard Deviation	0.1"	0.5°	0.5°

Figure 3.11 plots the error margin of the standard deviations for the geometric variations from the two approaches under different number of bends on a tube. The geometric variations on the tube are measured from one end to the other. It can be seen that the error margin is acceptably small but increases over the range of the number of bends. This is because the linearization errors accumulate as the number of bends increases.

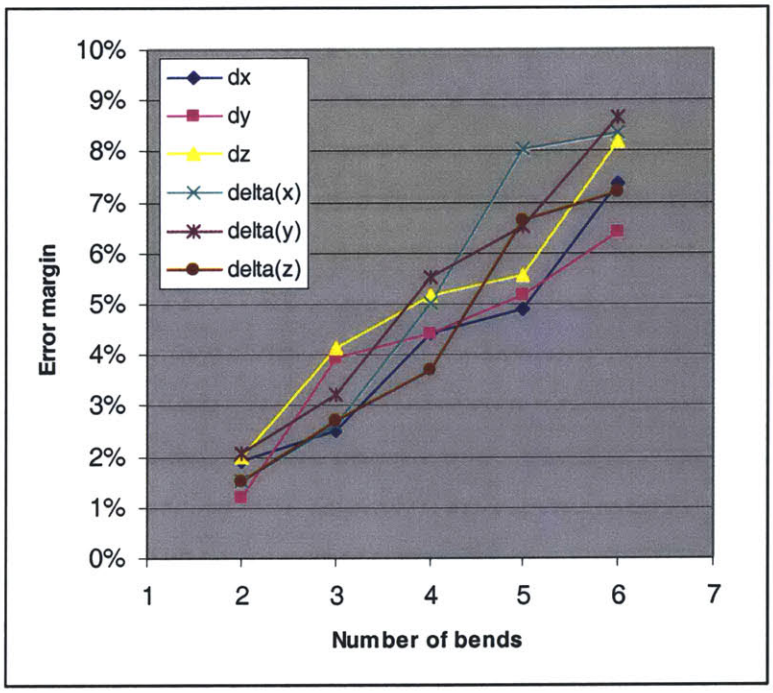

Figure 3.11: Results from the linearized HTM method and the simulation method under different number of bends

Generalization

This variation propagation model using matrix transform method can be extended to other manufacturing processes containing a series of bending cycles. For example, the variations in sheet metal bending can be analyzed through similar method. Equation (3.3) , (3.6) and (3.7) might need to be modified, depending on the coordinate system and the sequence of shooting, bending and rotation.

3.4.4 Variation Propagation in Assembly

In Section 3.3 we introduce the sensitivity matrices in the assembly operation in terms of the stiffness matrices of the tube and the mating structure. This section will demonstrate the detailed derivation.

Case I: Geometric Variation

There are two cases for the calculation of $\mathbf{S_3}$ and $\mathbf{S_4}$. If $\mathbf{Z}$ is the geometric variation vector, then

$$\mathbf{S_3} = (\mathbf{K_1} + \mathbf{K_2})^{-1}\mathbf{K_1} \tag{3.22}$$

$$\mathbf{S_4} = (\mathbf{K_1} + \mathbf{K_2})^{-1}\mathbf{K_2} \tag{3.23}$$

Equation (3.22) and (3.23) can be verified by the equilibrium of generalized forces at the mating points:

$$\mathbf{K}_1(\upsilon - \mathbf{X}') + \mathbf{K}_2(\upsilon - \mathbf{Y}) = \mathbf{0} \tag{3.24}$$

Manipulating the equation above, we get

$$\upsilon = (\mathbf{K}_1 + \mathbf{K}_2)^{-1}\mathbf{K}_1\mathbf{X}' + (\mathbf{K}_1 + \mathbf{K}_2)^{-1}\mathbf{K}_2\mathbf{Y} \tag{3.25}$$

where υ is the generalized displacement vector at the mating features and $\mathbf{Z} = \upsilon$ in this case. It implies that the assembled part variation can be interpolated by the variations on the two mating parts. Also stiffer part is more dominant in the output variation.

If the mating part is rigid, *i.e.*, $\mathbf{K_2} >> \mathbf{K_1}$, the output variation is then determined by the mating part variation, *i.e.*, $\mathbf{Z}=\mathbf{Y}$. The sensitivity matrices become

$$\mathbf{S}_3 = \mathbf{0} \tag{3.26}$$

$$\mathbf{S}_4 = \mathbf{I} \tag{3.27}$$

where $\mathbf{0}$ is the null matrix and $\mathbf{I}$ is the identity matrix.

Case II: Assembly Load

If $\mathbf{Z}$ is the assembly load vector, then

$$\mathbf{S}_3 = \mathbf{K}_1\left((\mathbf{K}_1 + \mathbf{K}_2)^{-1}\mathbf{K}_1 - \mathbf{I}\right) \tag{3.28}$$

$$\mathbf{S}_4 = \mathbf{K}_1(\mathbf{K}_1 + \mathbf{K}_2)^{-1}\mathbf{K}_1 \tag{3.29}$$

Equation (3.28) and (3.29) can be verified by the equation of elasticity:

$$\begin{aligned} \sigma &= \mathbf{K}_1(\upsilon - \mathbf{X}') \\ &= \mathbf{K}_1((\mathbf{K}_1 + \mathbf{K}_2)^{-1}\mathbf{K}_1\mathbf{X}' + (\mathbf{K}_1 + \mathbf{K}_2)^{-1}\mathbf{K}_2\mathbf{Y} - \mathbf{X}') \\ &= \mathbf{K}_1\left((\mathbf{K}_1 + \mathbf{K}_2)^{-1}\mathbf{K}_1 - \mathbf{I}\right)\mathbf{X} + \mathbf{K}_1(\mathbf{K}_1 + \mathbf{K}_2)^{-1}\mathbf{K}_2\mathbf{Y} \end{aligned} \tag{3.30}$$

where σ is the generalized force vector acting on the mating features of the incoming part and $\mathbf{Z} = \sigma$ in this case.

If the mating part is rigid, *i.e.*, $\mathbf{K_2} >> \mathbf{K_1}$ and $\upsilon = \mathbf{Y}$, Equation (3.30) becomes

$$\begin{aligned} \mathbf{Z} &= \mathbf{K}_1(\upsilon - \mathbf{X}') \\ &= \mathbf{K}_1(\mathbf{Y} - \mathbf{X}') \\ &= \mathbf{K}_1\mathbf{Y} - \mathbf{K}_1\mathbf{X}' \end{aligned} \tag{3.31}$$

Therefore, the sensitivity matrices are

$$S_3 = -K_1 \tag{3.32}$$

$$S_4 = K_1 \tag{3.33}$$

3.4.5 Direct Compliance Calculation

This section demonstrates a method to obtain the stiffness matrix of tube, $\mathbf{K_1}$, without FEM modeling. The proposed method takes the advantage of the geometric simplicity of the tube, since a tube can be modeled as a series of linear and curvilinear thin-wall cylinders.

The modeling procedure starts with dissecting the tube into linear and curvilinear sections. These sections are further divided at the points of interest. Their stiffness matrices can be obtained directly from the formulae handbook for structural elements (straight and circular thin-wall beams). In this paper the formulae are obtained from Pilkey's (1994) handbook. The next step is applying matrix operations to condense the section stiffness matrices and compose them into global stiffness matrix. An example in Figure 3.12 illustrates the process.

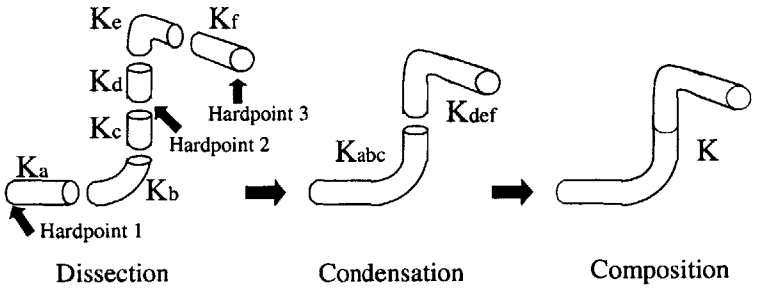

Figure 3.12: Procedure to compose global stiffness matrix

In the example above, we want to derive the stiffness matrix that links the generalized forces and generalized displacements on the three hardpoints. We first find the section stiffness matrices $\mathbf{K_a}$ through $\mathbf{K_c}$, which are three 12x12 matrices comprising six plus six degrees of freedom on both ends (2 nodes) of each section. They can be obtained directly from formula tables (Pilkey 1994) for straight and circular beam. Next we derive the stiffness matrix $\mathbf{K_{abc}}$, which is a 12x12 matrix comprising six plus six degrees of freedom on hardpoint 1 and 2. It can be obtained by condensing $\mathbf{K_a}$ through $\mathbf{K_c}$. Similarly, $\mathbf{K_{def}}$ is a 12x12 matrix comprising six plus six degrees of freedom on hardpoint 2 and 3, and can be obtained by condensing $\mathbf{K_d}$ through $\mathbf{K_f}$. The condensation process is illustrated below.

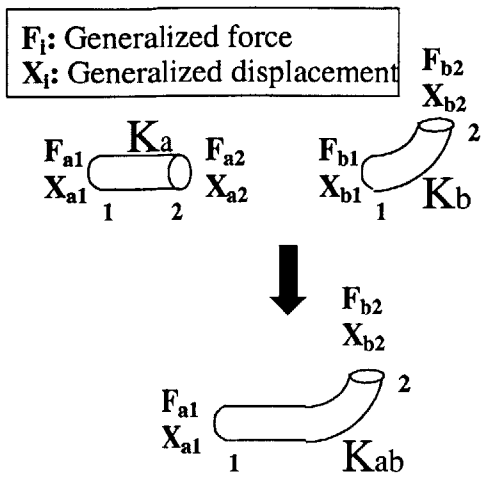

Figure 3.13: Illustration of stiffness matrix condensation

As shown in Figure 3.13, the second node of $\mathbf{K_a}$ is to be merged with the first node of $\mathbf{K_b}$, and the degrees of freedom on the node are to be eliminated (generalized force on the merging node is zero). Let $\mathbf{K}_a = \begin{pmatrix} \mathbf{K}_{a11} & \mathbf{K}_{a12} \\ \mathbf{K}_{a12}^T & \mathbf{K}_{a22} \end{pmatrix}$ and $\mathbf{K}_b = \begin{pmatrix} \mathbf{K}_{b11} & \mathbf{K}_{b12} \\ \mathbf{K}_{b12}^T & \mathbf{K}_{b22} \end{pmatrix}$, where $\begin{pmatrix} \mathbf{F}_{a1} \\ \mathbf{F}_{a2} \end{pmatrix} = \begin{pmatrix} \mathbf{K}_{a11} & \mathbf{K}_{a12} \\ \mathbf{K}_{a12}^T & \mathbf{K}_{a22} \end{pmatrix} \begin{pmatrix} \mathbf{X}_{a1} \\ \mathbf{X}_{a2} \end{pmatrix}$ and $\begin{pmatrix} \mathbf{F}_{b1} \\ \mathbf{F}_{b2} \end{pmatrix} = \begin{pmatrix} \mathbf{K}_{b11} & \mathbf{K}_{b12} \\ \mathbf{K}_{b12}^T & \mathbf{K}_{b22} \end{pmatrix} \begin{pmatrix} \mathbf{X}_{b1} \\ \mathbf{X}_{b2} \end{pmatrix}$. By solving $\mathbf{F}_{a2} + \mathbf{F}_{b1} = \mathbf{0}$ and $\mathbf{X}_{a2} = \mathbf{X}_{b1}$, the constitutive relation for the two-part system can be rewritten as $\begin{pmatrix} \mathbf{F}_{a1} \\ \mathbf{F}_{b2} \end{pmatrix} = \mathbf{K}_{ab} \begin{pmatrix} \mathbf{X}_{a1} \\ \mathbf{X}_{b2} \end{pmatrix}$, where $\mathbf{K}_{ab} = \begin{pmatrix} \mathbf{K}_{a11} - \mathbf{K}_{a12}(\mathbf{K}_{a22}+\mathbf{K}_{b11})^{-1}\mathbf{K}_{a12}^T & -\mathbf{K}_{a12}(\mathbf{K}_{a12}+\mathbf{K}_{b11})^{-1}\mathbf{K}_{b12} \\ -\mathbf{K}_{b12}^T(\mathbf{K}_{a22}+\mathbf{K}_{b11})^{-1}\mathbf{K}_{a12}^T & \mathbf{K}_{b22} - \mathbf{K}_{b12}^T(\mathbf{K}_{a22}+\mathbf{K}_{b11})^{-1}\mathbf{K}_{b12} \end{pmatrix}$, yielding a 12x12 matrix. By repeating this procedure, $\mathbf{K_{ab}}$ and $\mathbf{K_c}$ can be condensed into $\mathbf{K_{abc}}$.

The final step is to derive the global stiffness matrix $\mathbf{K}$, which is an 18x18 matrix that has six degrees of freedom on the three hardpoints and can be obtained from $\mathbf{K_{abc}}$ and $\mathbf{K_{def}}$. Let $\mathbf{K}_{abc} = \begin{pmatrix} \mathbf{K}_{abc11} & \mathbf{K}_{abc12} \\ \mathbf{K}_{abc12}^T & \mathbf{K}_{abc22} \end{pmatrix}$ and $\mathbf{K}_{def} = \begin{pmatrix} \mathbf{K}_{def11} & \mathbf{K}_{def12} \\ \mathbf{K}_{def12}^T & \mathbf{K}_{def22} \end{pmatrix}$, then $\mathbf{K} = \begin{pmatrix} \mathbf{K}_{abc11} & \mathbf{K}_{abc12} & \mathbf{0} \\ \mathbf{K}_{abc12}^T & \mathbf{K}_{abc22}+\mathbf{K}_{def11} & \mathbf{K}_{def12} \\ \mathbf{0} & \mathbf{K}_{def12}^T & \mathbf{K}_{def22} \end{pmatrix}$, in which the second node of $\mathbf{K_{abc}}$ and the first node of $\mathbf{K_{def}}$ are superimposed.

Example

The characteristic stiffness matrices that relate the generalized forces and displacements at the three install points is derived and shown as follows for the two example in Figure 3.2. Note that the bend radius is 1.5".

Design I:

8.12E+01	6.32E+00	1.96E+01	-1.82E+00	4.20E+01	-2.04E+01	-8.12E+01	-6.32E+00	-1.96E+01	-1.10E+02	-1.31E+02	5.13E+02					
6.32E+00	3.30E+01	4.61E+00	4.53E+01	3.42E+01	-3.33E+02	-6.32E+00	-3.30E+01	-4.61E+00	5.45E+01	-4.09E+00	-1.95E+01					
1.96E+01	4.61E+00	4.13E+01	-1.59E+01	3.82E+02	-3.57E+01	-1.96E+01	-4.61E+00	-4.13E+01	-2.55E+02	3.61E+01	1.18E+02					
-1.82E+00	4.53E+01	-1.59E+01	5.98E+02	-1.59E+02	-4.66E+02	1.82E+00	-4.53E+01	1.59E+01	-3.06E+02	-2.52E+01	-9.07E+01					
4.20E+01	3.42E+01	3.82E+02	-1.59E+02	4.34E+03	-3.22E+02	-4.20E+01	-3.42E+01	-3.82E+02	-2.38E+03	7.20E+01	2.07E+02					
-2.04E+01	-3.33E+02	-3.57E+01	-4.66E+02	-3.22E+02	3.92E+03	2.04E+01	3.33E+02	3.57E+01	-6.14E+02	-2.43E+01	-7.41E+01					
-8.12E+01	-6.32E+00	-1.96E+01	1.82E+00	-4.20E+01	2.04E+01	3.03E+02	3.95E+01	1.96E+01	1.10E+02	1.31E+02	7.54E+02	-2.22E+02	-3.32E+01	7.70E-07	2.86E-11	-2.60E-06	-1.12E+02
-6.32E+00	-3.30E+01	-4.61E+00	-4.53E+01	-3.42E+01	3.33E+02	3.95E+01	9.05E+01	4.61E+00	-5.45E+01	4.09E+00	6.10E+01	-3.32E+01	-5.75E+01	4.28E-07	-6.07E-07	-2.92E-06	-4.99E+02
-1.96E+01	-4.61E+00	-4.13E+01	1.59E+01	-3.82E+02	3.57E+01	1.96E+01	4.61E+00	8.04E+01	7.89E+00	5.93E+01	-1.18E+02	7.70E-07	4.28E-07	-3.90E+01	-2.62E+01	3.73E+02	2.92E-06
-1.10E+02	5.45E+01	-2.55E+02	-3.06E+02	-2.38E+03	-6.14E+02	1.10E+02	-5.45E+01	7.89E+00	4.56E+03	-8.54E+02	-8.12E+02	-3.73E-13	5.74E-06	2.47E+02	-5.25E+02	-2.36E+03	5.47E-05
-1.31E+02	-4.09E+00	3.61E+01	-2.52E+01	7.20E+01	-2.43E+01	1.31E+02	4.09E+00	5.93E+01	-8.54E+02	1.85E+03	-8.45E+02	-2.94E-05	-3.18E-06	-9.54E+01	-5.75E+01	1.78E+02	-6.82E-06
5.13E+02	-1.95E+01	1.18E+02	-9.07E+01	2.07E+02	-7.41E+01	7.54E+02	6.10E+01	-1.18E+02	-8.12E+02	-8.45E+02	1.24E+04	-1.27E+03	-4.15E+01	3.18E-06	1.34E-06	-6.82E-06	-1.16E+02
						-2.22E+02	-3.32E+01	7.70E-07	-1.29E-11	-2.94E-05	-1.27E+03	2.22E+02	3.32E+01	-7.70E-07	-2.86E-11	2.60E-06	1.12E+02
						-3.32E+01	-5.75E+01	4.28E-07	5.74E-06	-3.18E-06	-4.15E+01	3.32E+01	5.75E+01	-4.28E-07	6.07E-07	2.92E-06	4.99E+02
						7.70E-07	4.28E-07	-3.90E+01	2.47E+02	-9.54E+01	3.18E-06	-7.70E-07	-4.28E-07	3.90E+01	2.62E+01	-3.73E+02	-2.92E-06
						2.53E-11	-6.07E-07	-2.62E+01	-5.25E+02	-5.75E+01	1.34E-06	-2.53E-11	6.07E-07	2.62E+01	7.08E+02	-2.57E+02	5.95E-06
						-2.60E-06	-2.92E-06	3.73E+02	-2.36E+03	1.78E+02	-6.82E-06	2.60E-06	2.92E-06	-3.73E+02	-2.57E+02	4.30E+03	2.37E-05
						-1.12E+02	-4.99E+02	2.92E-06	5.47E-05	-6.82E-06	-1.16E+02	1.12E+02	4.99E+02	-2.92E-06	5.95E-06	2.37E-05	5.32E+03

Design II:

1.50E+02	2.68E+01	1.34E+01	-4.64E-06	4.59E+01	-9.19E+01	-1.50E+02	-2.68E+01	-1.34E+01	-1.15E-05	-4.34E+02	8.68E+02						
2.68E+01	5.28E+01	9.02E+00	1.46E+01	6.46E+01	-4.66E+02	-2.68E+01	-5.28E+01	-9.02E+00	1.13E+02	-5.46E+01	2.68E+01						
1.34E+01	9.02E+00	3.93E+01	-2.92E+01	3.70E+02	-6.46E+01	-1.34E+01	-9.02E+00	-3.93E+01	-2.25E+02	5.31E+01	5.46E+01						
-2.11E-05	1.46E+01	-2.92E+01	6.95E+02	-2.88E+02	-1.44E+02	2.11E-05	-1.46E+01	2.92E+01	-4.27E+02	-6.22E+01	-3.11E+01						
4.59E+01	6.46E+01	3.70E+02	-2.88E+02	4.23E+03	-5.42E+02	-4.59E+01	-6.46E+01	-3.70E+02	-2.18E+03	3.30E+01	1.04E+02						
-9.19E+01	-4.66E+02	-6.46E+01	-1.44E+02	-5.42E+02	5.05E+03	9.19E+01	4.66E+02	6.46E+01	-1.09E+03	1.04E+02	-1.23E+02						
-1.50E+02	-2.68E+01	-1.34E+01	4.64E-06	-4.59E+01	9.19E+01	3.00E+02	5.37E+01	2.68E+01	1.50E-06	-3.82E-04	5.67E-04	-1.50E+02	-2.68E+01	-1.34E+01	7.28E-05	4.59E+01	-9.19E+01
-2.68E+01	-5.28E+01	-9.02E+00	-1.46E+01	-6.46E+01	4.66E+02	5.37E+01	1.06E+02	1.80E+01	6.22E-07	1.42E-04	-3.12E-04	-2.68E+01	-5.28E+01	-9.02E+00	1.46E+01	6.46E+01	-4.66E+02
-1.34E+01	-9.02E+00	-3.93E+01	2.92E+01	-3.70E+02	6.46E+01	2.68E+01	1.80E+01	7.86E+01	-3.48E-05	1.55E-04	-1.32E-05	-1.34E+01	-9.02E+00	-3.93E+01	-2.92E+01	3.70E+02	-6.46E+01
-2.72E-05	1.13E+02	-2.25E+02	-4.27E+02	-2.18E+03	-1.09E+03	5.06E-06	-4.49E-05	4.40E-05	4.98E+03	-1.05E+03	-5.26E+02	2.21E-05	-1.13E+02	2.25E+02	-4.27E+02	-2.18E+03	-1.09E+03
-4.34E+02	-5.46E+01	5.31E+01	-6.22E+01	3.30E+01	1.04E+02	-3.78E-04	7.68E-05	2.28E-04	-1.05E+03	4.38E+03	-5.25E+03	4.34E+02	5.46E+01	-5.31E+01	-6.22E+01	3.30E+01	1.04E+02
8.68E+02	2.68E+01	5.46E+01	-3.11E+01	1.04E+02	-1.23E+02	5.57E-04	-3.16E-04	1.13E-05	-5.26E+02	-5.25E+03	1.23E+04	-8.68E+02	-2.68E+01	-5.46E+01	-3.11E+01	1.04E+02	-1.23E+02
						-1.50E+02	-2.68E+01	-1.34E+01	9.98E-06	4.34E+02	-8.68E+02	1.50E+02	2.68E+01	1.34E+01	-7.28E-05	-4.59E+01	9.19E+01
						-2.68E+01	-5.28E+01	-9.02E+00	-1.13E+02	5.46E+01	-2.68E+01	2.68E+01	5.28E+01	9.02E+00	-1.46E+01	-6.46E+01	4.66E+02
						-1.34E+01	-9.02E+00	-3.93E+01	2.25E+02	-5.31E+01	-5.46E+01	1.34E+01	9.02E+00	3.93E+01	2.92E+01	-3.70E+02	6.46E+01
						8.20E-05	1.46E+01	-2.92E+01	-4.27E+02	-6.22E+01	-3.11E+01	-8.20E-05	-1.46E+01	2.92E+01	6.95E+02	-2.88E+02	-1.44E+02
						4.59E+01	6.46E+01	3.70E+02	-2.18E+03	3.30E+01	1.04E+02	-4.59E+01	-6.46E+01	-3.70E+02	-2.88E+02	4.23E+03	-5.42E+02
						-9.19E+01	-4.66E+02	-6.46E+01	-1.09E+03	1.04E+02	-1.23E+02	9.19E+01	4.66E+02	6.46E+01	-1.44E+02	-5.42E+02	5.05E+03

Validation

We use Design II as the example to compare the direct compliance calculation method and FEM. Monte Carlo simulation is used to generate random geometric variations and then calculate the compensating force and moment by the two approaches. The result is shown in Figure 3.14, in which **X** is the index for geometric variation at one end of the tube with the other end fixed. The statistics for 1**X** is shown Table 3.4, where the bottom row contains the standard deviations of the geometric variations normalized by the tube dimensions. For multiple **X**, the statistics are multiplied according to the factor. For example, 2**X** means that the standard deviations in the table are doubled.

Table 3.4: Statistics on the geometric variations

Variation	dx	dy	dz	δx	δy	δz
Mean	0	0	0	0	0	0
Standard Deviation	0.1"	0.1"	0.1"	1°	1°	1°
Tube dimension	30"	20"	10"	30"	20"	10"
X	0.0033	0.005	0.01	0.0333 (°/inch)	0.05 (°/inch)	0.1 (°/inch)

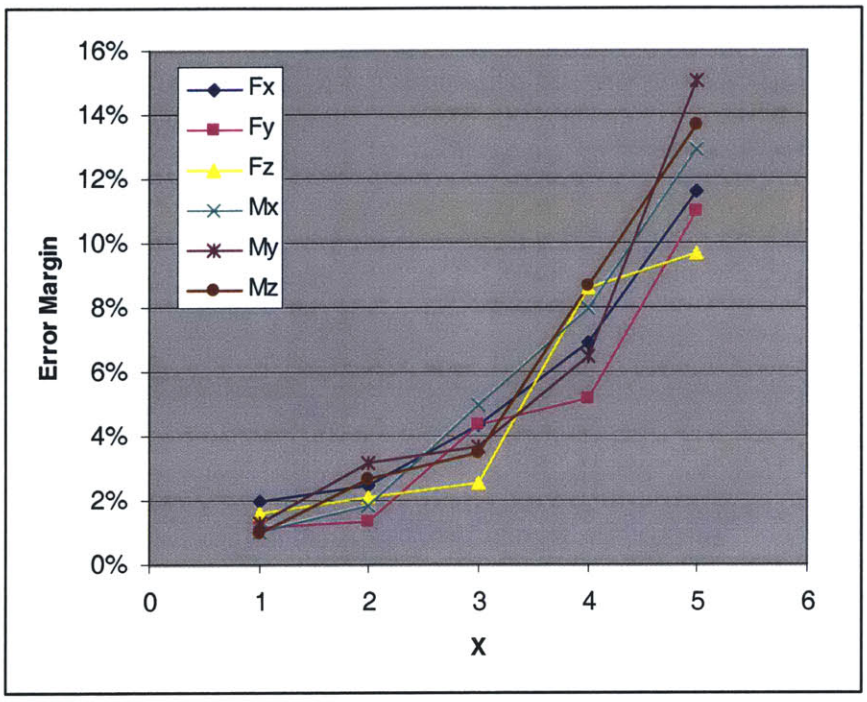

Figure 3.14: Simulation results from direct compliance calculation method and the FEM

From the plot it can be seen that the two methods have close results. However, the error increases nonlinearly as the level of variation increases. This is because the direct compliance calculation method us the stiffness matrix of the nominal shape of the tube as an approximation. When the geometric variation becomes large, this approximation becomes less accurate. The advantage of the direct compliance method is the computation time. For each simulation run, it only takes less than a second, while the FEM approach needs 10 seconds, not including the modeling time.

Generalization

This direct compliance calculation method can be extended to other cases where the parts can be decomposed into several standardized sections. For example, the sheet metal in Figure 3.15 can be dissected into several plates thus its stiffness matrix can be calculated directly.

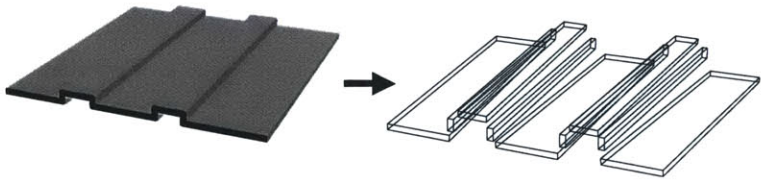

Figure 3.15: Another example of compliant part whose stiffness matrix can be calculated directly from matrix operations

3.5 YIELD RATES PREDICTION

3.5.1 Simulation with Numerical Method

One of the commonly used inspection methods is the gauge fitting. A part is rejected if it cannot fit in the gauges even with minor adjustment. Because of the complexity of the geometric relationship, the yield rate of such inspection cannot be derived in a close-form equation and numerical simulation is necessary. We use the tube inspection after the bending operation to illustrate the method.

Representation

Consider a tube inspected with multiple gauges with minor adjustment as shown in Figure 3.16. Let the actual position and orientation of one inspection point on the tube before adjustment be $\mathbf{t}_0^*$ and $\mathbf{o}_t^*$, where $\mathbf{t}_0^* = (t_0^{x*}, t_0^{y*}, t_0^{z*})$ and $\mathbf{o}_t^* = (o_t^{x*}, o_t^{y*}, o_t^{z*})$ represent the location and directional cosine in the global coordinate frame. The nominal position and orientation of the inspection point on the tube are $\mathbf{g}_0$ and $\mathbf{o}_g$, where $\mathbf{g}_0 = (g_0^x, g_0^y, g_0^z)$ and $\mathbf{o}_g = (o_g^x, o_g^y, o_g^z)$. The diameter of the tube is D, and the length and diameter of the gauge are L and c, respectively. The gauge is located and oriented according to the nominal inspection point on the tube.

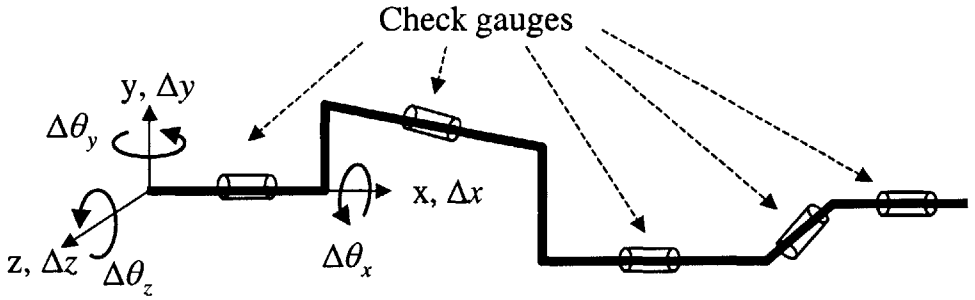

Figure 3.16: Schematic representation of the multi-gauge inspection with minor adjustment

The nominal inspection point and orientation, $\mathbf{g}_0$ and $\mathbf{o}_g$, can be calculated from the matrix transforms in Equation (3.4). The actual position and orientation of the inspection point before adjustment, $\mathbf{t}_0^*$ and $\mathbf{o}_t^*$, can be calculated from $\mathbf{g}_0$ and $\mathbf{o}_g$ plus the variations obtained from Equation (3.5), *i.e.*,

$$\mathbf{t}_0^* = \mathbf{g}_0 + d\mathbf{P} \tag{3.34}$$

$$\mathbf{o}_t^* = \mathbf{o}_g + \boldsymbol{\delta} \tag{3.35}$$

Let the adjustment in the six degree-of-freedom from the origin of the global coordinate frame to fit the tube into the gauge be Δx, Δy, Δz, $\Delta\theta_x$, $\Delta\theta_y$ and $\Delta\theta_z$. Define $\boldsymbol{\delta}_{\mathrm{A}} = \begin{pmatrix} 1 & -\Delta\theta_z & \Delta\theta_y \\ \Delta\theta_z & 1 & -\Delta\theta_x \\ -\Delta\theta_y & \Delta\theta_x & 1 \end{pmatrix}$ and $d\mathbf{P}_{\mathrm{A}} = \begin{pmatrix} \Delta x \\ \Delta y \\ \Delta z \end{pmatrix}$, then the position and orientation of the inspect point after adjustment become

$$\mathbf{t}_0 = \mathbf{t}_0^* + d\mathbf{P}_{\mathrm{A}} + \delta_A \times \mathbf{t}_0^* \tag{3.36}$$

$$\mathbf{o}_t = \boldsymbol{\delta}_{\mathrm{A}} \mathbf{o}_t^* \tag{3.37}$$

Figure 3.17 shows the enlarged local scheme around the inspection point, where $\mathcal{A}$ and $\mathcal{B}$ are the end planes on the gauge, with the center points $\mathbf{g}_1$ and $\mathbf{g}_2$, respectively. The two points, $\mathbf{t}_1$ and $\mathbf{t}_2$, are the intersections of the tube centerline with $\mathcal{A}$ and $\mathcal{B}$. Let $\mathbf{g}_1 = (g_1^x, g_1^y, g_1^z)$, $\mathbf{g}_2 = (g_2^x, g_2^y, g_2^z)$, $\mathbf{t}_1 = (t_1^x, t_1^y, t_1^z)$, and $\mathbf{t}_2 = (t_2^x, t_2^y, t_2^z)$, they can be solved from the following equations:

$$\mathbf{g}_1 = \mathbf{g}_0 + \frac{L}{2}\mathbf{o}_g \tag{3.38}$$

$$\mathbf{g}_2 = \mathbf{g}_0 - \frac{L}{2}\mathbf{o}_g \tag{3.39}$$

$$\frac{t_1^x - t_0^x}{o_t^x} = \frac{t_1^y - t_0^y}{o_t^y} = \frac{t_1^z - t_0^z}{o_t^z} \tag{3.40}$$

$$o_g^x\left(t_1^x - g_1^x\right) + o_g^y\left(t_1^y - g_1^y\right) + o_g^z\left(t_1^z - g_1^z\right) = 0 \tag{3.41}$$

$$\frac{t_2^x - t_0^x}{o_t^x} = \frac{t_2^y - t_0^y}{o_t^y} = \frac{t_2^z - t_0^z}{o_t^z} \tag{3.42}$$

$$o_g^x\left(t_2^x - g_2^x\right) + o_g^y\left(t_2^y - g_2^y\right) + o_g^z\left(t_2^z - g_2^z\right) = 0 \tag{3.43}$$

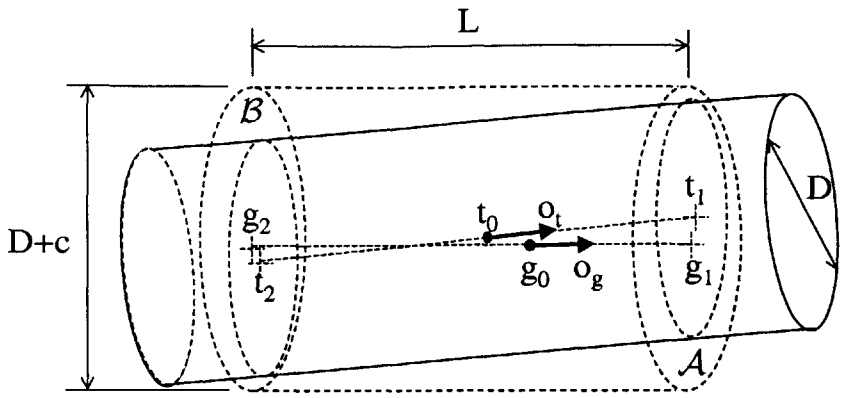

Figure 3.17: Schematic representation of gauge-tube fitting

Noninterference Criteria

If c<<L, then the intersections of the outer surface of the tube and the two end planes of the gauge, $\mathcal{A}$ and $\mathcal{B}$, are approximately circular with diameters of D. In this case, the criteria for noninterference fitting are when both of the intersected circles fall inside the end circles of the gauge, *i.e.*,

$$\left|\mathbf{t}_1 - \mathbf{g}_1\right| \le \frac{c}{2} \tag{3.44}$$

$$\left|\mathbf{t}_2 - \mathbf{g}_2\right| \le \frac{c}{2} \tag{3.45}$$

Finding the Feasible Adjustment

Repeat the foregoing procedures to obtain the noninterference criteria at each inspection point. Once the criteria are established, the inspection result with minor adjustment can be simulated by solving the following optimization problem, assuming that there are K inspection points.

$$\begin{aligned} &\underset{\delta_A, d\mathbf{P}_A}{Min} \quad Null \\ &S.T. \quad \left|\mathbf{t}_{1i} - \mathbf{g}_{1i}\right| \le \frac{c_i}{2} \\ &\qquad \left|\mathbf{t}_{2i} - \mathbf{g}_{2i}\right| \le \frac{c_i}{2} \\ &for \quad 1 \le i \le K \end{aligned}$$

Solving the optimization problem above is to find a feasible set of the adjustment that can fit the tube into the gauges without any interference. Therefore, if a feasible solution can be found, the tube is acceptable, otherwise the tube should be rejected. Figure 3.18 shows an example of a tube with geometric variations that can fit in the

gauges after the adjustment found from the optimization problem. This method is easy to implement because there are many software packages for solving such optimization problem, such as MS Excel.

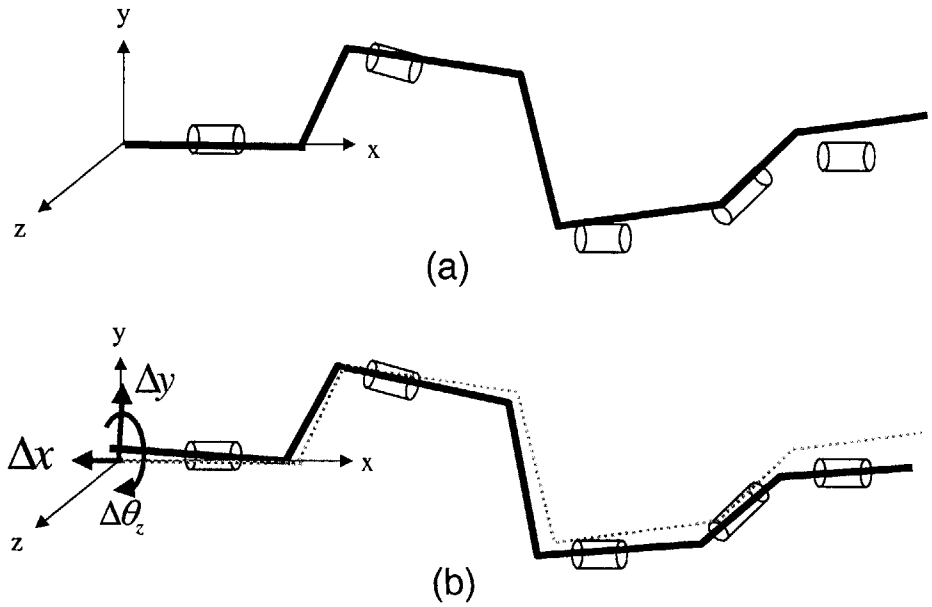

Figure 3.18: (a) A tube deviates from its nominal shape and cannot fit in the gauges (b) After the adjustment of rotating clockwise, moving upward and to the left, the tube can fit in the gauges and pass the inspection

Predicting Yield Rates by Simulation

Assume that in the assembly operation, the acceptance criteria are the direct upper and lower limits on the key characteristics, *i.e.* $\mathbf{Z}_{min} \leq \mathbf{Z} \leq \mathbf{Z}_{max}$. Then through the combination of Monte Carlo simulation and numerical optimization, the yield rates in the tube bending and assembly operations can be estimated. Figure 3.19 illustrates the procedures.

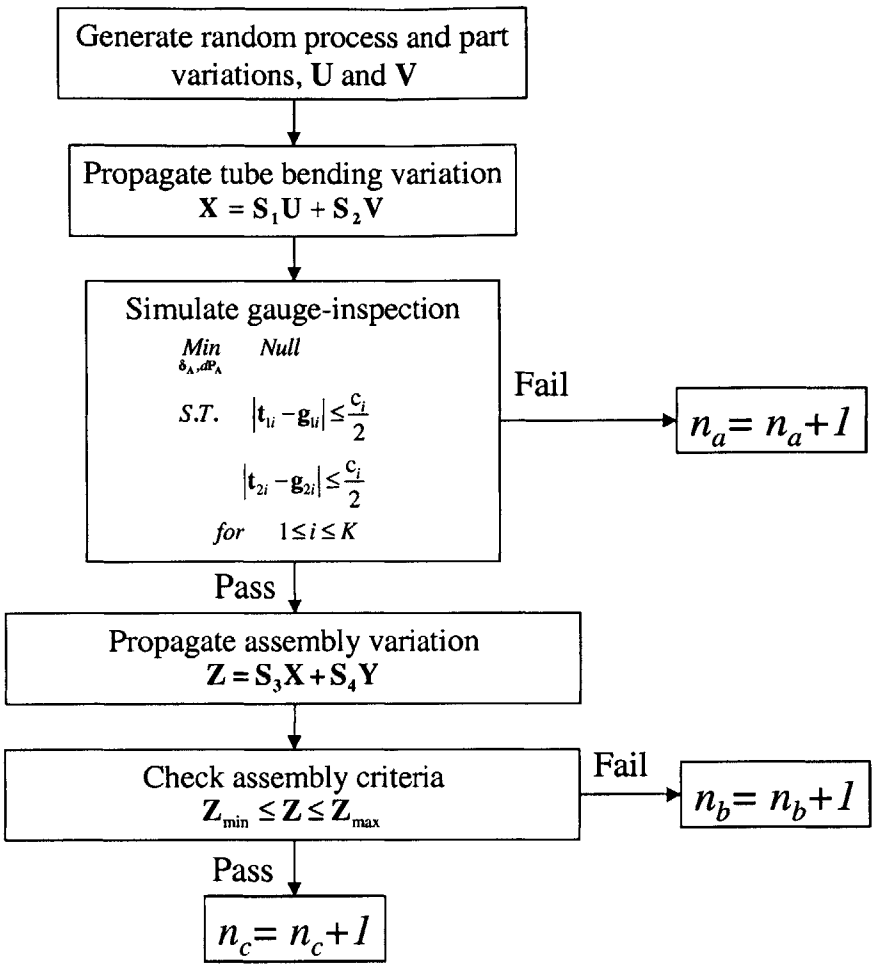

Figure 3.19: Yield rates prediction through Monte Carlo Simulation

In the figure above, n_a, n_b and n_c are the counters for rejected tube in tube bending, rejected tube in assembly, and accepted tubes in assembly, respectively. Random numbers are generated for the part and process variations as the input. These variations are propagated into the positions and orientations variations on the inspect points, then the optimization problem is used to simulate the inspection. If the feasible solution cannot be found, the tube is rejected and the counter n_a increases by one. Otherwise the variations propagate into variations in the assembly load or the assemble-part geometry. The variations in the assembly operation are checked by the acceptance criteria. If the criteria are not satisfied, the tube is rejected and n_b increases by one, otherwise the tube assembly is successful and n_c increases by one. The yield rate in tube bending operation, y_1, is estimated by $y_1 = \frac{n_b + n_c}{n_a + n_b + n_c}$. The yield rate in assembly operation, y_2, is estimated by $y_2 = \frac{n_b}{n_b + n_c}$.

Example

We use Design I in Figure 3.2 to exemplify this method. The statistics on the process variations are the same as Table 3.3. There are three gauges to validate the tube after the tube bending process. These gauges are located at the center of the three horizontal sections of the tube, as shown in Figure 3.20.

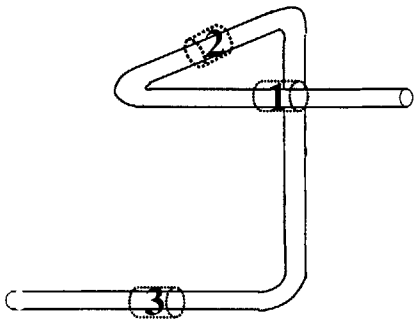

Tube diameter D=0.5"
Gauge length L=1.5"
Gauge clearance C=0.01"~0.1"

Figure 3.20: Gauge inspection for Design I

There are two install points in tube assembly: the two ends of the tube. The statistics for the geometric variations of the mating structure on install points are summarized in Table 3.5, where the bottom row contains the standard deviations of the structure variations normalized by the tube dimensions. The acceptance criterion for tube assembly is based on the assembly load, which requires that the resultant force in X, Y, Z directions at each install point cannot exceed 10 lbs, *i.e.* $\sqrt{F_x^2 + F_y^2 + F_z^2} \leq 10\ lbs$.

Table 3.5: Statistics on structure variations

Structure Variation	dx	dy	dz	δx	δy	δz
Mean	0	0	0	0	0	0
Standard Deviation	0.1"	0.1"	0.1"	3°	3°	3°
Tube dimension	30"	20"	10"	30"	20"	10"
Normalized S.D.	0.0033	0.005	0.01	0.1 (°/inch)	0.15 (°/inch)	0.3 (°/inch)

The simulation results for the inspections are shown in Figure 3.21. We vary the gauge clearance from 0.01 to 0.1 and plot the yield rates in tube bending operation (y_1) and assembly operation (y_2). It can be seen that as the gauge clearance increases (larger tolerance), y_1 increases and y_2 decreases. This is because larger clearance allows more tubes to pass the gauge inspection, but also increases the number of tubes with larger variations proceeded to the assembly operation. As the clearance becomes larger, y_1 approaches 100% and y_2 approaches 64%, which are the yield rates as if there is no inspection after the tube bending operation.

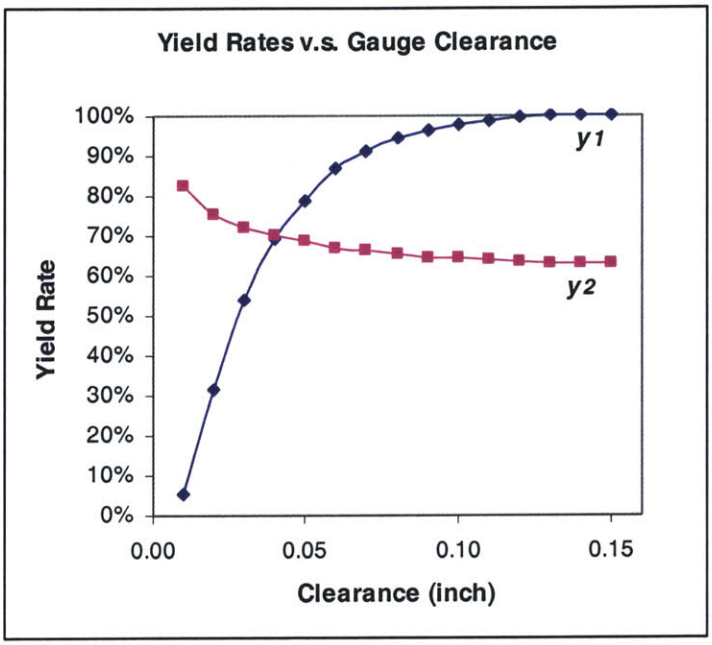

Figure 3.21: Yield rates under different sizes of gauge clearance

Generalization

The previous simulation method for tube inspection can be applied to other cases where the part features are inspected by fitting into the gauges with small kinematic adjustment. The following example illustrates a similar case: A sheet metal (**B**) with two holes needs to be inspected on a fixture (**A**) with two pegs, as shown in Figure 3.15. The holes on **B** are drilled and the locations of the holes are subjected to variations. The relative distance between the two holes is important for downstream operation thus is the key characteristic. The pegs on **A** are used to check this key characteristic and have slightly smaller diameters than their matching holes. During inspection the sheet metal can be moved or rotated to fit onto the pegs.

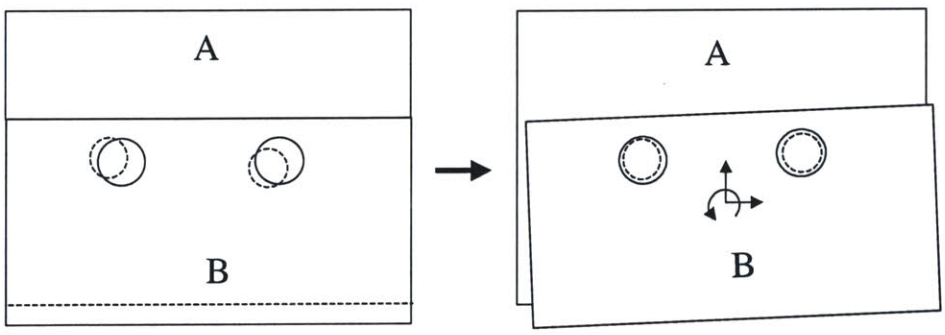

Figure 3.22: Another example of gauge inspection

The inspection result can be simulated as long as the positions and orientations of the features (the holes on **B**) and the gauges (the pegs on **A**) are modeled and the noninterference criteria for all the feature-gauge mates are constructed.

3.5.2 Gaussian Approximation

When the inspection method uses tolerance on the key characteristics, the analytical solution for the yield rate can be obtained. Assume that there is no inspection in tube bending operation and the tolerance set is imposed on the assembly load in the tube assembly operation. To predict the assembly yield rate, we need to know the statistical distribution of the assembly loads. Having the variation propagation models, we can predict the tube geometric variation, **X**, and the stiffness matrix, $\mathbf{K}_1$. Assuming that the structure variation, **Y**, and the stiffness matrix, $\mathbf{K}_2$, are known, the assembly loads at each install points can be predicted.

Case I: Rigid Mating Structure

In most cases the mating structure can be assumed rigid, *i.e.*, $\mathbf{K}_2 >> \mathbf{K}_1$. Therefore, Equation (3.25) becomes $\upsilon = \mathbf{Y}$, *i.e.*, the variation in final assembly equals the structure variation. Plugging $\upsilon = \mathbf{Y}$ in Equation (3.30), we get

$$\begin{aligned} \mathbf{Z} &= \mathbf{K}_1(\upsilon - \mathbf{X}) \\ &= \mathbf{K}_1(\mathbf{Y} - \mathbf{X}) \\ &= \mathbf{K}_1\mathbf{Y} - \mathbf{K}_1\mathbf{S}_1\mathbf{U} - \mathbf{K}_1\mathbf{S}_2\mathbf{V} \end{aligned} \tag{3.46}$$

$$E(\mathbf{Z}) = -\mathbf{K}_1\mathbf{S}_1E(\mathbf{U}) - \mathbf{K}_1\mathbf{S}_2E(\mathbf{V}) + \mathbf{K}_1E(\mathbf{Y}) \tag{3.47}$$

Assuming that **U**, **V**, and **Y** are independent and are normally distributed, then we can obtain

$$\begin{aligned} Var(\mathbf{Z}) = {} & \mathbf{K}_1\mathbf{S}_1Var(\mathbf{U})(\mathbf{K}_1\mathbf{S}_1)^T \\ & + \mathbf{K}_1\mathbf{S}_2Var(\mathbf{V})(\mathbf{K}_1\mathbf{S}_2)^T \\ & + \mathbf{K}_1Var(\mathbf{Y})\mathbf{K}_1^T \end{aligned} \tag{3.48}$$

$$pdf(\mathbf{Z}) = \frac{\exp(-\frac{1}{2}(\mathbf{Z} - E(\mathbf{Z}))^T Var(\mathbf{Z})^{-1}(\mathbf{Z} - E(\mathbf{Z})))}{\left(\sqrt{2\pi}\right)^{6n}\sqrt{|Var(\mathbf{Z})|}} \tag{3.49}$$

where n is the number of mating features. Let the tolerance set for assembly load on the assembled part be (**LSL**, **USL**), then the assemblability under geometric tolerance is

$$y_2 = \int_{\mathbf{LSL}}^{\mathbf{USL}} pdf(\mathbf{Z})d\mathbf{Z} \tag{3.50}$$

Case II: Non-rigid Mating Structure

Similar analysis can apply to the case where the mating structure is non-rigid, such as tube-to-tube assembly, compliant bracket at tiedowns, etc. In such cases, defining $\boldsymbol{\kappa}_U = (\mathbf{K}_1\mathbf{C}_1 - \mathbf{K}_1)\mathbf{S}_1$, $\boldsymbol{\kappa}_V = (\mathbf{K}_1\mathbf{C}_1 - \mathbf{K}_1)\mathbf{S}_2$, and $\boldsymbol{\kappa}_Y = \mathbf{K}_1(\mathbf{K}_1 + \mathbf{K}_2)^{-1}\mathbf{K}_2$, we get

$$\mathbf{Z} = \boldsymbol{\kappa}_U\mathbf{U} + \boldsymbol{\kappa}_V\mathbf{V} + \boldsymbol{\kappa}_Y\mathbf{Y} \tag{3.51}$$

$$E(\mathbf{Z}) = \boldsymbol{\kappa}_U E(\mathbf{U}) + \boldsymbol{\kappa}_V E(\mathbf{V}) + \boldsymbol{\kappa}_Y E(\mathbf{Y}) \tag{3.52}$$

$$Var(\mathbf{Z}) = \boldsymbol{\kappa}_U Var(\mathbf{U})\boldsymbol{\kappa}_U^T + \boldsymbol{\kappa}_V Var(\mathbf{V})\boldsymbol{\kappa}_V^T + \boldsymbol{\kappa}_Y Var(\mathbf{Y})\boldsymbol{\kappa}_Y^T \tag{3.53}$$

Plugging Equation (3.52) and (3.53) in (3.49), the assembly yield rate for non-rigid structure can be calculated in Equation (3.50).

Example

We use Design I and Design II in Figure 3.2 as an example. Assume the mating structure is rigid and no inspection after the tube bending operation. Using Equation (3.47)-(3.49) for both designs, we can predict the assembly yield rates under different levels of the structure variation.

The statistics of the process and structure variations are the same as Table 3.3 and Table 3.5, and the results are plotted in Figure 3.23. In the figure, **Y** is the index for the structure variation, in which 2**Y** means the standard deviations of the structure variations are twice as much as the ones in Table 3.5.

It can be seen that for Design I, the maximum yield is 79% when no structure variations exist, *i.e.*, the only effect is the tube variations. The yield declines as the structure variations increase, and reaches 56% at the estimated structure variation **Y**. The yield hits the minimum acceptable yield of 50% at 1.3**Y**, which is the maximum level of structure variations the tube can absorb. For Design II, the maximum yield is 97% without structure variations. The yield declines rapidly as the structure variations increase, falling below 50% at 0.8**Y**. At the estimated structure variation **Y**, the yield is only 28%. It approaches zero after 2.5**Y**.

The results show that Design II is more robust before 0.4**Y**, but after that Design I is more robust. This is because Design I is more compliant than Design II but also has one more bend that introduce more process variation. Therefore, when the structure variation is small (<0.4**Y**), the process variation dominates and Design I is more variable than Design II. As the result, the assemblability of Design I is inferior to Design II's. When structure variation increases and dominates (>0.4**Y**), the process variation becomes insignificant compared to structure variation and the design with more compliance to absorb the structure variation is more robust. Therefore, Design I has better assemblability than Design II.

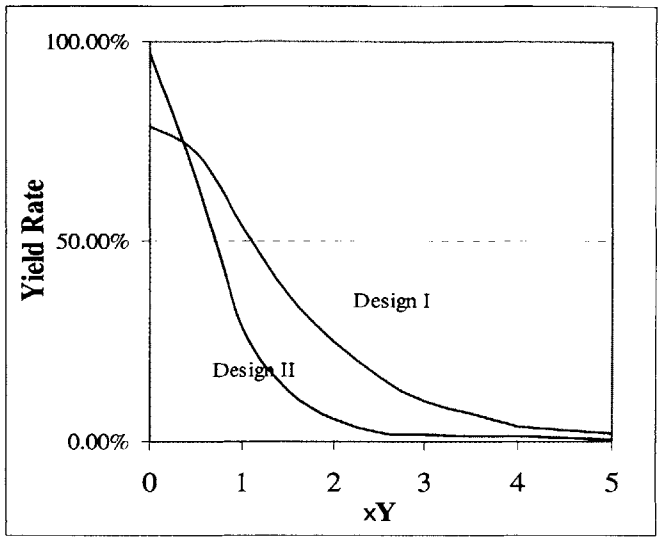

Figure 3.24: Assembly yield rates of the two designs under different levels of structure variations

3.6 CHAPTER SUMMARY

This chapter presents a variation model for compliant tube manufacturing and assembly, and uses an analytical approach to predict the geometrical variation, and compliance of tubes. Manufacturing and assembly yield rates are predicted through simulation. Gaussian approximation method is also used to calculate the yield rate in some restricted situations. The proposed approach significantly reduces the dependency on simulation and thus minimizes the computational efforts. Generalization of the approach is also discussed.

CHAPTER 4 PRODUCTION PREDICTION AND INVENTORY CONTROL IN AIRCRAFT TUBE PRODUCTION SYSTEMS

4.1 INTRODUCTION

In Chapter 1 we briefly introduce the characteristics of the tube production system. In this chapter we will elaborate the details and applied the Joint System Performance Model (JSPM) described in Chapter 2 to predict the cycle time performance and the system cost. We first use JSPM to represent the tube production system with inventory controlled by reordering-point (ROP). Secondly, we derive the statistical behavior of the order arrival under such inventory control system. We refer to Chapter 2 for the derivations of the processing aggregation, cycle time and WIP approximation, and system cost estimation. Thirdly, an example of tube production system is used to illustrate the method. Lastly, the extension of Concurrent Optimal Design for a production system with ROP inventory is discussed.

4.2 TUBE PRODUCTION SYSTEM WITH ROP INVENTORY

The demands for tubes are driven by the aircraft demands. Tubes are usually treated as the commodity in aircraft production, and are stored in the inventory controlled by reordering-point (ROP). A ROP inventory has three control variables: Reordering point, reordering quantity, and safety stock. Reordering point is the inventory level when an order should be issued for replenishment. The ROP is determined by the total demand during the time from ordering to delivery, *i.e.*, the manufacturing cycle time, plus the safety stock. The safety stock provides a buffer for demand and delivery uncertainties to prevent backlogs. The uncertainties include unexpected high demand before delivery, late delivery, or fewer delivered quantity than ordered. Figure 4.1 shows the changes in the inventory level and the control variables of a ROP inventory.

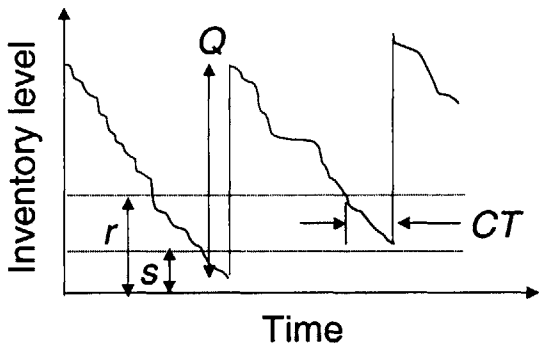

Figure 4.1: Inventory level and the control variables in a ROP inventory

Under such control system, the inventory issues an order of a predetermined quantity to the manufacturing plant when the stock of any of the tubes reaches the reordering point. The order arrives then trigger the tube manufacturing. The time interval between two orders for the same tube type may fluctuate due to the uncertainties in the aircraft

demand, the number of tubes consumed per assembly, and the number of tubes delivered from the manufacturing plant. The number of tubes consumed in assembly depends on the assembly yield rate of the tube. For example, if the assembly yield rate is only 50%, two tubes on average will be needed for one assembly. The number of tubes delivered from the manufacturing plant maybe lower to the ordered quantity, because of the yield loss during the manufacturing process. In general, the lower the assembly and manufacturing yield rates are, the more frequent the tubes will be ordered.

4.2.1 Model

The complete tube manufacturing process varies for different types of tube. Most includes four to five stages: tube bending for the desired tube shape, sawing and deburring to cut off the extra length, welding or swaging to mount the connectors onto the tubes, marking and final test to identify the tubes and detect any functionality problems (*e.g.*, leakage), and sometimes painting for erosion resistance. Figure 4.2 shows the schematic representation of the tube production system.

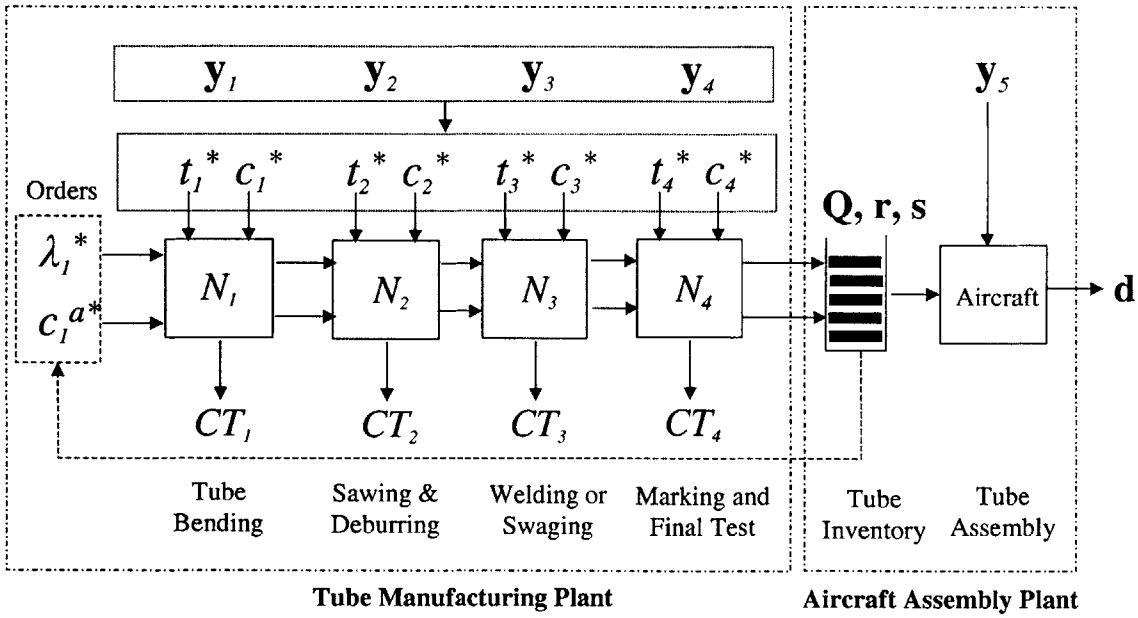

Figure 4.2: Representation of the queuing model for a tube production system with ROP Inventory

In the Figure 4.2, **d** is the vector of aircraft demands that comprises the average demands for all the aircrafts produced in the assembly plant. In the aircraft assembly plant, $\mathbf{y_5}$ is the vector of assembly yield rates, **Q**, **r** and **s** are the vector of reordering

quantity, vector of reordering point, and vector of safety stocks for all types of tubes, respectively[12].

In the tube manufacturing plant, $\mathbf{y}_1$ through $\mathbf{y}_4$ are the vector of yield rates for all the tubes processed at each of the manufacturing operations[13]. Other variables, including number of machines (N_i), aggregated average arrival rate the SCV of inter-arrival time (λ_1^* and c_1^{a*}), aggregated mean and SCV of processing time (t_i^* and c_i^*), and cycle time (CT_i) are the same as described in Section 2.3.2 of Chapter 2.

4.2.2 Inventory Control, Quality, and Cycle Time

It is noteworthy that the decision on the inventory control variables, **Q**, **r** and **s** are interdependent with the system performances of the manufacturing plant. We will discuss them as follows.

Ordering quantity influences cycle time. In Section 2.3.2 we can see that the batch-sizes affect the mean cycle time at each manufacturing stage. In general, large batch-sizes reduce the setups but increase the batch waiting. Therefore, they can be optimized to minimize the mean cycle time.

Cycle time influences reordering point and safety stock. The overall manufacturing cycle time determines the reordering point because the inventory needs to be sufficient to satisfy the tube demands before the tubes are delivered. In addition, longer mean manufacturing cycle time usually has larger variance, *i.e.*, delivery uncertainty, which results in the larger safety stock.

Yield rates influences reordering point and safety stock. The manufacturing and assembly yield rates also influence the inventory control variables. For example, low yield rates will either lead to larger ordering quantity to compensate the yield loss, which in turn influence the cycle time, reordering point and safety stock. In addition, lower yield rates increase the uncertainty in the delivered quantity, thus lead to larger safety stock.

4.3 ORDER ARRIVALS

The order arrival process for tube manufacturing depends on four variables: demand rate for aircrafts, ordering quantity, manufacturing yield rate, and assembly yield rate. Let the mean arrival rate and SCV of the inter-arrival time of the batch order for a tube type be λ and c^a, the mean demand rate and SCV of the demand interval for the aircrafts that need a certain type of tube be d and c^d, the ordering quantity be Q, the manufacturing yield rates be y_1 to y_4, and assembly yield rate be y_5.

---

[12] For m types of tubes in the system, $\mathbf{d} = (d_1, d_2, \ldots, d_m)$, $\mathbf{Q} = (Q_1, Q_2, \ldots, Q_m)$, $\mathbf{r} = (r_1, r_2, \ldots, r_m)$, $\mathbf{s} = (s_1, s_2, \ldots, s_m)$, and $\mathbf{y}_a = (y_a^1, y_a^2, \ldots, y_a^m)$

[13] Similarly, $\mathbf{y}_1 = (y_1^1, y_1^2, \ldots, y_1^m)$, etc.

4.3.1 Demand Satisfied per Order Delivery

We first want to find out how many demands of tubes can be satisfied with the ordering quantity of Q. Let n be the number of demands satisfied per delivered order. The derivation for n is similar to the multi-stage binomial process as described in Equation (2.13) and (2.16). Assuming that the number of tubes successfully passing through each stage is independent from each other, and letting $Y = \prod_{i=1}^{5} y_i$, we have,

$$E(n) = QY \tag{4.1}$$

$$Var(n) = QY(1-Y) \tag{4.2}$$

4.3.2 Mean and Variability of Order Inter-arrival Time

Assuming that the demand for tube is one per aircraft, the mean and variance of the inter-arrival time of the batch order can be expressed as

$$\frac{1}{\lambda} = E\left(\frac{n}{d}\right) = \frac{QY}{d} \tag{4.3}$$

$$\begin{aligned} \frac{c^a}{\lambda^2} &= E(n)\frac{c^d}{d^2} + \frac{1}{d^2}Var(n) \\ &= QY\frac{c^d}{d^2} + \frac{1}{d^2}QY(1-Y) \end{aligned} \tag{4.4}$$

Therefore, the mean arrival rate and SCV of the inter-arrival time for the batch order are

$$\lambda = \frac{1}{t^a} = \frac{d}{QY} \tag{4.5}$$

$$c^a = \frac{c^d + (1-Y)}{QY} \tag{4.6}$$

From the equations above it can be seen that both the mean arrival rate and the inter-arrival variability increases nonlinearly as the yield rates decreases. Furthermore, even though large order quantity can reduce the mean arrival rate and the arrival variability, it also increase the inventory carrying cost thus tradeoffs need to be made.

A reasonable assumption for the demand interval of the aircraft is that it is exponentially distributed. In this case the SCV of the demand interval, c^d, equals one, and Equation (4.6) becomes

$$c^a = \frac{2-Y}{QY} \tag{4.7}$$

The foregoing procedure gives the arrival rate and variability of a single tube type. To obtain the aggregated arrival rate and variability, λ_1^* and c_1^{a*}, as described in Equation (2.11) and (2.12), the procedure needs to be repeated for all the tube types manufactured in the plant.

4.4 PROCESSING AGGREGATION, CYCLE TIME, WIP AND COST

The mean and the variability ($t_1^* \sim t_4^*, c_1^* \sim c_4^*$) of the aggregated processing time at each of the four manufacturing stages can be calculated through the procedure described in Section 2.3.2.3. Similarly, the cycle time and WIP at each manufacturing stage can be calculated as described in Section 2.3.2.4 and 2.3.2.5. Finally, the system cost can be predicted as describe in Section 2.4.

4.5 INVENTORY CONTROL VARIABLES

From the previous sections it can be seen that there is a corresponding overall manufacturing cycle time for any reordering quantity. Once the cycle time is calculated, the reordering point and safety stock can be determined accordingly. Since the reordering point is the inventory level that can satisfy the demand during the cycle time plus the safety stock, it can be calculated by

$$r = \frac{d}{y_5} \cdot CT + s, \quad r < Q + s \tag{4.8}$$

There are many complex ways to determine safety stock based on the manufacturing cycle time and demand uncertainties (Eppen and Martin 1988, Fotopoulos *et. al.* 1988). In general, the larger the mean cycle time is, the larger the safety stock will be needed. Therefore, the simplest way to determine it is assigning a coefficient to the total demand during the cycle time, *i.e.*,

$$s = e \cdot d \cdot CT \tag{4.9}$$

where e is the safety coefficient. Equation (4.8) can be rewritten as

$$r = \frac{d}{y_5} \cdot CT \cdot (1+e) \tag{4.10}$$

In summary, the procedure to determined the control variables for ROP inventory is as follows:

- Determine the reordering quantity
- Predict the corresponding manufacturing cycle time

- From the cycle time, calculate the reordering point and safety stock

4.6 EXAMPLE

We use a specific tube line to illustrate the foregoing procedure. This line manufactures approximately 1,388 types of tubes. The order for each type of tube arrives every 20 to 164 days, with batch-sizes ranging from 1 to 37. We demonstrate the procedure by the following steps: arrival aggregation, batch processing time calculation for single parts, processing time aggregation, cycle time and WIP prediction, determination of inventory control variables, and system costs calculation.

4.6.1 Arrival Aggregation

The table bellow shows a portion of the total order arrivals for all tube types. The mean order arrival rate and the SCV of the inter-arrival time for each tube type are estimated by using Equation (4.5) and (4.7). For example, the batch arrival rate for part 1 is calculated by

$$\frac{0.69}{17 \cdot 90\%} = 0.0441$$

and the SCV of inter-arrival time is

$$\frac{2 - 90\%}{17 \cdot 90\%} = 0.0702$$

On top of the table, the aggregated arrival rate and the SCV of inter-arrival time for the product line are calculated based on all the 1,388 tube types through the procedure described in Section 2.3.2.2. In this example, the aggregated arrival rate is

$$\underbrace{0.0441 + 0.0391 + \cdots}_{\text{All 1,388 tube types}} = 28.1583$$

and the SCV of aggregated inter-arrival time is

$$\frac{0.0441 \cdot 0.0702 + 0.0391 \cdot 0.0664 + \cdots}{28.1583} = 0.1278$$

All the estimations are compared with the actual data. It can be seen that the estimation for mean arrival rate is more accurate than the estimation for the SCV of inter-arrival time (7% versus 22%). There are two possible reasons for the wider error margin in the latter. First, the actual variability in the demand interval may be larger than the variability from the assumption of exponential distribution. Second, since the mean arrival rates for the tubes are somewhat heterogeneous (0.05 to 0.006 orders/day), the approximation tends to be underestimated as discussed in Section 2.3.2.2.

Table 4.1: A portion of the overall order arrivals for the example product line

Aggregated			30.2312	28.1583	7%		0.1633	0.1278	22%	
	demand rate	Mean overall	Arrival rate (batch orders/day)			weight	SCV of Inter-arrival time			Ordering
Part #	(tubes/day)	yield rate	Actual	Estimated	Error		Actual	Estimated	Error	batch-size
1	0.69	90%	0.0433	0.0441	2%	0.0015	0.0797	0.0702	12%	17
2	0.69	96%	0.0413	0.0391	5%	0.0015	0.0675	0.0664	2%	18
3	0.69	87%	0.0414	0.0438	6%	0.0015	0.0717	0.0674	6%	18
4	0.69	92%	0.0435	0.0430	1%	0.0015	0.1068	0.0701	34%	17
5	0.69	93%	0.0406	0.0398	2%	0.0014	0.0888	0.0656	26%	19
6	0.69	91%	0.0430	0.0430	0%	0.0015	0.2417	0.0692	71%	18
7	0.69	98%	0.0402	0.0402	0%	0.0014	0.0733	0.0698	5%	18
8	0.69	99%	0.0419	0.0386	8%	0.0015	0.1541	0.0678	56%	18
9	0.69	100%	0.0435	0.0415	4%	0.0015	0.1534	0.0736	52%	17
10	0.69	95%	0.0439	0.0418	5%	0.0016	0.1010	0.0703	30%	17
11	0.69	85%	0.0423	0.0448	6%	0.0015	0.0752	0.0675	10%	18
12	0.69	87%	0.0407	0.0425	4%	0.0014	0.0580	0.0654	13%	19
13	0.69	94%	0.0431	0.0422	2%	0.0015	0.0873	0.0702	19%	17
14	0.69	86%	0.0401	0.0427	7%	0.0014	0.1259	0.0650	48%	19
15	0.69	94%	0.0404	0.0392	3%	0.0014	0.1485	0.0653	56%	19
16	0.69	89%	0.0407	0.0414	2%	0.0014	0.0709	0.0653	8%	19
17	0.69	98%	0.0435	0.0405	7%	0.0015	0.0821	0.0702	14%	17
18	0.69	97%	0.0451	0.0424	6%	0.0016	0.2130	0.0729	66%	17
19	0.69	92%	0.0437	0.0430	2%	0.0016	0.0964	0.0701	27%	17
20	0.69	99%	0.0413	0.0385	7%	0.0015	0.0614	0.0674	10%	18
⋮	⋮	⋮	⋮	⋮	⋮	⋮	⋮	⋮	⋮	⋮
⋮	⋮	⋮	⋮	⋮	⋮	⋮	⋮	⋮	⋮	⋮

4.6.2 Batch Processing Time

Table 4.2 shows an example for the calculation of the mean and SCV of the batch processing time for a single tube type. The yield rate, the mean and SCV of the batch setup time and single-part processing time at each workstation are obtained from the historical data. The mean and SCV of the arriving batch quantity at each workstation are calculated from Equation (2.13) and (2.17). For example, the mean arriving quantity at the welding/swaging workstation is

$$17 \cdot 95\% \cdot 100\% = 16.15$$

and the SCV is

$$\frac{1-95\% \cdot 100\%}{17 \cdot 95\% \cdot 100\%} + 0 = 0.0031$$

Note that the mean decreases and the SCV increases through the product line because of the yield loss.

Using Equation (2.18) and (2.20), the mean and SCV of the batch processing time of the part at each workstation can be calculated. For example, the mean batch processing time at the welding/swaging workstation is

$$14 + 16.15 \cdot 1.5 = 38.23$$

and the SCV is

$$\left(\frac{14}{38.23}\right)^2 \cdot 1 + \left(\frac{1.5}{38.23}\right)^2 \cdot \left(16.15 \cdot 1 + (16.15)^2 \cdot 0.0031\right) = 0.16$$

Table 4.2: Calculation of the mean and SCV of the batch processing time for a tube type

Part 1	Tube bending	Sawing & deburring	Welding/ swaging	Marking & final test
Mean setup time (min)	20	15	14	20
SCV of setup time	1.00	1.00	1.00	1.00
Mean single-part processing time (min)	1.00	0.50	1.50	1.10
SCV of single-part processing time	1.00	1.00	1.00	1.00
Quantity in batch	17.00	16.15	16.15	15.67
SCV of quantity in batch	0.0000	0.0031	0.0031	0.0049
Mean yield rate	95%	100%	97%	98%
Mean batch processing time (min)	**37.00**	**23.08**	**38.23**	**37.23**
SCV of batch processing time	**0.30**	**0.43**	**0.16**	**0.30**

4.6.3 Processing Time Aggregation

After the mean and SCV of the batch processing time for each tube type at each workstation are obtained, they can be aggregated into the mean and SCV of the processing time per arrival at each workstations. Table 4.3 shows a part of the worksheet for all tube types, where t^b and c^b are the mean and SCV of the batch processing time, respectively. The aggregated mean and SCV are calculated based on the relative arrival rates of all parts as described in Equation (2.21) and (2.24). For example, the aggregated mean batch-processing time at the welding/swaging workstation is

$$\frac{0.0441 \cdot 39.5780 + 0.0391 \cdot 41.0480 + \cdots}{28.1583} = 33.98$$

and the SCV is

$$\frac{0.0441 \cdot (0.0702)^2 \cdot (0.1501 + 1) + 0.0391 \cdot (0.0664)^2 \cdot (0.1409 + 1) + \cdots}{(33.98)^2 \cdot 28.1583} = 0.27$$

Table 4.3: Calculation of the processing time aggregation

		Tube bending		Sawing & deburring		Welding/Swaging		Marking & final test	
Aggregated	**28.1583**	**33.40**	**0.40**	**21.60**	**0.51**	**33.98**	**0.27**	**34.01**	**0.40**
Part #	Arrival rate (batch/day)	t^b	c^b	t^b	c^b	t^b	c^b	t^b	c^b
1	0.0433	37.0000	0.2984	23.5260	0.4144	39.5780	0.1501	37.8193	0.2941
2	0.0413	38.4000	0.2837	24.0160	0.3981	41.0480	0.1409	38.8434	0.2795
3	0.0414	38.1250	0.2877	23.8813	0.4025	40.6438	0.1433	38.5618	0.2834
4	0.0435	37.4400	0.2978	23.5456	0.4137	39.6368	0.1497	37.8603	0.2934
5	0.0406	38.6400	0.2804	24.1336	0.3943	41.4008	0.1388	39.0892	0.2762
6	0.0430	37.6538	0.2946	23.6504	0.4101	39.9512	0.1477	38.0793	0.2903
7	0.0402	37.5000	0.2969	23.5750	0.4127	39.7250	0.1491	37.9218	0.2925
8	0.0419	38.0400	0.2889	23.8396	0.4038	40.5188	0.1441	38.4748	0.2846
9	0.0435	36.6154	0.3107	23.1415	0.4279	38.4246	0.1581	37.0158	0.3063
10	0.0439	37.3846	0.2986	23.5185	0.4146	39.5554	0.1503	37.8036	0.2943
11	0.0423	38.1200	0.2877	23.8788	0.4025	40.6364	0.1434	38.5567	0.2835
12	0.0407	38.6800	0.2798	24.1532	0.3937	41.4596	0.1385	39.1302	0.2757
13	0.0431	37.4000	0.2984	23.5260	0.4144	39.5780	0.1501	37.8193	0.2941
14	0.0401	38.7917	0.2783	24.2079	0.3920	41.6238	0.1375	39.2445	0.2741
15	0.0404	38.7083	0.2794	24.1671	0.3932	41.5013	0.1382	39.1592	0.2753
16	0.0407	38.7200	0.2793	24.1728	0.3931	41.5184	0.1381	39.1712	0.2751
17	0.0435	37.4000	0.2984	23.5260	0.4144	39.5780	0.1501	37.8193	0.2941
18	0.0451	36.7692	0.3083	23.2169	0.4252	38.6508	0.1564	37.1734	0.3038
19	0.0437	37.4400	0.2978	23.5456	0.4137	39.6368	0.1497	37.8603	0.2934
20	0.0413	38.1250	0.2877	23.8813	0.4025	40.6438	0.1433	38.5618	0.2834
⋮	⋮	⋮	⋮	⋮	⋮	⋮	⋮	⋮	⋮
⋮	⋮	⋮	⋮	⋮	⋮	⋮	⋮	⋮	⋮

4.6.4 Cycle Time

Table 4.4 shows the calculation of the mean cycle time. Assuming no batch losses and a stable system, the aggregated batch arrival rate is the same through the line. To obtain the mean cycle time at each workstation, we need to calculate the utilization rates and the arrival variability. The utilization rate is obtained by multiplying the aggregated batch arrival rate and the processing time, then divided by the number of machines, as described in Equation (2.28). For example, the utilization rate at the tube bending workstation is calculated by

$$\frac{28.16 \text{ (batches/day)}}{16 \text{ (operating hours/day)} \times 60 \text{ (min/hour)}} \times 33.40 \text{ (min/batch)} = 97.97\%$$

Using Equation (2.30), the SCV of the inter-arrival time can be estimated by interpolating the SCVs of inter-arrival time and the processing time by the utilization rate of the upstream workstation. For example, the SCV of inter-arrival time at the welding/swaging workstation is

$$(63.36\%)^2 \cdot 0.51 + \left(1 - (63.36\%)^2\right) \cdot 0.39 = 0.44$$

The mean cycle time at each workstation is approximated by Equation (2.32). At the welding/swaging workstation, the mean cycle time is

$$\left(\frac{0.44+0.27}{2}\right)\cdot\left(\frac{99.67\%}{1-99.67\%}\right)\cdot 33.98+33.98=3,717 \text{ (min)}$$

The daily operating hours at the plant is 16 (two shifts), therefore, 3,717 minutes equals 3.87 days.

Table 4.4: Calculation of the mean cycle time at each workstation

	Tube bending	deburring	Welding/ Swaging	test
Aggregated batch arrival rate (batches/day)	28.16	28.16	28.16	28.16
Aggregated batch processing time (min)	33.40	21.60	33.98	34.01
Utilization rate	97.97%	63.36%	99.67%	99.76%
SCV of inter-arrival time	0.13	0.39	0.44	0.27
SCV of aggregated batch processing time	0.40	0.51	0.27	0.40
Number of machines	1	1	1	1
Average cycle time (days)	**0.48**	**0.04**	**3.87**	**5.03**
Total cycle time (days)	**9.42**			

It can be seen that the last two workstations have long cycle times due to the high utilization rates. The estimated mean total cycle time through the product line is 9.42 days, while the actual mean cycle time is 11.82 days thus is error margin is 20%. Figure 4.3 shows the actual distribution of the total cycle time for the product line.

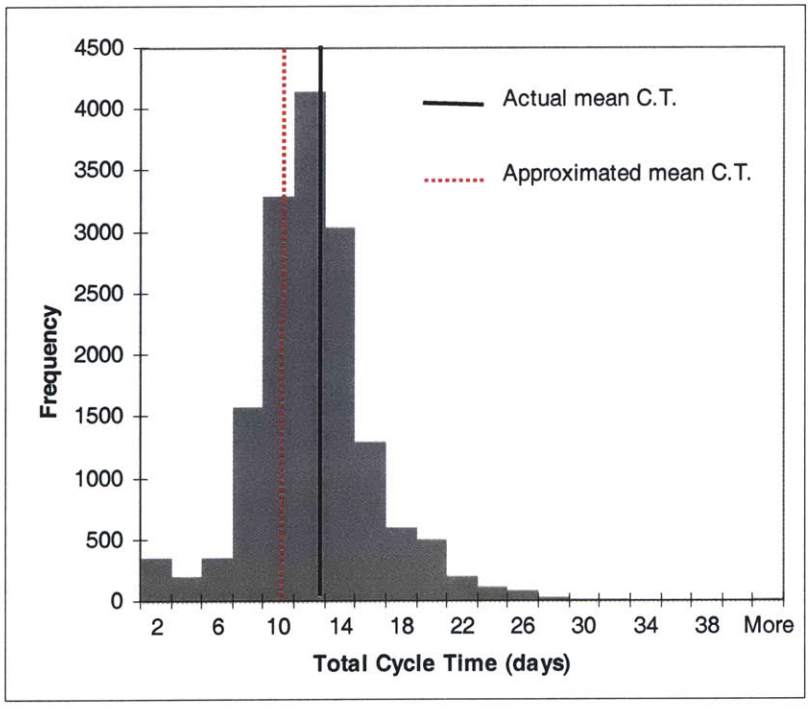

Figure 4.3: Actual distribution of total cycle time

4.6.5 Work-in-Process

Once the cycle time at each workstation is known, the work-in-process can be estimated by Little's Law. Using Equation (2.34), the mean WIPs are calculated for each tube type in the manufacturing plant. The average inventory level in the assembly plant is half of the reordering quantity plus the safety stock, since on average the inventory level runs down from $(Q+s)$ to s between two deliveries.

Table 4.5 shows an example of the WIP calculation. As an illustration, the mean WIP at the welding/swaging workstation is

$$\frac{0.69 \cdot 95\% \cdot 100\%}{90\%} \cdot 3.87 = 2.82$$

The safety stock is 10% of the reordering quantity, therefore, the average inventory level equals $\frac{17}{2} + 17 \cdot 10\% = 10.2$.

Table 4.5: Calculation of work-in-process

Part 1	Tube bending	Sawing & deburring	Welding/ Swaging	Marking & final test	Assembly
Mean demand rate (tubes/day)	0.69				
Mean overall yield rate	90%				
Mean yield rate	95%	100%	97%	98%	
Mean cycle time (days)	0.48	0.04	3.87	5.03	
Mean WIP	**0.37**	**0.03**	**2.82**	**3.56**	**13.50**
Total WIP	**20.27**				

4.6.6 Reordering Point And Safety Stock

Table 4.6 summarizes the calculation for the control variables of the ROP inventory. The safety coefficient equals 30%, therefore the safety stock after roundup is

$$17 \cdot 30\% = 5$$

The reordering point equals the total demand adjusted by the assembly yield loss during the cycle time, *i.e.*

$$\frac{0.69}{99.66\%} \cdot 9.42 = 7$$

Table 4.6: Calculation of the control variables for the ROP inventory

Part 1	Inventory
Mean demand rate (tubes/day)	0.69
Mean assembly yield rate	99.66%
Safety coefficient	0.30
Mean cycle time (days)	9.42
Reordering quantity	17
Reordering point	7
Safety Stock	5

4.6.7 System Cost

The costs incurred by each tube type per comprise scrap cost, inventory cost, and operation cost. Table 4.7 summarizes the calculation for a tube type. The scrap cost per unit time at each workstation is product of the mean batch arrival rate, mean batch quantity, mean yield loss, and the unit scrap cost. For example, the scrap cost at the welding/swaging workstation is

$$0.0028 \cdot 16.15 \cdot (1 - 97\%) \cdot \$30 = \$0.04$$

The inventory cost per unit time is obtained by multiplying the mean WIP and the inventory carrying cost per unit time. The operation cost per unit time equals the product of mean batch arrival rate, mean batch processing time, and the operation cost (labor and machine cost) per unit time. For example, the operation cost per unit time at the welding/swaging workstation equals

$$0.0028 \cdot 0.57 \cdot \$25 = \$0.039$$

The operation cost in assembly is not calculated because it is not driven by tube but the aircraft production.

Table 4.7: Calculation of total cost per hour for a tube type

Part 1	Tube bending	Sawing & deburring	Welding/ Swaging	Marking & final test	Assembly
Scrap cost per tube	$20	$25	$30	$35	$40
Inventory cost per tube per hour	$0.10	$0.13	$0.15	$0.18	$0.20
Operation cost per hour	$25	$25	$25	$25	$25
Mean batch arrival rate (batches/hour)	0.0028	0.0028	0.0028	0.0028	0.0028
Mean batch quantity	17.00	16.15	16.15	15.67	15.35
Mean yield rate	95%	100%	97%	98%	100%
Mean WIP	0.37	0.03	2.82	3.56	13.50
Mean batch processing time (hours)	0.56	0.36	0.57	0.57	
Mean scrap cost per hour	$0.0468	$0.0000	$0.0400	$0.0302	$0.0000
Mean inventory cost per hour	$0.0367	$0.0036	$0.4230	$0.6222	$2.7000
Mean operation cost per hour	$0.0383	$0.0248	$0.0390	$0.0390	
Mean total cost per hour	$0.1218	$0.0284	$0.5021	$0.6914	$2.7000
Total	**$4.0437**				

4.7 CONCURRENT OPTIMAL DESIGN AND INVENTORY CONTROL

In Section 2.6 we introduce the concept of Concurrent Optimal Design (COD) that minimize the system cost through part design, tolerancing, and batch-sizing. Therefore, there exists an optimal batch-size (reordering quantity) for any part type. Furthermore, since the reordering quantity determined the reordering point and safety stock as described in Section 4.5, the control variables for an ROP inventory can be determined simultaneously with COD. We will discuss COD by example in the next Chapter.

4.8 CHAPTER SUMMARY

This chapter elaborates the JSPM for the tube production system with inventories controlled by reordering points. The interactions among the inventory control variables, order arrivals, yield rates, and manufacturing cycle time are discussed. An example is used to demonstrate the procedure to predict the manufacturing cycle time, WIP, system costs, reordering point, and safety stock under a given reordering quantity. Since the reordering quantity can be optimized for minimum system costs in the formulation of COD as described in Section 2.6, the control variables for a ROP inventory can also be determined accordingly in COD.

CHAPTER 5 CONCURRENT OPTIMAL DESIGN AND OPTIMAL VARIATION REDUCTION FOR AIRCRAFT TUBE PRODUCTION

5.1 INTRODUCTION

In the previous two chapters we demonstrate the procedures of predicting the quality and production performances under specific part design and system configurations for aircraft tube production. This chapter will illustrate the concept of Concurrent Optimal Design (COD) as described in Chapter 2 by using aircraft tube design and production as an example. In addition, we will examine the sensitivity of COD to the source variation and determined the optimal investment strategy for the variation reduction.

5.2 SUMMARY OF APPROACH

In Section 2.6.2 we discussed the procedure and formulation for COD. Figure 5.1 summarizes the steps used for the aircraft tube production case. The first step is exploring the design alternatives that satisfy all functional requirements and constraints. Secondly, based on the methods described in Chapter 3, predict the yield rates in tube bending and assembly under different gauge clearances for each design. Thirdly, using the methods described in Chapter 4, predict the cycle time and WIP at each workstation and convert them into system cost. Fourthly, use mathematical programming method to find the optimal set of batch-sizes that minimizes the system cost for each combination of design alternative and gauge clearance. Lastly, choose the combination of design, gauge clearance and batch-sizes that minimize the system cost.

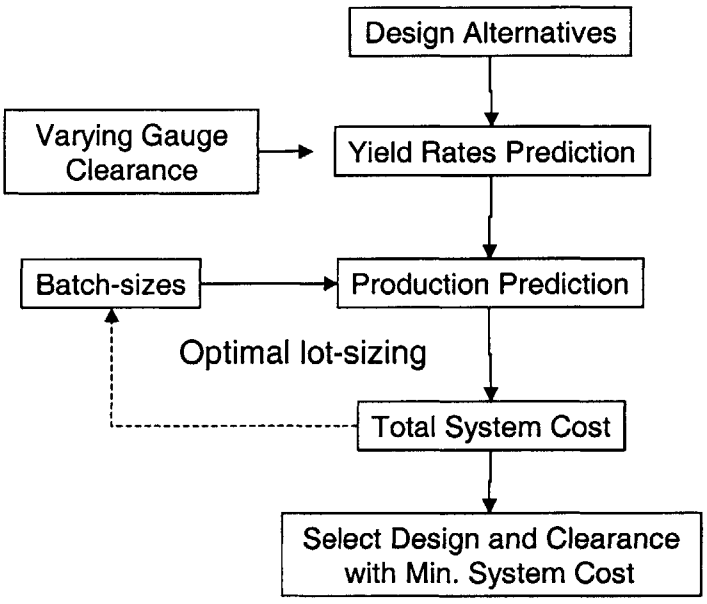

Figure 5.1: Flowchart of the procedure of COD for aircraft tube production

Repeating the COD procedure for different level of source variations (*e.g.*, process variation and structure variation), the optimal investment decision can be made by comparing the associated benefit from the reduction of total system cost and the cost for variation reduction. This is illustrated in Section 5.8.

5.3 DESIGN ALTERNATIVES

A tube needs to be designed to connect two points, point 1 and point 2, in the interior of the aircraft. It will be used to carry fluid for hydraulic control system. Due to the constraint of maximum pressure drop of the carrying fluid from point 1 to point 2, the maximum number of bends allowed on the tube is five. In addition, the spatial constraints require that the tube be within the envelope of 30"x30"x20", and the weight constraint limits the maximum tube length to 90". The specifications, material properties and inspection methods are listed below

- Outer diameter: ½"
- Wall thickness: 1/32'
- Bend radius: 1 ½"
- Elastic module E=1.60E+07 psi
- Shear module G=5.95E+06 psi
- Poison ratio=0.34
- Inspection in tube bending operation: Three cylindrical gauges with length of 1.5" and to-be-determined clearance ranging from 0.01"~0.15"
- Inspection criteria in the assembly operation: The resultant loads at both install points cannot exceed 10 lbs.

Four designs alternatives satisfying the aforementioned design criteria are shown in Figure 5.2. The name of the design indicates the number of bends on the tube, *e.g.*, B2 has two bends, B3 and three bends, etc. The dash-lined cylinders indicate the gauge locations for inspection after tube bending operation.

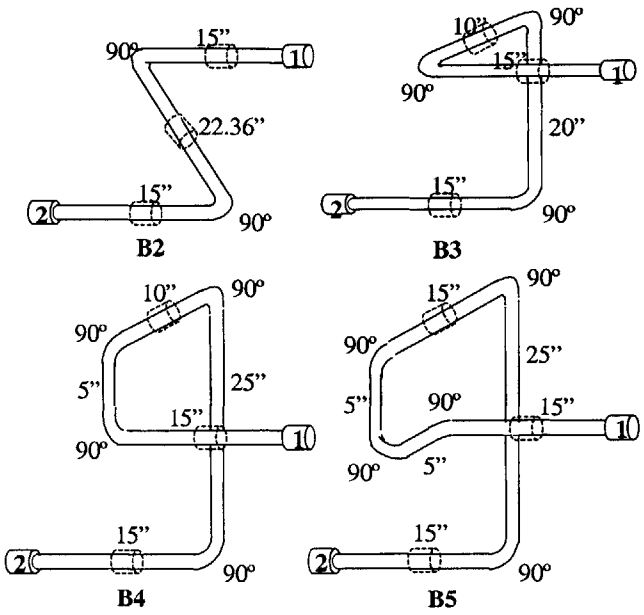

Figure 5.2: Four tube design alternatives

5.4 YIELD RATES PREDICTION

Assume the statistics for the process variations in tube bending and the geometric variations of the mating structure are the same as Table 3.3 and 3.5. Following the steps of variation propagation in tube bending and assembly as described in Chapter 3, the yield rates in tube bending (y_1) and assembly operations (y_5) are predicted with varying gauge clearance through simulation.

Figure 5.3 shows simulation result of the yield rates in tube bending operation for the four design alternatives under varying gauge clearance. It can be seen that the yield rate increases as the clearance is relaxed. In addition, under the same gauge clearance, the tube with more bends has lower yield rate because each additional bend introduces three variation sources (shooting distance, bending, and rotation angles).

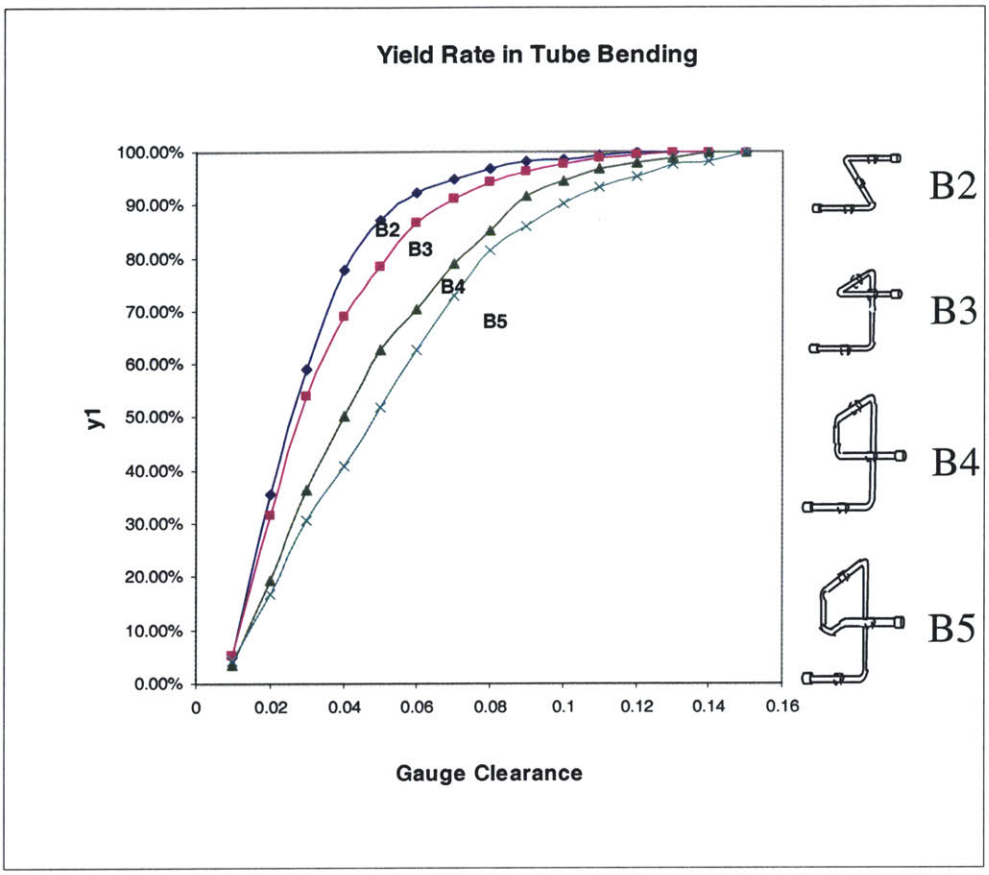

Figure 5.3: Yield rate in tube bending for the four design alternatives

Figure 5.4 shows the result of the assembly yield rates. It can be seen that the assembly yield rate increases as the clearance is relaxed because more tubes with larger variations are passed onto the assembly operation. Besides, the designs with more bends tend to have higher assembly yield rates because they have larger compliance to absorb the variations. However, there is a notable phenomenon in the assembly yield rates of B3 and B4: When the gauge clearance is large (>0.03), the assembly yield rate of B4 is smaller than B3, but when the gauge clearance is small (<0.03), it is larger than B3. This is because B4 has both larger tube variation and compliance. When the gauge clearance is large so that larger tube variations are permissible, the effect of larger tube variations of B4 overwhelms its larger compliance thus results in lower assembly yield rate. However, when the gauge clearance is small so that only small tube variations are allowed for both B3 and B4, the larger compliance of B4 leads to higher assembly yield rate.

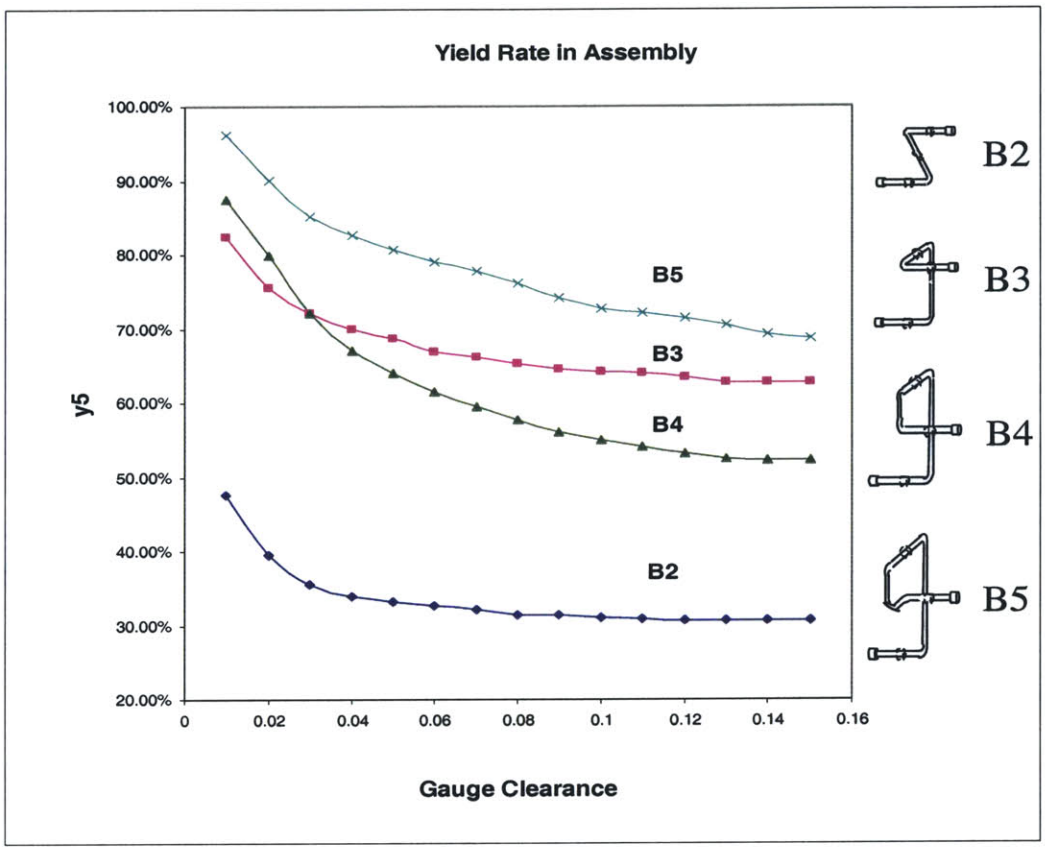

Figure 5.4: Yield rate in assembly for the four design alternatives

5.5 PRODUCTION SYSTEM PREDICTION

In order to illustrate the effect of a single part in the production system, we simplify the tube production by assuming only ten tube types manufactured in an imaginary system. Table 5.1 summarizes the production system. All the notations follow the ones used in Chapter 2. In the system, Part #1 is the tube to be designed and is highlighted. All the production variables at each stage of production (demand, yield rates, setup time, processing time, etc) are shown in the spreadsheet. The yield rates of tube bending and assembly of Part #1 are subject to change based on the selection of tube design and gauge clearance (tolerance), as described in the previous section. In addition, the reordering quantities (batch-sizes) of all part types are also subject to change to minimize the total system cost. These changing variables are highlighted in red font.

Table 5.1: Summary of the production system

Arrival					Tube Bending									Sawing & deburring								
Aggregated		6.27		0.03	CT=	88.7	u= 55%			C^d=	0.0392	83.87	0.07	CT=	44.77	u= 28%			C^d=	0.0464	43.1	0.13
Part #	d (per day)	λ	Y	c^a	Q	c^Q	s (min)	c^s	t (min)	c	y	t^b	c^b	Q	c^Q	s (min)	c^s	t (min)	c	y	t^b	c^b
1	30	0.90	57%	0.04	58	0.00	20.00	1.00	1.00	1.00	90%	78.19	0.07	52.37	0.00	15.00	1.00	0.50	1.00	100%	41.18	0.14
2	30	0.59	85%	0.02	60	0.00	20.00	1.00	1.00	1.00	96%	80.04	0.07	57.64	0.00	15.00	1.00	0.50	1.00	100%	43.82	0.12
3	30	0.59	83%	0.02	61	0.00	20.00	1.00	1.00	1.00	94%	81.14	0.07	57.47	0.00	15.00	1.00	0.50	1.00	100%	43.74	0.13
4	30	0.59	81%	0.02	62	0.00	20.00	1.00	1.00	1.00	92%	82.28	0.07	57.30	0.00	15.00	1.00	0.50	1.00	100%	43.65	0.13
5	30	0.59	80%	0.02	63	0.00	20.00	1.00	1.00	1.00	90%	83.45	0.07	57.11	0.00	15.00	1.00	0.50	1.00	100%	43.55	0.13
6	30	0.60	78%	0.02	65	0.00	20.00	1.00	1.00	1.00	88%	84.66	0.06	56.90	0.00	15.00	1.00	0.50	1.00	100%	43.45	0.13
7	30	0.60	76%	0.02	66	0.00	20.00	1.00	1.00	1.00	86%	85.91	0.06	56.68	0.00	15.00	1.00	0.50	1.00	100%	43.34	0.13
8	30	0.60	74%	0.03	67	0.00	20.00	1.00	1.00	1.00	84%	87.20	0.06	56.44	0.00	15.00	1.00	0.50	1.00	100%	43.22	0.13
9	30	0.60	73%	0.03	69	0.00	20.00	1.00	1.00	1.00	82%	88.53	0.06	56.19	0.00	15.00	1.00	0.50	1.00	100%	43.10	0.13
10	30	0.61	71%	0.03	70	0.00	20.00	1.00	1.00	1.00	80%	89.90	0.06	55.92	0.00	15.00	1.00	0.50	1.00	100%	42.96	0.13

Welding									Marking and final inspection									Inventory			Assembly
CT=	113	u= 64%			C^d=	0.042	98.307	0.04	CT=	85.49	u= 53%			C^d=	0.051	80.59	0.07	e= 20%			
Q	c^Q	s (min)	c^s	t (min)	c	y	t^b	c^b	Q	c^Q	s (min)	c^s	t (min)	c	y	t^b	c^b	Q	r	s	y
52.37	0.00	14.00	1.00	1.50	1.00	98%	92.55	0.04	51.32	0.00	20.00	1.00	1.10	1.00	95%	76.45	0.08	58	11	12	89%
57.64	0.00	14.00	1.00	1.50	1.00	98%	100.46	0.03	56.49	0.00	20.00	1.00	1.10	1.00	95%	82.14	0.07	60	11	13	95%
57.47	0.00	14.00	1.00	1.50	1.00	98%	100.21	0.03	56.33	0.00	20.00	1.00	1.10	1.00	95%	81.96	0.07	61	11	13	95%
57.30	0.00	14.00	1.00	1.50	1.00	98%	99.95	0.03	56.15	0.00	20.00	1.00	1.10	1.00	95%	81.77	0.07	62	11	13	95%
57.11	0.00	14.00	1.00	1.50	1.00	98%	99.66	0.03	55.96	0.00	20.00	1.00	1.10	1.00	95%	81.56	0.07	63	11	13	95%
56.90	0.00	14.00	1.00	1.50	1.00	98%	99.35	0.03	55.76	0.00	20.00	1.00	1.10	1.00	95%	81.34	0.07	65	11	13	95%
56.68	0.00	14.00	1.00	1.50	1.00	98%	99.02	0.03	55.55	0.00	20.00	1.00	1.10	1.00	95%	81.10	0.07	66	11	14	95%
56.44	0.00	14.00	1.00	1.50	1.00	98%	98.67	0.04	55.32	0.00	20.00	1.00	1.10	1.00	95%	80.85	0.07	67	11	14	95%
56.19	0.00	14.00	1.00	1.50	1.00	98%	98.29	0.04	55.07	0.00	20.00	1.00	1.10	1.00	95%	80.57	0.07	69	11	14	95%
55.92	0.00	14.00	1.00	1.50	1.00	98%	97.88	0.04	54.80	0.00	20.00	1.00	1.10	1.00	95%	80.28	0.08	70	11	14	95%

In the spreadsheet, the cycle time and WIP at each workstation and the control variables of the inventory are calculated using the procedure described in Chapter 4.

5.6 SYSTEM COST PREDICTION WITH OPTIMAL BATCH-SIZES

The cost factors in the production system are summarized in Table 5.2, where CS is the scrap cost per tube, CI is the inventory carrying cost per tube per hour, and CO is the operation cost per hour. Both scrap cost and inventory cost increase through the line because more value is added to the tubes during the production. The scrap cost in assembly is high because it includes not only the cost of a finished tube, but also the cost of interrupting the production of the whole aircraft.

Table 5.2: Summary of costs in the production system

	Raw	Tube bending			Sawing & deburring			Welding			Marking & final test			Assembly	
Part #	material	CS	CI	CO	CS	CI	CO	CS	CI	CO	CS	CI	CO	CS	CI
1	$20.00	$20.00	$0.10	$20.00	$22.00	$0.10	$15.00	$24.00	$0.11	$25.00	$26.00	$0.12	$20.00	$60.00	$0.13
2	$20.00	$20.00	$0.10	$20.00	$22.00	$0.10	$15.00	$24.00	$0.11	$25.00	$26.00	$0.12	$20.00	$60.00	$0.13
3	$20.00	$20.00	$0.10	$20.00	$22.00	$0.10	$15.00	$24.00	$0.11	$25.00	$26.00	$0.12	$20.00	$60.00	$0.13
4	$20.00	$20.00	$0.10	$20.00	$22.00	$0.10	$15.00	$24.00	$0.11	$25.00	$26.00	$0.12	$20.00	$60.00	$0.13
5	$20.00	$20.00	$0.10	$20.00	$22.00	$0.10	$15.00	$24.00	$0.11	$25.00	$26.00	$0.12	$20.00	$60.00	$0.13
6	$20.00	$20.00	$0.10	$20.00	$22.00	$0.10	$15.00	$24.00	$0.11	$25.00	$26.00	$0.12	$20.00	$60.00	$0.13
7	$20.00	$20.00	$0.10	$20.00	$22.00	$0.10	$15.00	$24.00	$0.11	$25.00	$26.00	$0.12	$20.00	$60.00	$0.13
8	$20.00	$20.00	$0.10	$20.00	$22.00	$0.10	$15.00	$24.00	$0.11	$25.00	$26.00	$0.12	$20.00	$60.00	$0.13
9	$20.00	$20.00	$0.10	$20.00	$22.00	$0.10	$15.00	$24.00	$0.11	$25.00	$26.00	$0.12	$20.00	$60.00	$0.13
10	$20.00	$20.00	$0.10	$20.00	$22.00	$0.10	$15.00	$24.00	$0.11	$25.00	$26.00	$0.12	$20.00	$60.00	$0.13

Using the production information in Table 5.1 and the cost information in Table 5.2, the total system cost for each design alternatives can be calculated under different set of batch-sizes and the yield rates of Part #1, y_1 and y_5, obtained from different scenarios of design and gauge clearance.

For each combination of y_1 and y_5, the batch-sizes can be optimized for the minimal total system cost through integer programming method. It is easy to implement in the package software such as Solver in MS Excel.

With optimal batch-sizes, the total system cost for each design under the varying gauge clearance is plotted in Figure 5.5, where the diamond-shaped dot indicates the gauge clearance that minimizes the total system cost.

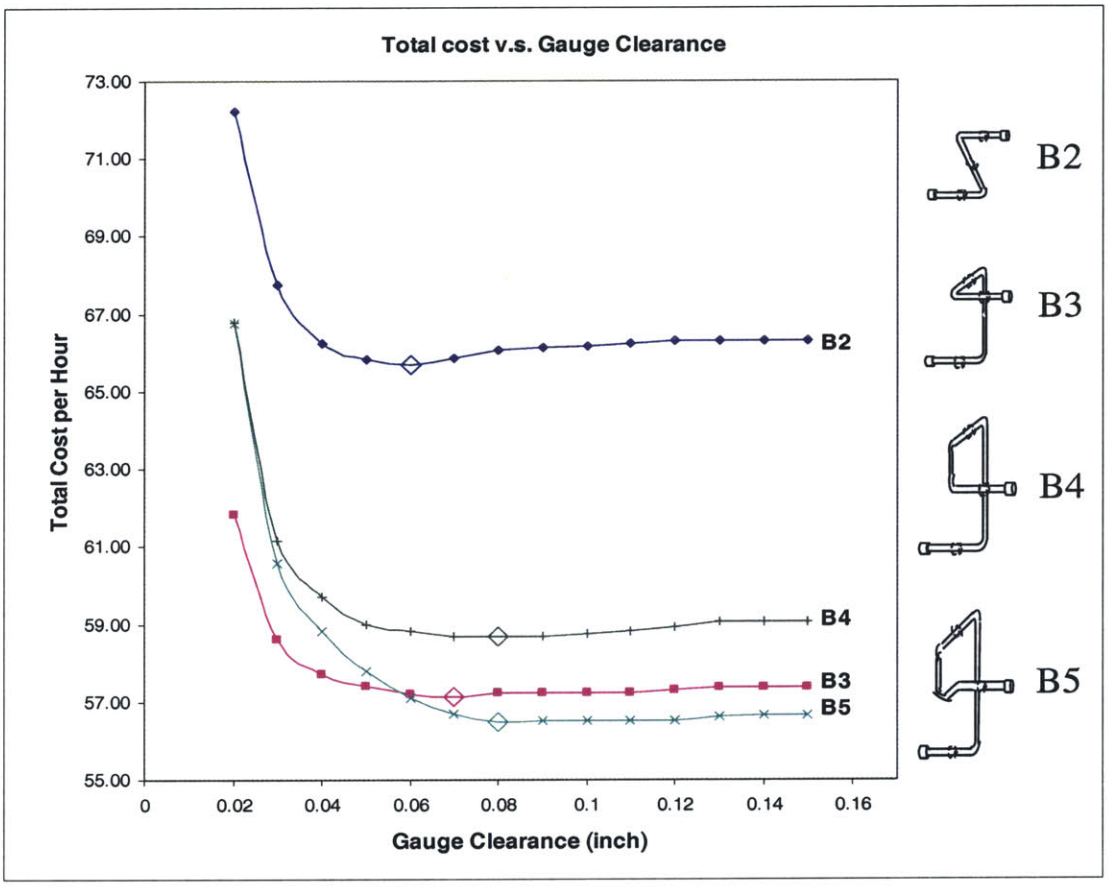

Figure 5.5: Total costs for the four design alternatives under varying gauge clearance

5.7 OPTIMAL DESIGN, TOLERANCE AND BATCH-SIZES

From Figure 5.5 it can be seen that design B5 with gauge clearance of 0.08 leads to the minimal system cost of $56.47 per hour. The optimal batch-sizes for this scenario are listed in Table 5.3.

Table 5.3: Optimal batch-sizes

Part #	**1**	2	3	4	5	6	7	8	9	10
Q	**69**	60	61	62	63	64	66	67	68	70

5.8 OPTIMAL VARIATION REDUCTION

The result of COD is subject to change when the source variations, *i.e.*, process variations and structure variation, are changed. This is because any changes in the source variations influence the resultant yield rates, thus the result in COD. For example, the inaccurate information about the variations, or the implementation of variation reduction schemes will lead to different optimal design, tolerance and batch-sizes. Figure 5.6 shows the result of assembly yield rates for the four design alternatives after 20% variation reduction in the mating structure. Here the 20% variation reduction means 20% decrease in the standard deviation for each of the geometric variation in the six degrees-of-freedom. Compared to Figure 5.4, it can be seen that all the yield rate curves are lifted up with different magnitudes.

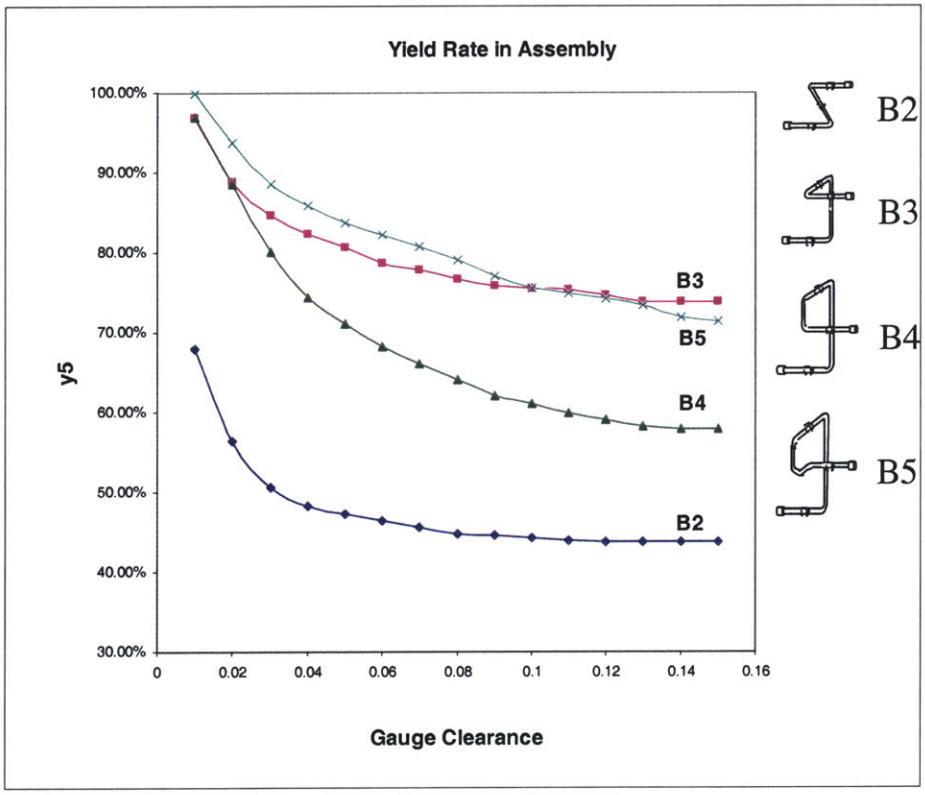

Figure 5.6: Assembly yield rates after 20% variation reduction in the mating structure

The result for total costs is shown in Figure 5.7. It can be seen that with 20% variation reduction in the mating structure, B3 replaces B5 as the optimal design. This is because after the variation reduction, the compliance of B3 becomes sufficient to absorb the variation, plus the fact that B3 has smaller tube variation than B5 due to its fewer bends. The new optimal total cost becomes $55.99 per hour.

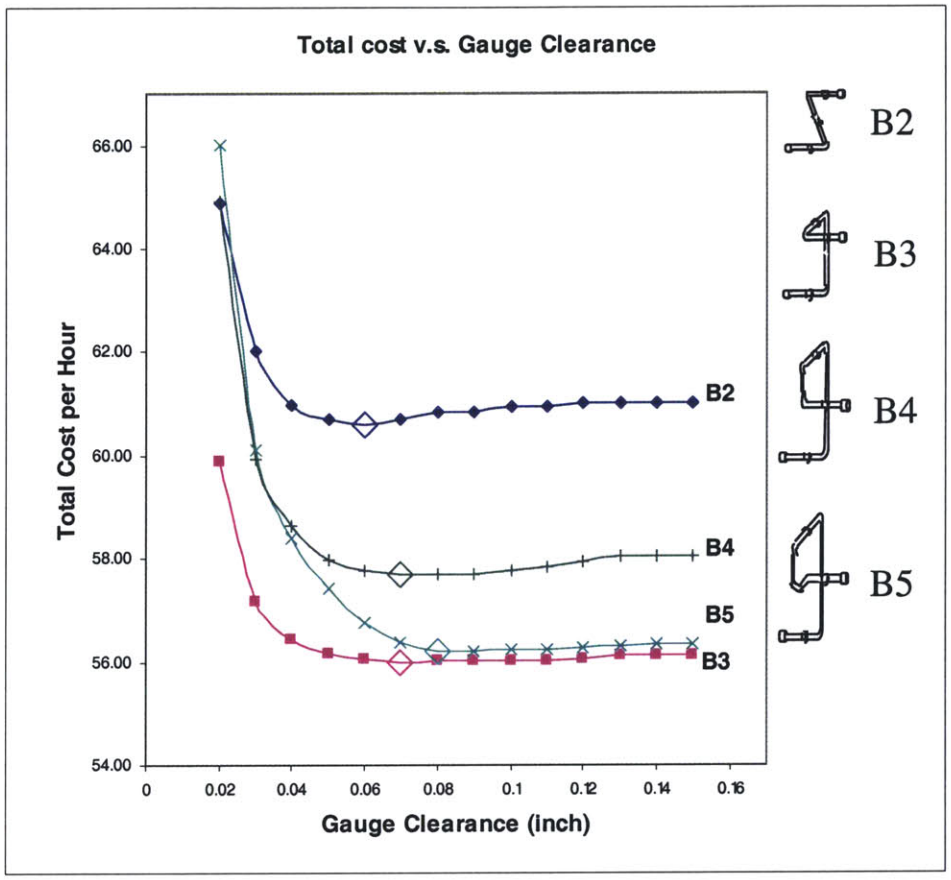

Figure 5.7: Total costs after 20% variation reduction in the mating structure

Figure 5.8 shows the result of optimal total cost under different levels of variation reduction in the mating structure. It can be seen that there is a diminishing marginal effect. This is because as the structure variation becomes smaller, the assembly yield rate is more dominated by the tube variation.

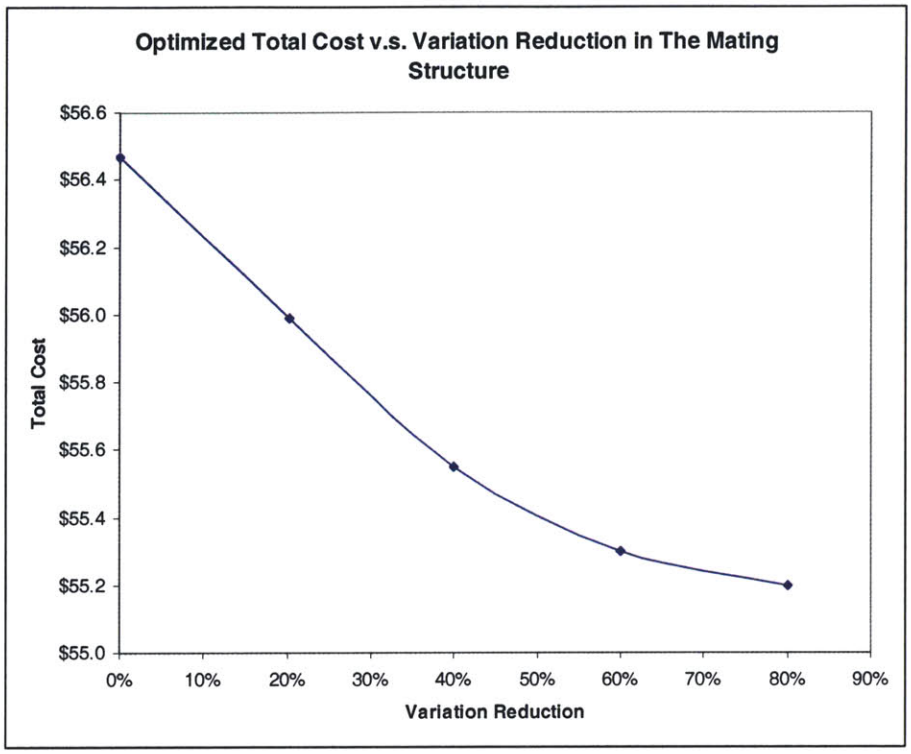

Figure 5.8: Optimized total cost per hour under different levels of variation reduction in the mating structure

In order to find the optimal level of variation reduction, the benefit from variation reduction needs to be compared to the associated cost. Assume that the cost is $5/hour per 20% variation reduction for the mating structure, the reduction in the optimal total cost compared to the optimal total cost without variation reduction and net saving are shown in Figure 5.9. It can be seen that the optimal level of variation reduction in the mating structure is 44%.

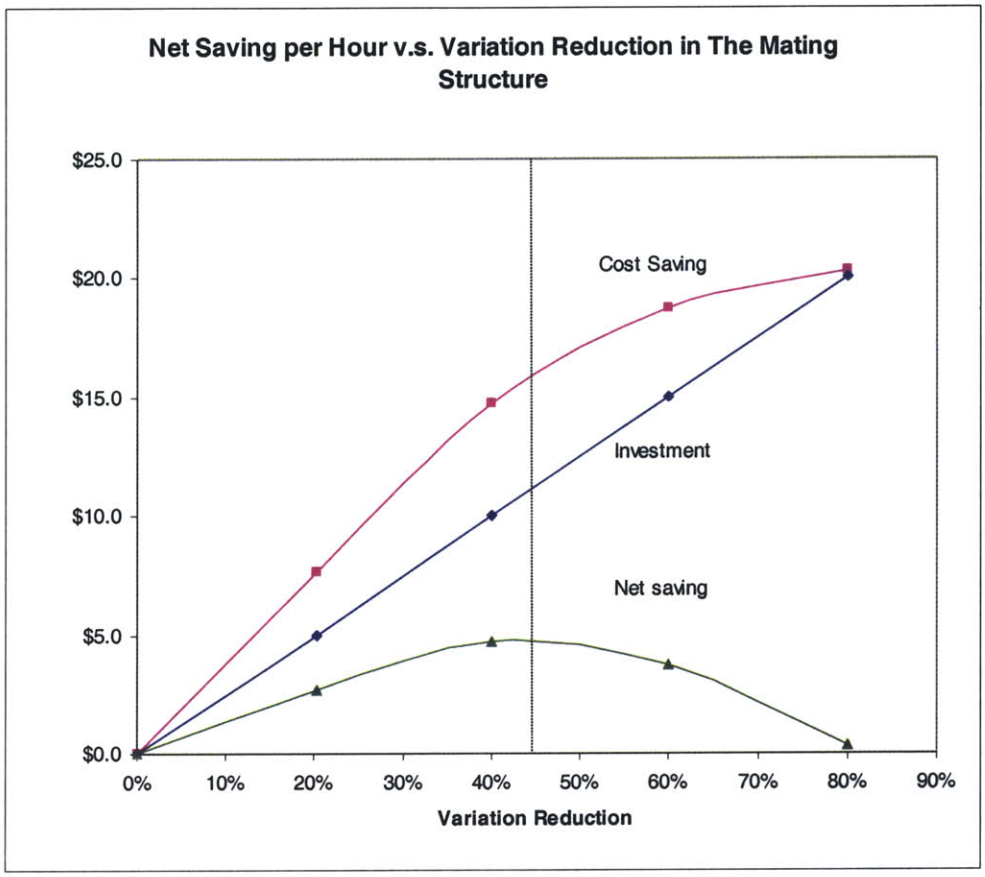

Figure 5.9: Optimal variation reduction in the mating structure

5.9 DISCUSSION

There are some findings from the results in Figure 5.5. They are discussed below.

Number of Bends and Optimal Design

Increase the number of bends on a tube can potentially, but not necessarily, decrease the total system cost. The reason for it is the effects of number of bends on the two yield rates as discussed in Section 5.4. From Figure 5.5, it can be seen that B4 has higher total cost curve than B3, even though it has one more bend. This is because the effect of increased tube variations is greater than the effect of increased compliance by the extra bend in B4.

Number of Bends and Optimal Clearance

Generally speaking, optimal tolerancing seeks to make the best tradeoff among the yield rate at the current stage and the downstream yield rates. In the case of tube production, it can be seen from Figure 5.5 that the designs with more bends have larger optimal gauge clearance. This is because even though more bends lead to higher tube variations, they also allow the tube shape to have larger compliance (higher assembly

robustness). Therefore, the gauge clearance can be relaxed to increase the yield rate in tube bending with a little sacrifice in the assembly yield rate.

Shape of Total Cost Curve

The shape of the total cost curve under the varying gauge clearance has some traits and will be discussed in this section. The curve of B2 is used as an illustration as shown in Figure 5.10. Starting from the optimal clearance, as the clearance decreases, the loss in y_1 (yield rate in tube bending) faster and larger than the gain in y_5 (yield rate in assembly) thus increases the total cost severely. The production system becomes unstable (the utilization rate at the bottleneck workstation approaches 100%) thus the total cost soars up to infinity as the clearance becomes too small. On the other side, as the clearance increases from the optimal point, the loss in y_5 slightly overwhelms the gain in y_1 thus increases the total cost. As the clearance becomes very large, y_1 approaches 100% and y_5 approaches the assembly yield rate without inspection in tube bending, as indicated by the asymptote.

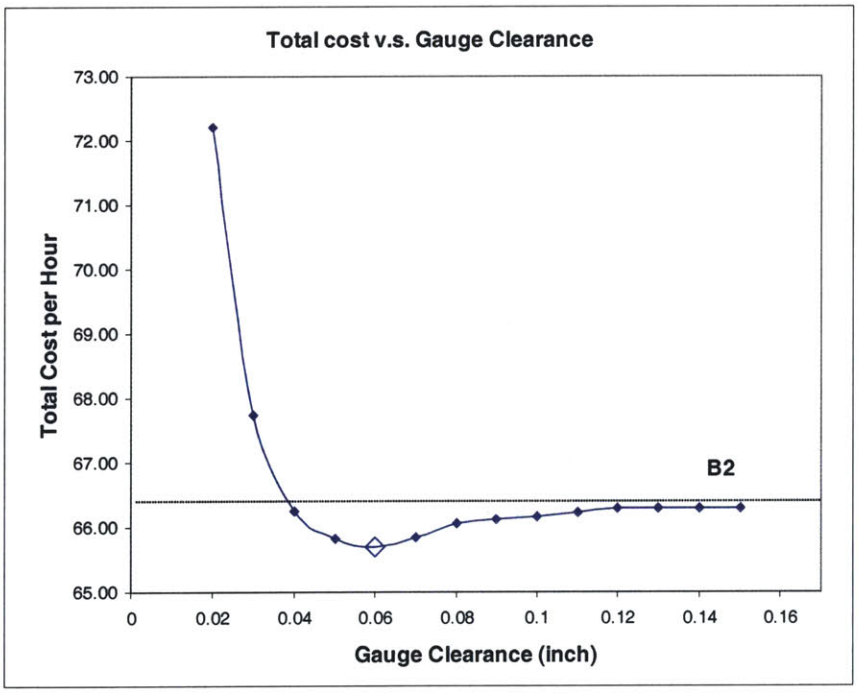

Figure 5.10: Shape of the total cost curve under the varying gauge clearance

5.10 CHAPTER SUMMARY

This chapter illustrates the procedure of Concurrent Optimal Design and optimal variation reduction by using aircraft tube production as an example. The result shows that part design, tolerancing and batch-sizes can and should be optimized simultaneously to achieve the minimum system cost. The investment decision for optimal variation reduction is also analyzed by comparing the associated benefit and cost. It is noted that

any changes in the design and tolerance for one part will not only affect the optimal batch-size decision of the part, but all other parts produced in the system. In addition, the accuracy and reduction in the source variation will affect the result of COD. Finally, the impact of the number of bends of a tube on the optimal tube design and gauge clearance, as well as the shape of the total cost curve under the varying tolerance are discussed.

CHAPTER 6 CONCLUSION

6.1 KEY FINDINGS

The key findings in the research are grouped into three categories. The first is robust design and optimal tolerancing. The second is production and inventory control. The third is guidelines for tube design. They are discussed as follows.

6.1.1 Robust Design and Optimal Tolerancing

Part design and tolerance will not only affect the quality, but also the production performance. From Joint System Performance Model we see that both part design and tolerance influence the yield rates, and the yield rates in turn affect the production performances, such as manufacturing cycle time, inventory, and cost. Over-strict tolerance may improve the downstream quality marginally, but can also deteriorate the system performances severely.

There are tradeoffs in the robust design at different stages of the manufacturing process. Traditional robust design techniques seek to minimize the variation at a single manufacturing operation through process adjustment or part design. However, most manufacturing processes comprise multiple operations. For robust design through process adjustment, Suri (1999) pointed out that in order to minimize the end-of-line variations, the process parameters at each stage need to be tuned and optimized simultaneously. Maximizing the robustness at each stage will not necessarily lead to the minimum end-of-line variations. Unlike the robust design by process adjustment where the process parameters at different stages can be tuned independently, robust design through part design is more complex because the any design change will affect the robustness at all stages thus tradeoffs need to be made. The example is shown in Chapter 3 that there is a tradeoff between the robustness in tube bending and the robustness in tube assembly.

Robust design and optimal tolerancing should be conducted simultaneously at all stages of the manufacturing process. Following the previous statement, robust design needs to consider the whole manufacturing process rather than a single operation because there are tradeoffs. However, the variation at each stage can also be controlled through tolerancing and there are also tradeoffs as shown in Section 3.5. Therefore, robust design and optimal tolerancing should be conducted concurrently through all stages of the manufacturing process.

Robust design and optimal tolerancing should seek to optimize the system performance, not just the quality. Traditional robust design uses quality as the only performance measure. However, it might not lead to the minimum system cost considering other performance measures. For example, suppose that the yield rates for the four design alternatives described in Chapter 5 are changed due to the changes in source variations and inspection method, as shown in Figure 6.1, and the other conditions stay the same. The optimization results by minimizing overall yield loss and the total system cost are shown in Figure 6.2. It can be seen that the results are different. The optimal

design and gauge clearance (tolerance) for the minimum yield loss is B5 and 0.12", while design B3 and the gauge clearance of 0.11" minimize the total system cost. The difference in the total system cost per hour is \$1.64-\$1.56=\$0.08. Therefore, optimizing the quality in robust design and optimal tolerancing will only lead to a local optimum. In order to achieve the global optimum, the total system cost needs to be considered.

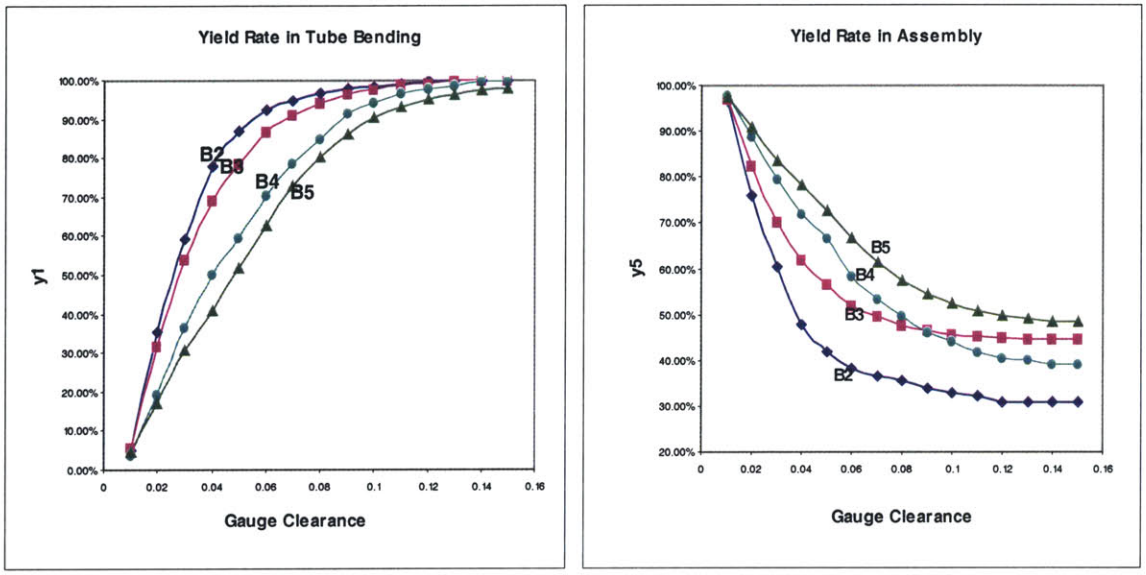

Figure 6.1: Modified yield rates for the four designs

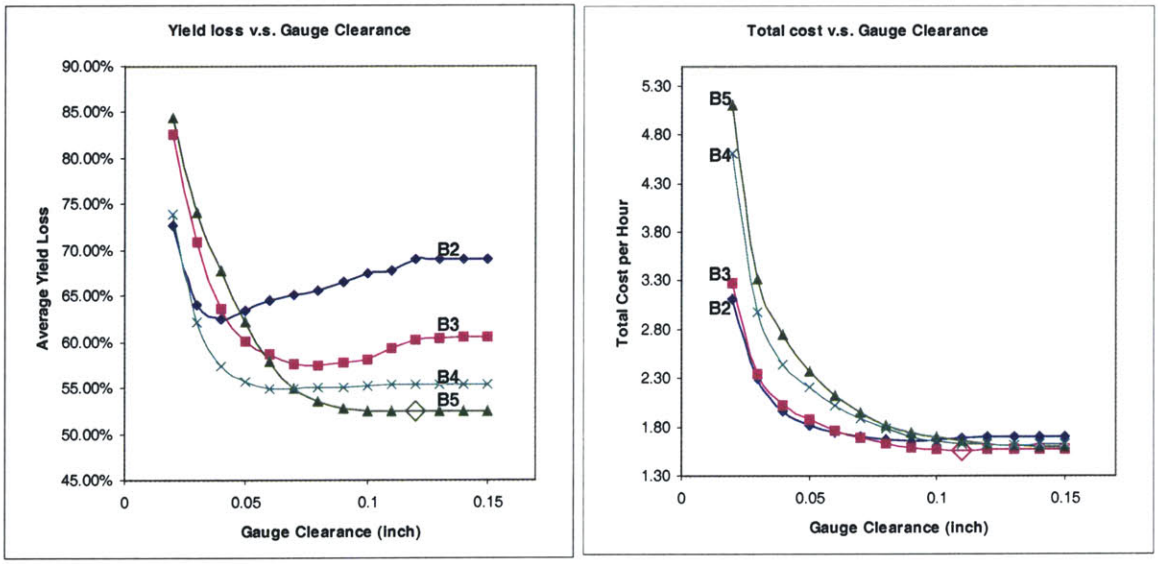

Figure 6.2: Optimization results by minimizing overall yield loss (left) and total system cost (right)

6.1.2 Production and Inventory Control

There is an optimal set of batch-sizes and inventory control variables corresponding to any set of part designs and tolerances. From Chapter 5 it can be seen that the optimal batch-sizes and inventory control variables are dependent on the decision of part design and tolerancing of any part type in the system. Any change in a part design or tolerance will influence the optimal set of batch-sizes and inventory control variables for all other parts.

Production optimization should start with design and tolerance optimization. Following the previous statement, the optimal batch-sizing and inventory control are passive optimizers. Therefore, in order to attain the best result, production optimization should always start with the part design and tolerance optimization.

Zero-defect is not always the optimal quality control policy. One of the paradigms of lean manufacturing is zero-defect quality control. However, it is not always the optimal policy. It can be seen from the example in Chapter 5 that imposing strict tolerance in the upstream operation to ensure the downstream quality will lead to very disastrous result. It will not be the optimal control policy unless the downstream quality cost is extremely high and the processing time, operation and scrap cost in the workstation is negligible, which is rarely the case. Therefore, zero-defect should be a goal for continuous process variation reduction, rather than quality control tool.

Single-piece flow is a possible consequence after design and process optimization, not the means. In Chapter 4 we see that there is an optimal set of batch-sizes. Unless they all turn out to be ones, single-piece flow will lead to very severe result in that it boosts the setups, workstation utilization, and ultimately the manufacturing cycle time. Therefore, single-piece flow should be the goal for continuous process improvement, such as setup reduction, variability elimination, etc., rather than batching policy.

6.1.3 DFM/A Guidelines for Tube Design

The number of bends on a tube should be minimized while providing sufficient compliance. It can be seen from Section 3.4 that increasing the number of bends will increase the variation in the shape of the tube, because more process variations are introduced. Therefore, the number of bends should always be minimized while the tube routing can still provide sufficient compliance.

A tube should be designed to have sufficiently long projected sections perpendicular to the direction of the geometric variations of the mating structure. In order to provide compliance to absorb the structure variation, the tube needs to have sufficiently long projected section perpendicular to the direction of each variation, as shown in Figure 6.3. This is because the bending and torsional deformations of these perpendicular sections can provide degree-of-freedom for adjustment in the direction of the variation.

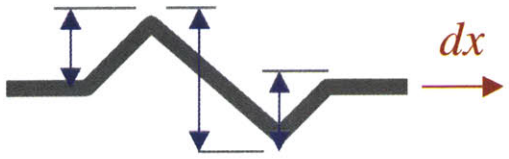

Figure 6.3: Perpendicular sections to provide compliance for the variation vector

Orthogonal or symmetric routing of tube is preferred to decouple the compensating loads. Non-orthogonal routing will induce loads in other directions when compensating the variation in one direction. Figure 6.4 shows examples of the effect of tube routing on its stiffness matrix. It can be seen that with a certain number of bends, non-orthogonal routing tends to have larger non-diagonal components in the stiffness matrix, which increase the chance of exceeding the load allowance. Therefore, orthogonal routing can not only facilitate the control of compensating loads by decoupling, but also potentially increase the assemblability.

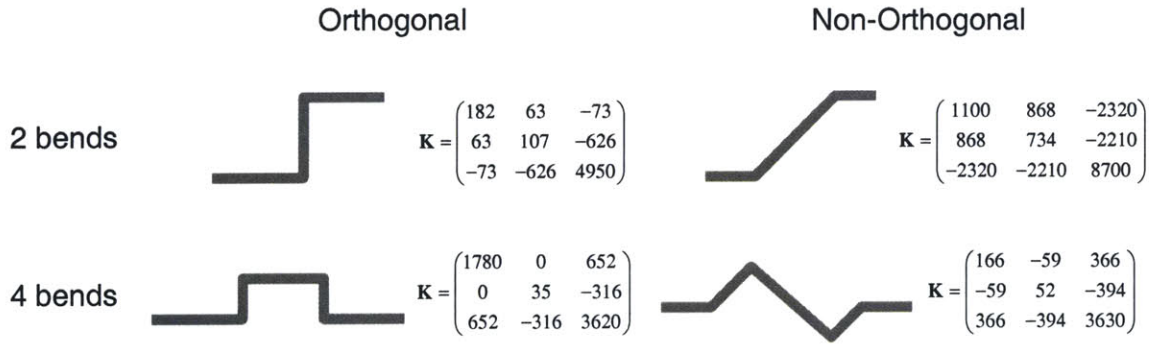

Figure 6.4: Examples of tube routings and the corresponding stiffness matrices

6.2 CONTRIBUTIONS

Major contributions of the thesis are summarized as follows:

- Introduced a system model, Joint System Performance Model (JSPM), to evaluate the system performances under the variability in a manufacturing system. The effects of part design, tolerancing, and process variations are projected onto the manufacturing cycle time, WIP and cost, rather than just quality variation.

- Provided a direct way for estimating the cost function for quality loss and tolerancing through Joint System Performance Model.

- Proposed an integrated optimization framework, Concurrent Optimal Design (COD), for simultaneous optimization of part design, tolerancing, and batch-sizing. It is pointed out that these three issues are interdependent thus need to be

conducted together to achieve the global optimum. A case study is used to illustrate the procedure.

- Demonstrated the approach for optimal investment strategy for variation reduction through JSPM and COD. Similar analysis can be applied to the investment strategy for capacity expansion, setup reduction, demand regulation, etc.

- Derived the variation propagation model for tube bending and assembly with minimum computational requirement. The proposed method provides analytical solution directly and eliminates the need for intensive CAD modeling and FEM simulation, thus enable the design optimization for tubes. Guidelines for the DFM/A of tubes are also drawn from the model.

- Research is being implemented at Boeing's next-generation design automation system

6.3 GENERALIZATION OF METHODS

The methods described in this thesis can be generalized. JSPM and COD in Chapter 2 are described in generic forms. There are two challenges in applying them to other cases. The first is deriving the sensitivity matrices for variation propagation at each stage of the process, as exemplified by the tube production system in Chapter 3. The second is adapting the queueing model for the production system. The general approaches of obtaining the sensitivity matrices are discussed in Section 2.2.4. Beside the process model for tube bending and assembly derived in this thesis, many researchers have modeled different types of manufacturing processes, such as stretch forming (Suri 1999), multi-chip modules (Frey and Otto 1996), injection molding (Kazmer and Barkan *et al.* 1996), welded aluminum automotive frames (Suri and Otto 1998), which can be used to derive the sensitivity matrices for these processes.

The queueing model for production prediction described in this thesis assumes a simplified multi-item and batching production system that has infinite buffers, no batch-splitting, and flow line with push system. For more complex cases, such as systems with finite buffers, complex routing or pull system, other queueing models need to be considered. Papadopoulos *et al.* (1993) provide a comprehensive review on this subject. However, the concept of JSPM that combines yield prediction and production prediction remains the same for different queueing models.

The modeling methods used in the quality prediction for tube production can also be generalized. These methods include applying homogeneous transform matrix for variation propagation in a bending operation, using matrix operation for direct compliance calculation for part with simple geometry, and utilizing nonlinear programming to simulate the gauge inspection. Their generalization issues are discussed in Section 3.4.3, 3.4.5 and 3.5.1, respectively.

6.4 FUTURE RESEARCH

There are some opportunities for future research. First, generalizing JSPM to more complex manufacturing systems with finite buffers instead of flow-line system with infinite buffers. Since many plants in reality adopt different types of manufacturing systems, and usually deploy finite buffers instead of infinite ones, the current assumptions of JSPM may not be always realistic and applicable. Secondly, estimating the distribution of manufacturing cycle time rather than just the average value. This is because the lead-time quoting in industry usually follows a pre-determined service rate, *i.e.*, the probability that the order will be delivered on time. In order to quote the lead-time based on the service rate, the distribution of the manufacturing cycle time is necessary. Thirdly, other potential performance measures, such as flexibility, quality and lead-time dependent demand, need to be incorporated into JSPM. Finally, more sophisticated cost model is needs to accommodate the other performance measures.

6.5 THESIS SUMMARY

This thesis demonstrates that concurrent engineering can be achieved through modeling so that tradeoffs and optimum decisions can be made analytically. A novel system modeling method, Joint System Performance Model, is introduced. Based on the model, a simultaneous optimization method, Concurrent Optimal Design, is formulated. The proposed method is demonstrated through a case study in the aircraft tube production system. The result shows that the decisions in part design, tolerancing, and batch-sizes can significantly improve the system performance without any investment. Many insights are drawn from the study and provide a different aspect from the current research in related areas.

REFERENCES

1. Asada, H. and Slotine, J.-J. E. (1986) *Robot Analysis and Control.* John Wiley & Sons, Inc., New York.
2. Bertrand, J.W.M. (1985) "Multiproduct Optimal Batch Sizes with In-process Inventories and Multiwork Centres" *IIE Transactions* 17 p.157-163
3. Bjorke, O. (1978) *Computer Aided Tolerancing*, Tapir Publication, Trondheim, Norway
4. Boothroyd, G., and Dewhurst, P. (1983) "Design for Assembly-Selecting the Right Method" *Machine Design* 55: (25), p.94-98
5. Boothroyd, G., and Dewhurst, P. (1988) "Product Design for Manufacturing and Assembly" *Manufacturing Engineering* 100: (4), p.42-46
6. Box, G.E., Hunter, W.G., and Hunter, J.S. (1978) *Statistics for Experimenters.* John Wiley & Sons, Inc., New York
7. Chang, M. (1996) *Modeling the Assembly of Compliant, Non-Ideal Parts.* Ph.D. Thesis. MIT, Boston
8. Chen, T.J. and Thornton, A.C. (1999) "Quantitative Selection of Inspection Plans" *ASME Design Theory and Methodology Conference*, Las Vegas, NV
9. Clausing, D. (1993) *Total Quality Development* ASME press, New York
10. Clausing, D., Pugh, S. (1991) "Enhanced Quality Function Deployment" *Proceedings of the Design Productivity International Conference*, Honolulu p.15-25
11. Cook R.D. and Young, W.C. (1985) *Advanced Mechanics of Materials.* McMillan Publishing Co., New York.
12. Cook, N. (1984) *Mechanics and Materials for Design.* McGraw-Hill Book Co., New York.
13. Daniel, F., Weil R., and Bourdet, P. (1986) "Computer Aided Tolerancing and Dimensioning in Process Planning" *CIRP Annals*, 35: (1), p. 381-386
14. DeVor, R.E., Chang, T.-H. and Sutherland, J.W. (1992) *Statistical Quality Design and Control.* MacMillan Publishing Co., New York.
15. Dewhurst, P., Boothroyd, G. (1988) "Early Cost Estimating in Product Design" *Journal of Manufacturing Systems* 7: (3) p.183-191
16. Diplaris SC, Sfantsikopoulos MM (2000) "Cost-tolerance function: A new approach for cost optimum machining accuracy" *International Journal of Advanced Manufacturing Technology* 16: (1) p. 32-38
17. Dong, Z. (1997) "Tolerance Synthesis by Manufacturing Cost Modeling and Design Optimization" *Advanced Tolerancing Techniques.* John Wiley & Sons, New York, p. 233-260.
18. Eppen, G.D., Martin, R.K. (1988) "Determining Safety Stock in The Presence of Stochastic Lead Time And Demand" *Management Science* 34: (11), p. 1380-1390
19. Evans, B. (1988) "Simultaneous Engineering" *Mechanical Engineering* 110: (2) p.38-39
20. Fotopoulos, S., Wang, M.C., and Rao, S.S. (1988) "Safety Stock Determination with Correlated Demands And Arbitrary Lead Times" *European Journal of Operational Research* 35: (2), p.172-181
21. Frank, B. (1993) "Pipe and Tube Bending: a Refresher Course." *Welding Design & Fabrication* 66, p. 72-73

22. Frey, D. (1997) *Using Product Tolerances to Drive Manufacturing System Design.* Ph.D. Thesis. MIT, Boston.
23. Frey, D. and Otto, K. (1996) "The Process Capability Matrix: A Tool for Manufacturing Variation Analysis at the System Level" *ASME Design Theory and Methodology Conference*, Sacramento, CA
24. Fritzinger, D. (1997) "A Quick Course in Bending Tubes. " *Machine Design.* 69, p. 67-68
25. Gao, J., Chase, K.W. and Magleby, S.P. (1998) "Generalized 3-D Tolerance Analysis of Mechanical Assemblies with Small Kinematic Adjustments" *IIE Transactions* 30, p. 367-377
26. Gao, J., Chase, K.W. and Magleby, S.P. (1995) "Comparison of Assembly Tolerance Analysis by The Direct Linearization And Modified Monte Carlo Simulation Methods" *ASME Design Engineering Technical Conference*, Boston, MA. Sep., p. 17-20, DE-82(1), 353-360.
27. Govil, M.K., Magrab, E.B. (1999) "Designing for Time-to-Market: Predicting the Effects of Product Design on the Production Rate" *ASME Design Engineering Technical Conference*, Las Vegas, NV
28. Guilford, J. and Turner, J.U. (1993) "Advances Tolerance Analysis and Synthesis for Geometric Tolerances" *ASME Manufacturing Review*, December
29. Hauser, J., Clausing, D. (1988) "The House of Quality" *Harvard Business Review* 66, p.63-73
30. Herrmann, J.W. and Chincholkar, M.M. (2000) "Design for Production: A Tool for Reducing Manufacturing Cycle Time" *ASME Design For Manufacturing Conference*, Baltimore, MD
31. Hopp, W.J. and Spearman, M.L. (1996) *Factory Physics.* Irwin/McGraw-Hill, Boston
32. Hu, S.J. (1997) "Stream-of-Variation Theory for Automotive Body Assembly." *CIRP Annals* 46: (1), p. 1-6
33. Jönsson, H., Silver, E.A. (1985) "Impact of Processing and Queueing Times on Order Quantities" *Material Flow* 2, p.221-230
34. Karmarkar U.S. (1987) "Lot-sizes, Lead Times, and In-process Inventories" *Management Science* 33: (3) 409-418
35. Karmarkar, U.S., Kekre, S., Kekre, S. (1992) "Multi-item Batching Heuristics for Minimization of Queueing Delays" *European Journal of Operational Research* 58: (1) 99-111
36. Karmarkar, U.S., Kekre, S., Kekre, S., and Freeman, S. (1985) "Lot-sizing and Lead-time Performance in A Manufacturing Cell" *Interfaces* 15: (2), p.1-9
37. Kazmer, D., P. Barkan, *et al.* (1996) "Quantifying Design and Manufacturing Robustness Through Stochastic Optimization Techniques" *ASME Design Automation Conference*, Irvine, CA
38. Kleinrock, L. (1975) *Queueing Systems, Volume I: Theory* John Wiley & Sons
39. Kleinrock, L. (1976) *Queueing Systems, Volume II: Computer Applications* John Wiley & Sons
40. Kuik R, Tielemans P.F.J., (1999) "Lead-time variability in a Homogeneous Queueing Model of Batching" *International Journal of Production Economics* 59: (1-3), p.435-441

41. Lambrecht M.R., Vandaele N.J. (1996) "A General Approximation for The Single Product Lot-sizing Model with Queueing Delays" European Journal of Operational Research 95: (1) p.73-88
42. Lee, D.J. and Thornton, A.C. (1996) "The Identification and Use of Key Characteristics in the Product Development Process" *ASME Design Theory and Methodology Conference*, Irvine, CA
43. Lee, J., Long, Y., and Hu, S.J. (2000) "Robustness Evaluation for Compliant Assembly Systems" *ASME Design For Manufacturing Conference*, Baltimore, MD
44. Liu, S.C. and Hu, S.J. (1997) "Variation Simulation for Deformable Sheet Metal Assemblies Using Finite Element Methods" *Journal of Manufacturing Science and Engineering*, 119, p. 368-374
45. Liu, S.C., Hu, S.J. and Woo, T.C. (1996) "Tolerance Analysis for Sheet Metal Assemblies" *Journal of Mechanical Design* 118, p. 62-67
46. Montgomery, D.C. (1984) *Design and Analysis of Experiments.* John Wiley & Sons Inc., New York.
47. Papadopoulos, H.T., Heavey, C. and Browne, J. (1993) *Queuing Theory in Manufacturing Systems Analysis and Design.* Chapman and Hall, London
48. Parsaei, H.R. and Sullivan W.G. (1993) *Concurrent Engineering* Chapman & Hall, New York.
49. Pilkey, W. (1994) *Formulas for Stress, Strain, and Structural Matrices.* John Wiley & Sons, Inc., New York.
50. Shimano, B.E. (1978) *The Kinematic Design and Force Control of Computer Controlled Manipulators.* Ph.D. Thesis. Stanford University, Stanford, CA.
51. Slocum, A. H. (1992) *Precision Machine Design.* Prentice Hall, Inc., New Jersey.
52. Soman, N.A. (1996) *A Model of the Assembly of Compliant Parts.* Ph.D. Thesis. MIT, Boston
53. Suri, R. and Otto, K. (1998) "Process Capability to Guide Tolerancing in Manufacturing Systems" *NAMRC XXVII*, Berkeley, CA NAMRI/SME
54. Suri, R. (1999) *An Integrated System Model for Variation Reduction in Manufacturing Systems.* Ph.D. Thesis. MIT, Boston.
55. Suri, R. and Otto, K. (1999) "Variation Modeling for Sheet Stretch Forming Manufacturing System" *Annals of CIRP.*
56. Szykman, S. amd Cagan, J. (1996) "Synthesis of Optimal Non-orthogonal Routes" *Journal of Mechanical Design* 118: (3), p. 419-424
57. Szykman, S., Cagan, J. and Weisser, P. (1998) "An Integrated Approach to Optimal Three Dimensional Layout and Routing" *Journal of Mechanical Design* 120: (3), p. 510-512
58. Takahashi, K., Suzuki, H. and Kimura, F. (1991) "Tolerance Analysis in Machine Assembly by Classifying Part Contact State" *Proceedings of CIRP Seminar on Computer Aided Tolerancing*, p. 57-76
59. Turner, J.U. (1990) "Relative Positioning of Parts in Assemblies using Mathematical Programming" *Computer-Aided Design*, 22: (7), p. 394-400, September
60. Turner, J.U. and Gangoiti, A.B. (1991) "Tolerance Analysis Approaches in Commercial Software" *Concurrent Engineering Issues, Technology, and Practice*, 1: (2), p. 11-23

61. Veeramani, D. and Joshi, P. (1997) "Methodologies for Rapid And Effective Response to Requests for Quotation" *IIE Transactions* 29, p.825-838
62. Veeramani, D. and Mehendale, T. (1999) "Online Design and Price Quotations for Complex Product Assemblies: The Case of Overhead Cranes" *ASME Design for Manufacturing Conference*, Las Vegas, NV
63. Veitschegger, W.K. and Wu, C.H. (1986) "Robot Accuracy Analysis Based on Kinematics." *IEEE Journal of Robotics and Automation* RA-2: (3), p. 171-179
64. Wei, Y.-F. and Thornton, A.C. (2000) "Tube Production and Assembly Systems: The Impact of Compliance and Variability on Yield" *ASME Design Automation Conference*, Baltimore, MD
65. Wei, Y.-F. and Thornton, A.C. (2000) "Robust Design for Tube Bending and Assembly" submitted to *Journal of Mechanical Design*
66. Whitney, D., Gilbert, O.L. and Jastrzebski, M. (1994) "Representation of Geometric Variation Using Matrix Transforms for Statistical Tolerance Analysis in Assembly" *Research in Engineering Design* 6, p. 51-70
67. Whitt, W. (1983) "The Queueing Network Analyzer" *The Bell System Technical Journal* 62: (9), p.2779-2815
68. Yano, C.A., Lee, H.L. (1995) "Lot Sizing with Random Yields: A Review" *Operations Research*, 43 (2), p. 311-334
69. Yao, D.D.W., Chaudhry, M.L., Templeton, J.G.C., (1984) "Analyzing the Steady-State Queue GIX/G/1" *Journal of the Operational Research Society* 35: (11), p.1027-1030
70. Zhang, C., Wang, H.P., and Li, J.K. (1992) "Simultaneous Optimization of Design and Manufacturing Tolerances with Process (Machine) Selection" *Annals of CIRP*, 41 (1), p. 569-572
71. Zipkin, P.H. (1986) "Models for Design and Control of Stochastic Multi-item Batch Production Systems" *Operation Research*, 34 (1), p. 91-104